Title
Nuclear Magnetic Resonance Experiments with dc SQUID Amplifiers

Author
Heaney, M.B.

Publication Date
1990-11-01

LBL-30095

Lawrence Berkeley Laboratory
UNIVERSITY OF CALIFORNIA

Materials & Chemical Sciences Division

Nuclear Magnetic Resonance Experiments with dc SQUID Amplifiers

M.B. Heaney
(Ph.D. Thesis)

November 1990

Prepared for the U.S. Department of Energy under Contract Number DE-AC03-76SF00098.

DISCLAIMER

LBL-30095

Nuclear Magnetic Resonance Experiments with dc SQUID Amplifiers

Michael Benedict Heaney

Ph.D. Thesis

Department of Physics,
University of California
Berkeley, CA 94720

and

Materials Sciences Division
Lawrence Berkeley Laboratory
University of California
Berkeley, CA 94720

November 1990

This work was supported by the Director, Office of Energy Research, Office of Basic Energy Sciences, Materials Sciences Division of the U.S. Department of Energy under contract number DE-AC03-76SF00098.

Nuclear Magnetic Resonance Experiments with dc SQUID Amplifiers

by

Michael Benedict Heaney

Abstract

The development and fabrication of dc SQUIDs (Superconducting QUantum Interference Devices) with $Nb/Al_2O_3/Nb$ Josephson junctions is described. A theory of the dc SQUID as a radio-frequency amplifier is presented, with an optimization strategy that accounts for the loading and noise contributions of the postamplifier and maximizes the signal-to-noise ratio of the total system. The high sensitivity of the dc SQUID is extended to high field NMR. A dc SQUID is used as a tuned radio-frequency amplifier to detect pulsed nuclear magnetic resonance at 32 MHz from a metal film in a 3.5 Tesla static field. A total system noise temperature of 11 K has been achieved, at a bath temperature of 4.2 K. The minimum number of nuclear Bohr magnetons observable from a free precession signal after a single pulse is about 2×10^{17} in a bandwidth of 25 kHz. In a separate experiment, a dc SQUID is used as a rf amplifier in a NQR experiment to observe a new resonance response mechanism. The net electric polarization of a $NaClO_3$ crystal due to the precessing electric quadrupole moments of the Cl nuclei is detected at 30 MHz. The sensitivity of NMR and NQR spectrometers using dc SQUID amplifiers is compared to the sensitivity of spectrometers using conventional rf amplifiers. A SQUID-based spectrometer has a voltage sensitivity which is comparable to the best achieved by a FET-based spectrometer, at these temperatures and operating frequencies.

Acknowledgements

I would first like to thank my research advisor, Professor John Clarke, for his support and advice during my stay at Berkeley. I would also like to thank Professor Erwin Hahn for teaching me about NQR and NMR, and for his many memorable jokes. I am very grateful to Cristian Urbina and Fred Wellstood, who spent a lot of time patiently teaching me how to fabricate and test Josephson junctions and SQUIDs. Fred Wellstood provided much invaluable guidance and help during my graduate school career, and made many useful suggestions during the writing of this dissertation. Fred's noble character and devotion to physics will always be an inspiration to me. Tycho Sleator led the way on the inverse Stark effect experiment. His personality and sense of humor greatly enhanced the collaboration. Dave Newitt and Larry Wald were both deeply involved in the high field SQUID NMR experiments, and made many contributions. Non Fan provided some assistance in SQUID fabrication. I would like to thank Katalin Voros, Bob Hamilton, and the staff of the Microlab for their excellent help in device fabrication.

I would like to thank my family for their support during graduate school. I would especially like to thank my grandmother, Mrs. Winifred Anner, for a lifetime of encouragement and support of my academic endeavors. Finally, I thank Kirsten Daehler for her invaluable support, and for adding so much fun to graduate school.

This work was funded by the Director, Office of Energy Research, Office of Basic Energy Sciences, Materials Sciences Division of the U.S. Department of Energy under contract number DE-AC03-76SF00098.

TABLE OF CONTENTS

Chapter 1: Introduction

1.1 Outline of this dissertation

This chapter provides a general introduction to the principles of the dc SQUID, and describes previous applications of superconductive devices to magnetic resonance experiments.

Chapter 2 describes the fabrication of dc SQUIDs and Q-spoilers used in the experiments described in later chapters, and includes a study of the stability of Nb/NbOx/PbIn Josephson junctions. These junctions exhibit critical currents which decrease with use, and show visible degradation of the PbIn layer following exposure to moisture. The development of a $Nb/Al_2O_3/Nb$ SQUID is described, using a system and junction process developed by Savo et al. (1987). These SQUIDs show no change in critical currents or visible degradation of layers after a year of use and exposure to moisture.

Chapter 3 reviews the theory of the dc SQUID as an rf amplifier. Optimization of the signal-to-noise ratio for a SQUID inductively coupled to a tuned circuit yields an optimization condition $M^{opt} \approx (LL_T/Q)^{1/2}(1 + T_N^{pa}/T)^{1/4}$, where M^{opt} is the optimum mutual inductance between the SQUID and the tuned circuit, L is the inductance of the SQUID loop, L_T is the total inductance of the tuned circuit, Q is the quality factor of the tuned circuit, T_N^{pa} is the noise temperature of the postamplifier, and T is the temperature of the tuned circuit.

Chapter 4 provides a brief derivation of the theoretical signal-to-noise ratio in NMR, and explains the optimization of signal averaging in NMR. When one pulse is applied, maximum signal-to-noise ratio is achieved when the pulse tips the spins by 90°. When more than one pulse are averaged together, the maximum signal-to-noise ratio for a given experimental time is attained when each pulse tips the spins by less than 90°. This is due to the finite spin-lattice relaxation time.

Chapter 5 describes the development of a pulsed NMR spectrometer using a dc SQUID amplifier for measurements at 32 MHz in a 3.5 Tesla static magnetic field. The spectrometer was used to observe NMR signals from a variety of metallic samples. The spectrometer noise temperature was measured to be 11 K, and the spin sensitivity was measured to be about 2.5×10^{17} nuclear Bohr magnetons in a 25 kHz bandwidth.

Chapter 6 describes an earlier experiment, in which a NQR spectrometer using a dc SQUID amplifier was used to detect the electric polarization induced in a $NaClO_3$ crystal by the precessing ^{35}Cl nuclear quadrupole moments.

Chapter 7 compares the advantages and disadvantages of SQUID-based NMR and NQR spectrometers with conventional spectrometers, and makes suggestions for future work.

1.2 The dc SQUID

The dc SQUID (Superconducting QUantum Interference Device) was first built by Jaclevic, Lambe, Mercereau, and Silver (1964) not long after Josephson's prediction of the effect which now bears his name (Josephson, 1962). The dc SQUID is a loop of superconducting material interrupted by two Josephson junctions, as shown schematically in Fig. 1.1(a). The loop has inductance L, and each junction has a critical current I_0. For high quality junctions, such as the ones used in this dissertation, two resistors R shunting each junction are deliberately added to the junction to make it non-hysteretic. The junction will be non-hysteretic when $\beta_c \equiv 2\pi I_0 R^2 C/\Phi_0 \leq 1$ (Stewart, 1968), where I_0 is the critical current of one junction, Φ_0 is the quantum of flux $h/2e = 2 \times 10^{-15}$ Wb, and C is the intrinsic capacitance of the junction. For thin film SQUIDs, the inductance of the junction itself can be neglected, and the junction areas can each be modeled as a capacitor, resistor, and Josephson junction in parallel. This is the resistively shunted junction (RSJ) model, first developed by Stewart (1968) and McCumber (1968).

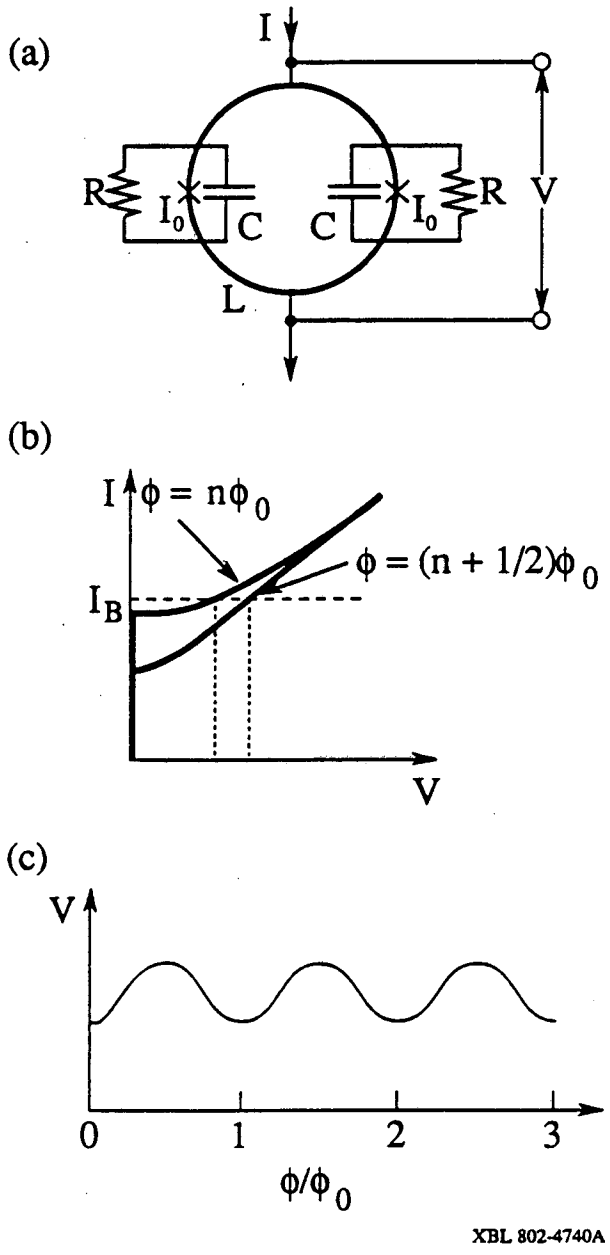

Fig. 1.1 (a) Schematic circuit diagram of the dc SQUID.
(b) Time-averaged current-voltage (I-V) characteristic of the dc SQUID.
(c) Voltage versus flux (V-Φ) curve of the current-biased dc SQUID.

The time-averaged current-voltage (I-V) characteristic of a non-hysteretic SQUID is shown in Fig. 1.1(b). A SQUID will be non-hysteretic when $\beta \equiv 2\pi I_0/\Phi_0 \leq 1$. For small currents, all of the current applied to the SQUID tunnels through the two junctions as supercurrents and there is no voltage across the SQUID. The supercurrent through one junction is given by the dc Josephson equation $I_1 = I_0 \sin \delta_1$, where I_0 is the critical current of the junction and δ_1 is the phase difference of the macroscopic wavefunction across that junction. Once the applied current exceeds the critical current, a voltage V appears across the junction as given by the ac Josephson equation $\hbar\dot{\delta} = 2eV$. This voltage induces current flow through the capacitor and resistor in parallel with the junction. As the applied current is increased to values much greater than the critical current, the time-averaged current through the junction decreases, and most of the dc current flows through the resistor. The large-current asymptote of the time-averaged I-V in Fig. 1.1(b) is just the I-V of the two shunt resistors in parallel.

The phase differences across the two junctions are related by $\delta_2 - \delta_1 = 2\pi\Phi/\Phi_0 + 2\pi n$, where Φ is the total flux in the SQUID loop (which is the sum of the externally applied flux and the self-induced flux) and n is an integer. The fact that the phase difference depends on the applied flux causes a modulation of the I-V of the SQUID periodic in the flux quantum, as shown in Fig. 1.1(b). This flux modulation allows the SQUID to be used as a sensitive flux-to-voltage transducer. In ordinary operation, a constant current is driven through the SQUID at a value $I \approx 2.5\ I_0$. Any flux entering the SQUID loop will then cause a change in voltage across the SQUID. The voltage versus flux (V-Φ) curve will then vary periodically, as shown qualitatively in Fig. 1.1(c).

Much insight into the behavior of the dc SQUID can be gained by studying mechanical analogs (Fulton, 1977). For example, the behavior of the voltage and circulating current vs. time in a dc SQUID (Tesche and Clarke, 1977) is readily understood by watching the behavior of two coupled pendulums, a mechanical analog for the dc SQUID.

To use the SQUID as a linear transducer, a fixed external flux is applied to the SQUID to flux-bias the SQUID at a point of maximum slope on the V-Φ curve. For small applied flux, the output voltage across the SQUID is then approximately linear in the input flux. By inductively coupling the SQUID to a tuned RLC circuit, as shown in Fig. 1.2, the SQUID and tuned circuit can be used as a voltage amplifier. The tuned circuit consists of a signal voltage V_{in}, a resistance R_i, a capacitance C_i, an inductance L_p, and a much smaller inductance L_i used to couple the tuned to the SQUID inductance L, via the mutual inductance M. The tuned circuit is tuned to the frequency of the signal voltage V_{in}, so that the current in the tuned circuit is approximately $I_{in} = V_{in}/R_i$ (note that this treatment neglects several effects which will be treated in more detail in Ch. 2). This signal current I_{in} induces a flux ϕ_x in the SQUID loop, given by $\phi_x = MI_{in}$. If this flux ϕ_x is small compared to a flux quantum, it will induce a voltage $V_{out} = \phi_x V_\phi$ across the SQUID, where V_ϕ is the maximum slope of the V-Φ curve of Fig. 1.1(c). The tuned circuit and SQUID thus function as a tuned linear amplifier, with output voltage related to input voltage by $V_{out} = (MV_\phi/R_i)\, V_{in}$. The voltage gain MV_ϕ/R_i can be over 100 for nominal SQUID parameters.

There are three intrinsic sources of noise in this voltage amplifier: the resistor R_i and the two resistors R. They all produce Nyquist noise which limits the ultimate sensitivity of the SQUID voltage amplifier. If one expresses sensitivity in terms of noise temperature, the SQUID voltage amplifier has a total noise temperature of $T_N^\Sigma = T_{Ri} + T_N$, where T_{Ri} is the temperature of the resistor R_i, and T_N is the noise temperature of the SQUID. The noise temperature of the SQUID is $T_N \approx 7(\omega L/R)T$, where the factor of 7 comes from nonlinear effects in the SQUID, ω is the signal frequency, L is the inductance of the SQUID loop, and T is the temperature of the two resistors R. For a signal frequency of 30 MHz, nominal SQUID parameters, and a bath temperature of 4.2 K, the theoretical SQUID noise temperature is $T_N \approx 0.3$ K. This is significantly lower than conventional room temperature amplifier noise temperatures at these frequencies, which have noise temperatures of 30 K or

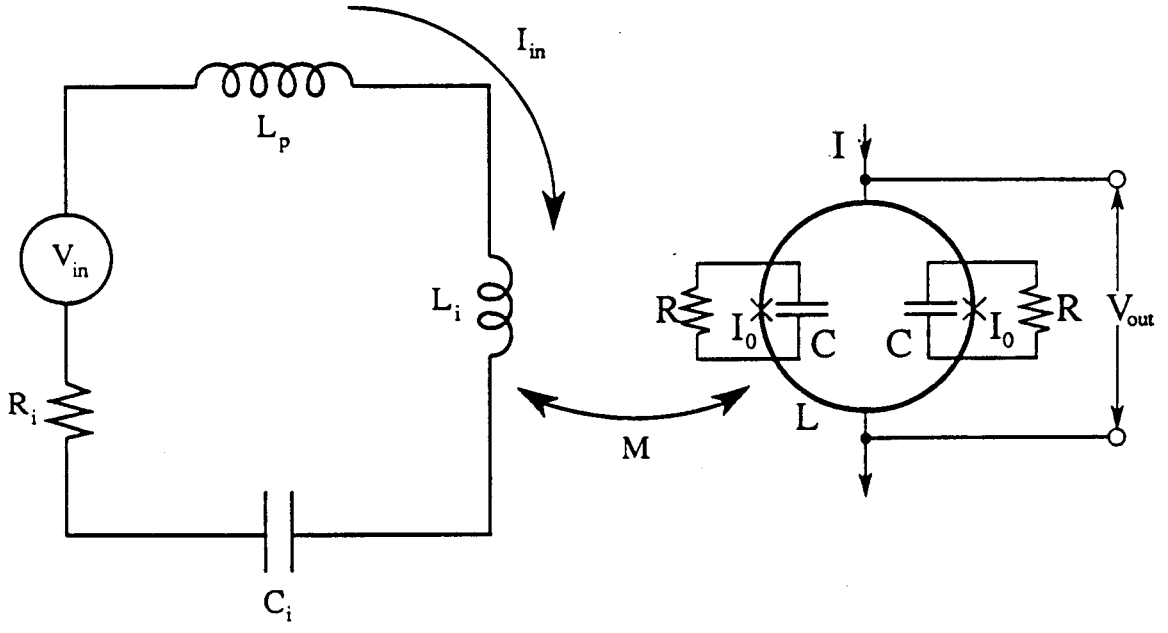

Fig. 1.2 Schematic circuit diagram of a tuned circuit inductively coupled to a dc SQUID.

higher. The low noise temperature of the dc SQUID makes it very attractive as a more sensitive rf amplifier for magnetic resonance experiments, where signals are small and many experiments are limited by lack of sensitivity.

However, there are disadvantages to using a dc SQUID as an rf amplifier for magnetic resonance experiments. As a linear amplifier, the SQUID is limited to the detection of small signals, due to the sinusoidal nature of the V-Φ curve. The SQUID must be kept at a temperature below about 9 K, necessitating the use of liquid helium. The tuned circuit must also be kept at about the same temperature: otherwise the Nyquist noise from the circuit will dominate the total noise temperature of the system, and the benefit of using a SQUID instead of a conventional amplifier will be minimal. For example, if the tuned circuit is at room temperature, using a conventional amplifier with a 30 K noise temperature will give a total system noise temperature of about 310 K, while using a SQUID will give a total system noise temperature of about 290 K. Using a SQUID instead of a conventional amplifier in this situation gives only a 6% improvement in noise temperature. If the sample to be studied is conducting, then it too will have Nyquist noise and must be kept at low temperatures to get much advantage from using a SQUID amplifier. This greatly limits the type of samples and problems for which the SQUID amplifier will be useful. For example, magnetic resonance studies of living biological organisms would not benefit much from the use of a SQUID amplifier. The SQUID is also sensitive to rf pulses, which can permanently shift the flux-bias point of the SQUID, rendering it useless as a linear amplifier. This problem might be remedied by improved decoupling between the transmitter and receiver circuits, or the use of a feedback circuit to return the SQUID to the optimum flux-bias point after the end of the rf pulse.

1.3 Applications to magnetic resonance

Superconducting devices have a long history of application to NMR, with the goal of improving the sensitivity. Silver et al. (1967) used a voltage-biased Josephson junction

to detect the ferromagnetic resonance (FMR) of ^{59}Co in zero external field at 218 MHz. Day (1972) used an rf SQUID to detect changes in longitudinal magnetization M_z in a 0.7 Tesla field (an rf SQUID is similar in form to a dc SQUID, except it has only one Josephson junction). Meredith et al. (1973) used an rf SQUID to measure changes in M_z with the continuous wave (cw) technique. Jach (1976) used an rf SQUID to detect changes in M_z in an NQR experiment. Webb (1977) used an rf SQUID to detect changes in M_z at low frequencies after application of an rf pulse, as well as cw NMR and adiabatic fast passage. Pickens et al. (1984) used an rf SQUID to detect changes in M_z after acoustic excitation.

Most of this work involved detection of changes in longitudinal magnetization M_z at low frequencies. Enholm et al. (1980) were the first to use an rf SQUID to detect transverse magnetization M_x at low frequencies after cw excitation, in a static field of 15 mT.

It is well known that the dc SQUID is is the most sensitive low frequency amplifier. Accordingly, recently workers have begun to use dc SQUIDs for low frequency NMR. The use of a dc SQUID allows NMR and NQR to be done at frequencies below 100 kHz with a broad bandwidth and improved sensitivity. For example, Friedman et al. (1986) used a dc SQUID to detect transverse magnetization at 50 kHz following a pulse, in a static field of 1.5 mT. Fan et al. (1988) used a dc SQUID to detect transverse magnetization at 55 kHz after a pulse, in a 6 mT field. Chang et al. (1989) used a dc SQUID to detect low frequency NQR with a cw technique.

However, the most useful and widespread NMR techniques are based on detection of transverse magnetization $M_{x,y}$ at high frequencies. DC SQUIDs have only recently been developed as radiofrequency amplifiers. A Q-spoiler based on a series array of hysteretic Josephson junctions has also been developed (Hilbert et al., 1985). This allowed the use of high Q receiver circuits without the usual serious ringdown problems. These new developments allowed Hilbert et al. (1985) to use a dc SQUID to detect the transverse

magnetization at 30 MHz following an rf pulse in an NQR experiment. Freeman et al. (1986) used a dc SQUID to detect transverse magnetization at 2 MHz in a 60 mT field. Since the voltage sensitivity in NMR is proportional to $B_0^{3/2}$ if the Q of the receiver circuit is held constant (where B_0 is the static magnetic field) there is motivation to extend dc SQUID NMR to higher fields. Chapter 5 describes some attempts to do so.

References

1. Savo, B., F. C. Wellstood, and J. Clarke, 1987, "Low Frequency Excess Noise in Nb-Al_2O_3-Nb Josephson Tunnel Junctions," Appl. Phys. Lett. 50, 1757.

2. Jacklevic, R. C., J. Lambe, J. E. Mercereau, and A. H. Silver, 1964, "Quantum interference effects in Josephson tunnelling," Phys. Rev. Lett. 12, 159.

3. Josephson, B. D., 1962, "Possible new effects in superconductive tunnelling," Phys. Rev. Lett. 1, 251.

4. Stewart, W. C., 1968, "Current-voltage characteristics of Josephson junctions," Appl. Phys. Lett. 12, 277.

5. McCumber, D. E., 1968, "Effect of ac impedance on dc voltage-current characteristics of superconductor weak-link junctions," J. Appl. Phys. 39, 3113.

6. Tesche, C. D., and J. Clarke, 1977, "DC SQUID: noise and optimization," J. Low Temp. Phys. 29, 301.

7. Fulton, T. A., 1977, "Equivalent circuits and analogs of the Josephson effect," in Superconductor Applications: SQUIDs and Machines, B. B. Schwartz and S. Foner, Eds. (Plenum Press, New York).

8. Silver, A. H., and J. E. Zimmerman, 1967, "Multiple quantum resonance spectroscopy through weakly connected superconductors," Appl. Phys. Lett. 10, 142.

9. Day, E. P., 1972, "Detection of NMR using a Josephson-junction magnetometer," Phys. Rev. Lett. 29, 540.

10. Meredith, D. J., G. R. Pickett, and O. G. Symko, 1973, "Application of a SQUID magnetometer to NMR at low temperatures," J. Low Temp. Phys. 13, 607.

11. Jach, T., 1976, "Detection of nuclear quadrupole resonance via induced longitudinal magnetization," Appl. Phys. Lett. 28, 49.

12. Webb, R. A., 1977, "New technique for improved low-temperature SQUID NMR measurements," Rev. Sci. Instrum. 48, 1585.

13. Pickens, K. S., D. I. Bolef, M. R. Holland, and R. K. Sundfors, 1984, "Superconducting quantum interference device detection of acoustic nuclear quadrupole resonance of ^{121}Sb and ^{123}Sb in antimony metal," Phys. Rev. B30, 3644.

14. Enholm, G. J., J. P. Ekstrom, M. T. Loponen, and J. K. Soini, "Transversal SQUID NMR," Cryogenics 19, 673.

15. Friedman, L. J., A. K. M. Wennberg, S. N. Ytterboe, and H. M. Bozler, "Direct detection of low-frequency NMR using a dc SQUID," Rev. Sci. Instrum. 57, 410.

16. Fan, N. Q., M. B. Heaney, J. Clarke, D. Newitt, L. L. Wald, E. L. Hahn, A.Bielecki, and A. Pines, 1988, "Nuclear Magnetic Resonance with dc SQUID Preamplifiers," IEEE Trans. Magn. 25, 1193.

17. Chang, J., C. Conner, E. L. Hahn, H. Huber, and A. Pines, 1989, "Direct detection of aluminum-27 resonance with a SQUID spectrometer," J. Magn. Reson. 82, 387.

18. Hilbert, C., J. Clarke, T. Sleator, and E. L. Hahn, 1985, "Nuclear quadrupole resonance detected at 30 MHz with a dc superconducting quantum interference device," Appl. Phys. Lett. 47, 637.

19. Freeman, M. R., R. S. Germain, R. C. Richardson, M. L. Roukes, W. J. Gallagher, and M. B. Ketchen, 1986, "Low-temperature nuclear magnetic resonance with a dc SQUID amplifier," Appl. Phys. Lett. 48, 300.

Chapter 2: SQUID and Q-spoiler fabrication

2.1 Introduction

In this chapter I will describe the fabrication procedures for the SQUIDs and Q-spoilers used in this dissertation. I will also describe some earlier studies on the stability of Nb/NbOx/PbIn junctions and the development of the all-niobium SQUID, and discuss some remaining problems in SQUID technology.

A schematic of a SQUID with a 4-turn spiral input coil is shown in Fig. 2.1. The SQUIDs are thin film planar devices similar in design to those described by Ketchen and Jaycox (1982). The body of the SQUID is a square washer of niobium about 1 mm on a side, interrupted by a vertical slit. The input coil lies on top of the SQUID body, and is electrically isolated from the SQUID body by an insulating SiO layer. The input coil enters from the right side, spirals around to the center of the SQUID body, and exits via an underpass (vertical dotted line).

A close-up of the junction area is also shown in Fig. 2.1. The two junction areas are defined by two square holes in the insulating SiO layer near the upper left and upper right sides of the shunts. The shunts for both junctions are defined by a single CuAu structure.

2.2 Fabrication procedures

I fabricated the SQUIDs in the Cory Hall microlab and 137 LeConte Hall using conventional photolithographic techniques. The SQUIDs are fabricated 36 at a time on 2" diameter oxidized silicon wafers which are 14-16 mil thick, have 5-10 Ω-cm resistivity, 1,100 nm oxide thickness, and (100) orientation. The diameter of the wafer was chosen many years ago, when 2" was fairly common in industry. Today most processing is done on larger diameter wafers, and few vendors still stock 2" diameter wafers.

Wafers thinner than 12 mil have been used by the Clarke group, with unsatisfactory results. The fabrication procedure includes steps where the wafer is gripped on one edge

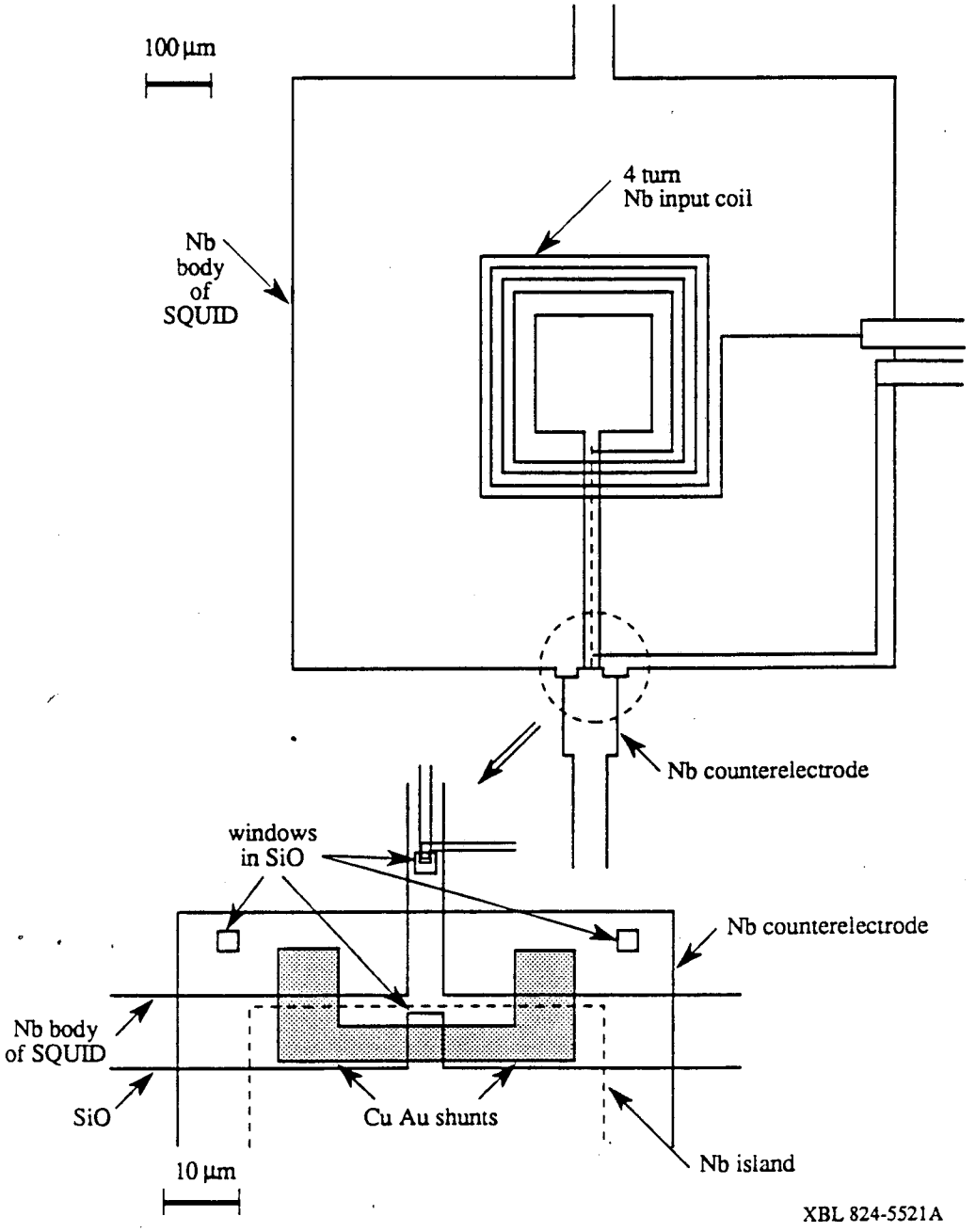

Fig. 2.1 Schematic of a Nb/Al_2O_3/Nb dc SQUID with a 4-turn input coil.

with a tweezer and stirred in a glass beaker of fluid. I have found that wafers thinner than about 14 mil tended to break too easily during this and other processing steps. High resistivity and a thick oxide layer are desirable to avoid any conduction through the wafer. Thinner oxide layers are occasionally "punched through" when making electrical contact to the SQUID. The crystal orientation of the wafer is fairly important. Wafers with other orientations are more difficult to dice along the directions defining the individual SQUID chips. A diamond saw could overcome this problem, but the diamond saw process involves wetting the wafer while it is being cut. The slurry of wafer dust from the cutting gets into the junction windows and is then impossible to remove without destroying the nearby resist. The dicing is done with an automated wafer scriber using a dry process. This produces less wafer dust, and any dust falling in the junction windows can usually be removed with a jet of nitrogen gas.

The fabrication procedure for the SQUIDs is as follows. I first clean the wafer in Pierce detergent for 10 minutes, to remove any grease or dust. The wafer is then exposed to HMDS vapor for 3 minutes. This promotes adhesion of the photoresist to the wafer. Shipley 1450J photoresist is then spun onto the wafer at 6 krpm for 30 seconds. The wafer is next heated on a 70°C hot plate for 3 minutes, to dry and harden the photoresist. The wafer is placed in chlorobenzene held at 18-19°C for 10 minutes. The chlorobenzene hardens the surface of the photoresist. This causes undercutting of the photoresist when it is developed, which aids in liftoff of subsequently deposited films. After removal from chlorobenzene, the wafer is blown dry with a jet of nitrogen gas and placed on the 70°C hot plate for 3 minutes.

The first photolithography exposure is the shunts. Most of the photolithography masks used for SQUID fabrication are modifications of masks designed by Wellstood. The exposures are done with a Canon 4× Projection Mask Aligner with the exposure set at 5.0 and the focus set at 968. The SQUIDs are exposed in sets of 4. Each of the 9 exposure areas on the wafer is done with manual alignment, since the automatic alignment feature of

the Canon can give poor alignment. After exposure, the wafer is developed in Microposit Developer Concentrate for 45 seconds, transferred to a DI water stopbath, rinsed under DI water and blown dry. After examination of the developed photoresist pattern under a microscope, I bring the wafer as quickly as possible to 137 LeConte Hall for shunt deposition.

A 1 nm layer of titanium is first evaporated onto the wafer. This acts as an adhesion layer between the wafer and the shunt. I have obtained good adhesion this way, although others have had more success with chromium instead of titanium at this step. A mixture of gold and copper (33wt% Cu) is evaporated to a thickness of 30 nm to serve as the resistive shunt. The photoresist is then lifted off in acetone to leave the shunt structure.

I then clean the wafer in Pierce detergent and place it in the sputter system. A 200 nm thick niobium film is sputter deposited on the wafer. Vacuum grease is used to anchor and thermally ground the wafer during the sputter process. After Nb deposition the wafer is again cleaned in Pierce detergent to remove the vacuum grease on the back of the wafer.

The wafer is exposed to HMDS for 5 minutes, and Shipley 1400-17 photoresist is spun on at 5 krpm for 30 seconds. I then bake the wafer at 90°C on a hot plate for 3 minutes, then expose it to the SQUID body mask in the Canon at an exposure setting of 5.9. The photoresist is developed in a diluted mixture of Microposit Developer Concentrate (50% H_2O) for 25 seconds, stopbathed, rinsed, blown dry, and heated on the 90°C hot plate for 1.5 minutes. The exposed Nb is etched away in a 0.56 Torr SF_6O_2 plasma for about 2 minutes to define the body of the SQUID and the contact pads. The etch is stopped by visual inspection. I then put the wafer in diluted Microposit 1112A Remover (50% H_2O) to remove the photoresist, clean it in acetone, rinse it in water, blow it dry, and clean in Pierce detergent for 20 minutes.

I next deposit two SiO layers to form an insulating barrier with holes defining the junction areas and contacts to the input coil crossover strip and shunt. Wellstood has developed a cross-strip junction process to replace the IBM dot junction process

(Wellstood, 1988). This new method gives much more satisfactory results: the photoresist dots defining the junction windows were often difficult to lift off. The wafer is exposed to HMDS for 5 minutes, Shipley 1400-31 photoresist is spun on, heated at 70°C for 3 minutes, soaked in chlorobenzene for 10 minutes, blown dry, and heated at 70°C for three minutes. The first window mask is exposed on the Canon with an exposure setting of 5.0. The photoresist is developed for 20 seconds in Microposit Developer Concentrate, stopbathed, rinsed, and blown dry. A 1 nm Ti adhesion layer is evaporated onto the wafer, immediately followed by a 200 nm thick SiO layer. Previously, Cr had been used for the adhesion layer. This often produced shorts on the SQUID, possibly due to the fact that Cr sublimates and the deposition rate is thus difficult to control. Wellstood switched to the IBM technique of using Ti for adhesion, with satisfactory results (Wellstood, 1988). The photoresist is then removed by soaking the wafer in acetone and diluted Microposit 1112A Remover (50% H_2O). The wafer is cleaned in Pierce detergent, and the second SiO layer is fabricated in the same manner, except to a thickness of 300 nm.

The next layer is 300 nm Nb for the input coils and contact pads. I first ion mill the Nb base layer for 40 seconds to remove dirt and oxide, thus ensuring good contact to the crossover strip. I then pattern this layer for liftoff, following all of the same steps as the shunt layer. The Canon is set at an exposure of 5.5, and the photoresist is developed for 45 seconds. The turns of the coils are defined by photolithography and plasma etch steps similar to the first Nb layer.

A final photoresist layer of Shipley 1450J is applied to define the counterelectrode area. The wafer can now be diced with the wafer scriber in 137 LeConte, and individual SQUIDs completed as needed.

Nominal SQUID parameters are L = 0.4 nH, C = 0.5 pF, R = 8 Ω, L_i = 5.6 nH and M = 1.2 nH (for a 4-turn input coil), and I_0 = 3 μA. These parameters give $\beta \approx 1$ and $\beta_c \approx 0.3$.

The Q-spoiler is a series array of 21 $10 \times 10\ \mu m^2$ cross-strip Josephson junctions. These arrays are fabricated 9 on a wafer using a procedure similar to the above SQUID procedure, although simpler in steps. A Nb base layer is deposited as described above, followed by a photoresist layer defining the $10 \times 10\ \mu m^2$ junction areas. The junctions are completed as described in the next section, the only difference being the oxidation time (60 seconds) and the relative gas concentration (20vol% O_2).

2.3 The Nb/NbOx/PbIn process

The original junction technology in the Clarke group was based on Nb/NbOx/PbIn junctions. Proceeding on an individual chip, I ion mill the base Nb for 1 minute in 2.5 mTorr Ar to clean the Nb and remove native oxide. In a second pumpdown, the base Nb is oxidized for about 45 seconds in an 8 mTorr Ar (5vol% O_2) rf discharge. Then PbIn (5wt% In) is evaporated to a thickness of 300 nm to form the counterelectrode. The indium reduces the hillocks in the Pb and forms a stable oxide on top of the Pb which improves the chemical stability. The photoresist is lifted off in acetone, and the SQUID is ready for testing. A schematic of the Nb/NbOx/PbIn junction cross-section is shown in Fig. 2.2(a). There are actually two junctions in this figure. The large junction on the right is formed incidentally to the SQUID junctions, and is in series with the entire SQUID. This large junction has a critical current much larger than the SQUID junctions, and has no effect on the SQUID.

2.4 Junction stability

A major problem with the Nb/NbOx/PbIn SQUIDs is their sensitivity to moisture, which causes degradation of the Pb. When removed from liquid helium, water may condense on the SQUID unless it is enclosed in a vacuum can. With repeated cycling, the critical currents gradually decrease until the SQUID becomes useless. The critical currents also gradually decrease if the junctions are just left in air at room temperature,

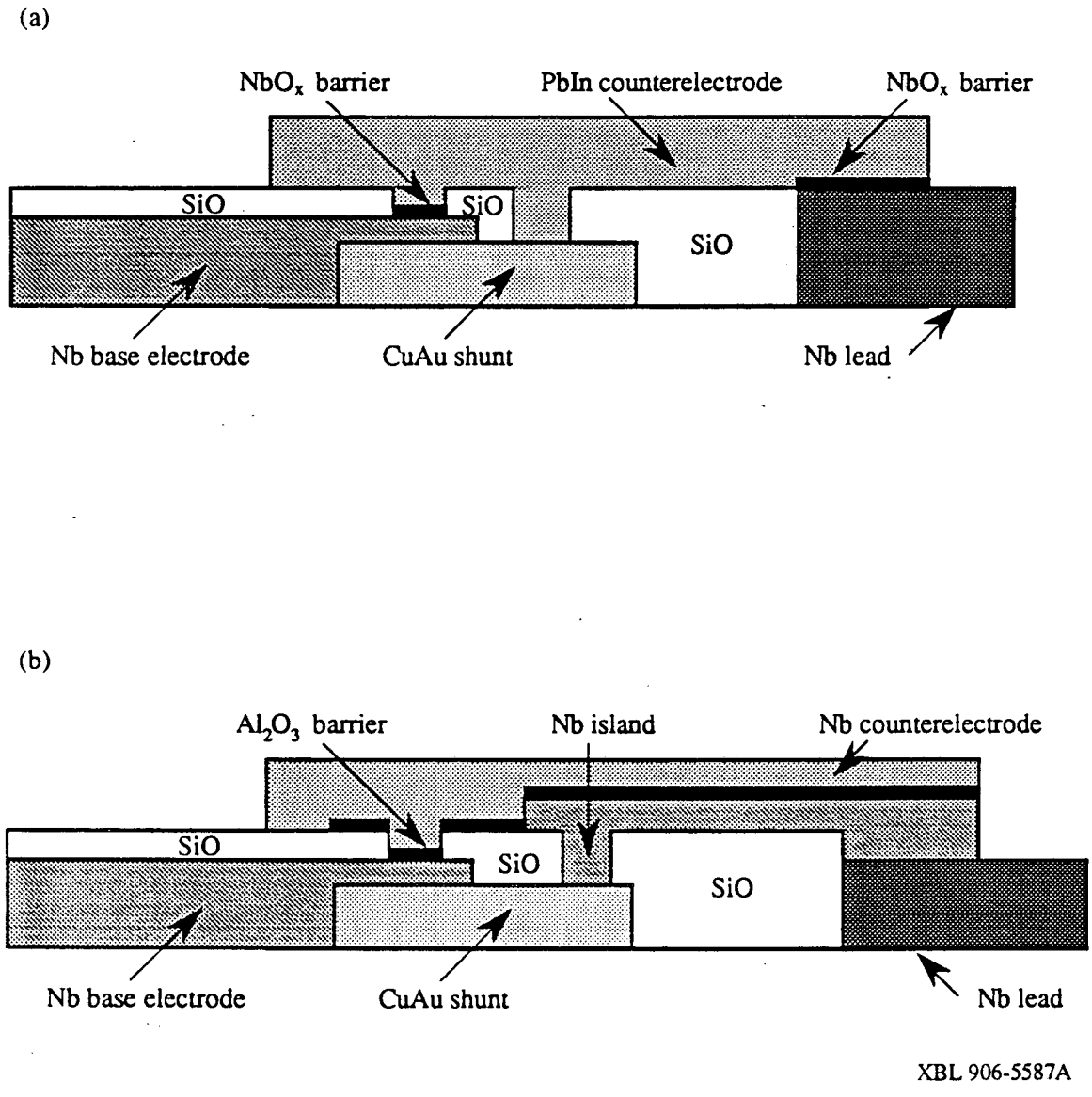

Fig. 2.2 Cross-sectional schematic of a SQUID Josephson junction with shunt:
(a) Nb/NbOx/PbIn junction,
(b) Nb/Al2O3/Nb junction.

presumably because of chemical reactions proceeding at room temperature. SQUIDs can be stored for long periods of time in a freezer without decreases in critical current. Protecting the SQUID with a plastic bag after removal from helium helps somewhat, as it prevents large amounts of water from condensing on the SQUID.

One possible solution is to enclose the SQUID in a vacuum-tight can which is warmed to room temperature before opening. This has been effective in slowing the junction deterioration. This technique adds to the experimental complexity, and is not always feasible.

I attempted to determine the cause of the decrease in critical current in $10 \times 10\ \mu m^2$ Nb/NbOx/PbIn cross-strip Josephson junctions, and devised a sealed brass container for junctions (and potentially SQUIDs) which would prevent the decrease in critical current. As one test, the critical currents of 5 junctions stored in a sealed glass desiccator (with no desiccant) were periodically removed from the desiccator and their critical currents measured over the course of 71 days. The general instability of the critical currents is shown in Fig. 2.3. This figure shows the average critical current of the 5 junctions, normalized to their initial average critical current, as a function of time. The fast initial decrease in critical currents is also commonly seen in Nb/NbOx/PbIn SQUIDs. The average critical current decreases by about 10%. This experiment did not demonstrate the eventual decrease towards zero critical current that is observed in the $2 \times 2\ \mu m^2$ area SQUID junctions. It is generally observed that the $10 \times 10\ \mu m^2$ cross-strip junctions do not show as much sensitivity to moisture as the SQUID junctions.

To examine the effect of water vapor on the Nb/NbOx/PbIn junctions more specifically, 3 junctions were stored in a sealed glass desiccator (with no desiccant) containing a dish of water. After 6 days the junctions were removed from the vessel and their critical currents were measured. The average critical current had decreased by about 15%. One of the junctions showed a marked change in its I-V characteristic, as shown in Fig. 2.4(a). This junction initially had a leakage current of 0.07 mA measured at 2 mV. For

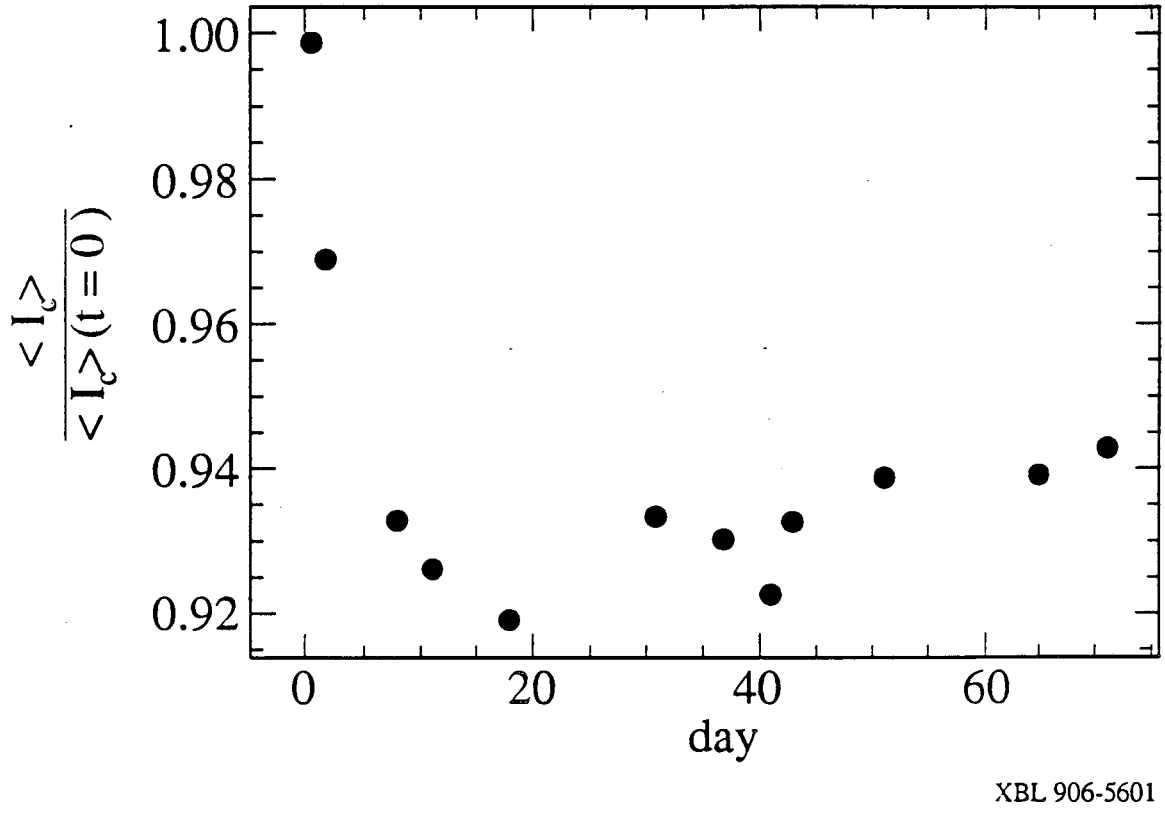

Fig. 2.3 Critical current variation with time of Nb/NbOx/PbIn $10 \times 10\ \mu m^2$ cross-strip junctions, stored in a sealed glass jar.

(a)

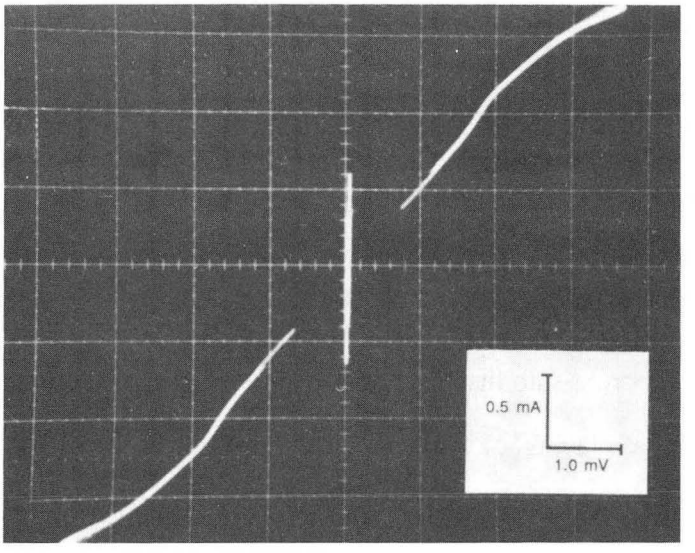

(b)

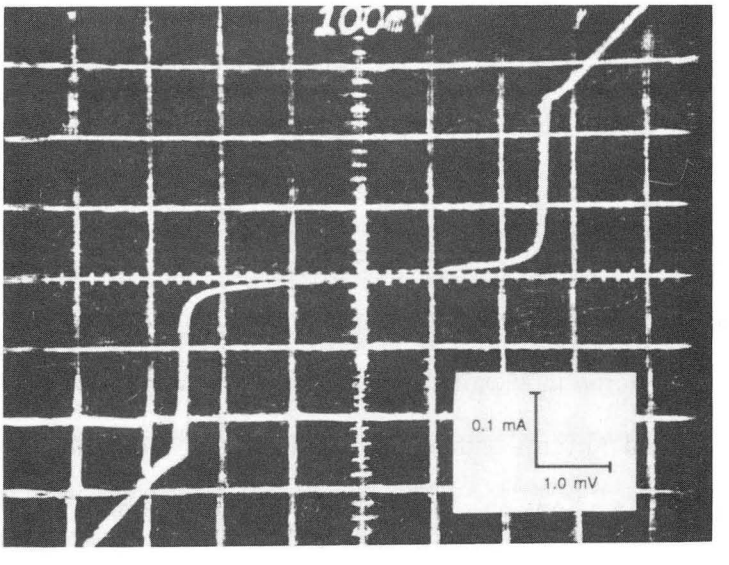

XBB 900-9449

Fig. 2.4 (a) Current-voltage (I-V) characteristic of a Nb/NbOx/PbIn 10x10 μm^2 cross-strip junction stored in a sealed glass jar with a dish of water after 6 days.

(b) I-V characteristic of a typical Nb/NbOx/PbIn 10x10 μm^2 cross-strip junction.

comparison, a typical junction I-V is shown in Fig. 2.4(b). After storage in a moist environment, the leakage current increased to 1.25 mA. A very similar effect was seen with a fourth junction after 22 days of storage under identical conditions. An examination of these two junctions under a microscope revealed discolored regions at the junctions and on the Pb counterelectrode near the junction area, probably due to chemical corrosion.

I did another experiment to determine if storing junctions in an inert gas would have any effect on the critical current stability. Two sets of junctions were fabricated under identical conditions: the base layers, oxide barriers, and counterelectrodes of both sets were fabricated simultaneously. One set was sealed in a brass container filled with 1 Atm of helium gas. Only one junction of this set could be measured. The can remained sealed for the duration of the experiment: I-V characteristics were measured using hermetically sealed feedthroughs. The second set was left on a laboratory table exposed to air. After 18 days the average critical current of the junctions exposed to air had decreased by about 70%, and the critical current of the junction sealed in helium gas had decreased by about 34%.

In conclusion, the critical currents of Nb/NbOx/PbIn junctions are not stable, and generally decrease with time. The observed rate of decrease in the critical currents of the junctions exposed to air is typical for what has been seen in Nb/NbOx/PbIn SQUIDs exposed to air. Junctions stored in a sealed glass desiccator (without desiccant) have smaller decreases in critical currents with aging than do similar junctions left exposed to room air. Junctions stored in a humid environment sometimes exhibit dramatic changes in leakage current and visible degradation of the lead counterelectrode. The single junction stored in a sealed brass can containing helium gas showed a decrease in critical current smaller than the decrease observed for junctions fabricated simultaneously under identical conditions and left exposed to room air, yet larger than the decrease observed for junctions fabricated on a different day under similar conditions and stored in a sealed glass desiccator (without desiccant). This suggests that storage in an inert gas environment may slow the critical current decay. Variations in junction fabrication conditions from day to day or room

humidity may also be a factor in junction stability. Although only a small number of junctions were measured in this study, the effects are very large.

2.5 The $Nb/Al_2O_3/Nb$ process

In an attempt to overcome the lifetime and stability problems with the PbIn junction technology, we have developed an all-niobium process for dc SQUID fabrication. The new all-niobium process was first used to fabricate junctions by Savo et al. (1987). The SQUID process is very similar. I process the wafer as described in Sec. 2.2, up to dicing of the wafer. At this point the SQUID may be completed by either the old Nb/NbOx/PbIn junction technology, or the new Nb/AlOx/Nb junction technology. For the latter case, I clean the Nb base electrode by ion milling for 80 seconds in 1.8 mTorr of argon at 400 V and a current density of 50 $\mu A/cm^2$. Then 6 nm of Al is sputtered onto the wafer in a vacuum of 6×10^{-7} Torr at 0.5 nm/sec. Then about 7 mTorr of Ar (40vol% O_2) is bled into the chamber, and the pressure is held constant for 80 minutes, to allow saturation to occur. The system is then evacuated, and the Nb counterelectrode is sputter deposited to a thickness of 200 nm in 8 mTorr argon. The best base pressure obtained was about 3×10^{-7} Torr. I initially tried fabricating $Nb/Al_2O_3/Nb$ SQUIDs using all of the same photolithography masks from the Nb/NbOx/PbIn process. These masks had no Nb island covering the CuAu shunt, so Al was deposited directly on the CuAu shunt and oxidized before deposition of the Nb counterelectrode. I found that SQUIDs fabricated in this manner exhibited shunt resistances that increased irreproducibly with cycling in liquid helium to values up to five times the original shunt resistance. The addition of the Nb island between the CuAu shunt and the Al_2O_3 layer removed this problem. A schematic of the $Nb/Al_2O_3/Nb$ junction cross-section is shown in Fig. 2.2(b). This can be compared with the Nb/NbOx/PbIn junction cross-section shown in Fig. 2.2(a).

Pictures of a completed $Nb/Al_2O_3/Nb$ SQUID with a 4-turn input coil are shown in Fig. 2.5. The leads to the input coil enter from the left, and the leads to the

(a)

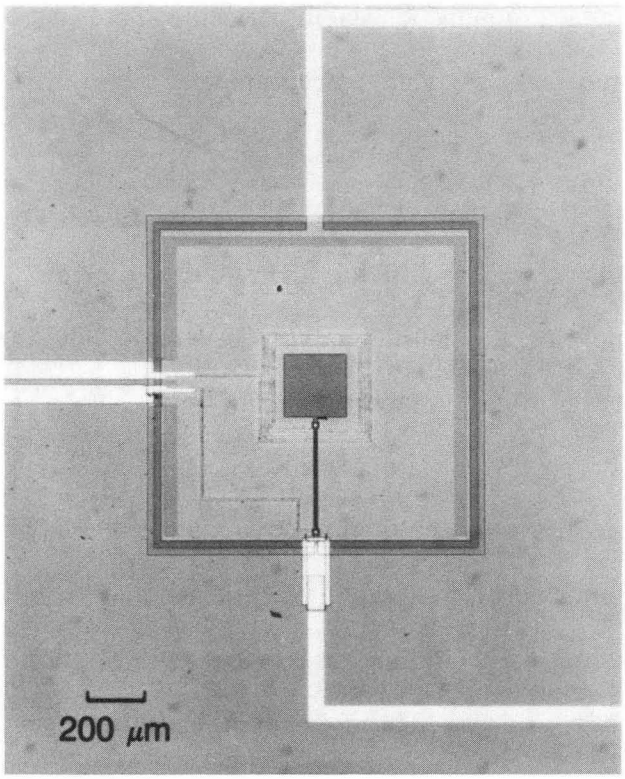

(b)

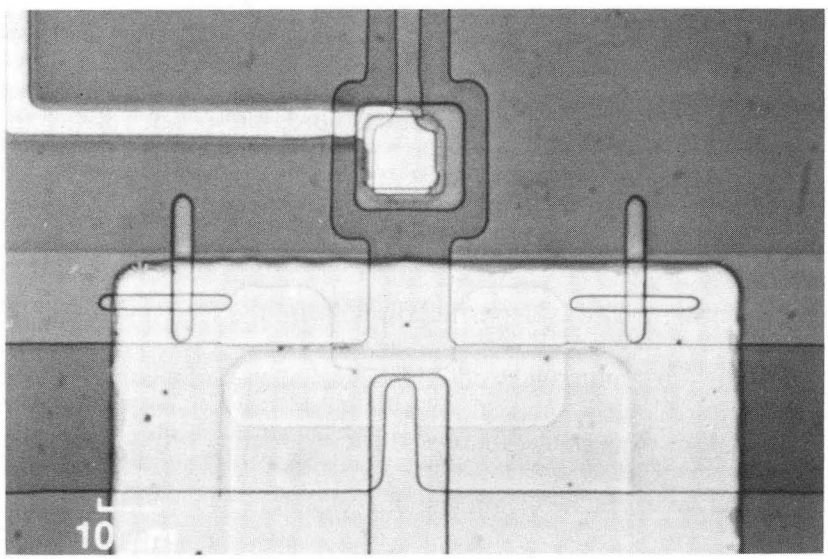

XBB 900-9368

Fig. 2.5 Photographs of a completed Nb/Al_2O_3/Nb dc SQUID with a 4-turn spiral input coil:
(a) complete device,
(b) close-up of junction and shunt area.

SQUID enter from the right. The edges of the two SiO layers can be seen just outside the edges of the Nb washer forming the SQUID body. The fainter pattern just inside the Nb washer is a residual shadow formed during the etching step which defines the 4-turn coil. The close-up picture shows the two junction areas, each defined by the intersection of two trenches in the insulating SiO layers. The underpass and connection for the input coil can also be seen.

The new Nb/Al_2O_3/Nb SQUIDs show no detectable decrease in critical currents after many hundreds of cyclings in liquid helium and exposure to water condensation over the course of a year. This represents an improvement in the robustness of the Clarke group SQUIDs. I have successfully fabricated dozens of the Nb/Al_2O_3/Nb SQUIDs. These SQUIDs have been used to detect high frequency NMR and NQR signals (Fan et al., 1988), low frequency NMR and NQR signals (Fan et al., 1990), and to measure low frequency noise in Josephson transmission lines (Hansen et al., 1991).

2.6 SQUID mount and bias electronics

The SQUID is attached with vacuum grease to a slot in a G-10 fiberglass mount, and enclosed in a superconducting niobium tube. The mount has a small 20-turn copper coil glued into a hole in the fiberglass directly beneath the SQUID slot, which is used to provide the flux bias. The current bias is provided by a separate pair of wires connected across the SQUID itself. Contacts to the SQUID and input coil are made by pressing tinned copper wires into the niobium pads on the SQUID chip. This usually provides a superconducting point contact.

The current bias and flux bias for the SQUID are produced by the circuit shown in Fig. 2.6. This circuit produces from 0 to 56 μA for both sets of bias wires. The circuit is powered by a 15 V rechargeable battery located inside the screened room.

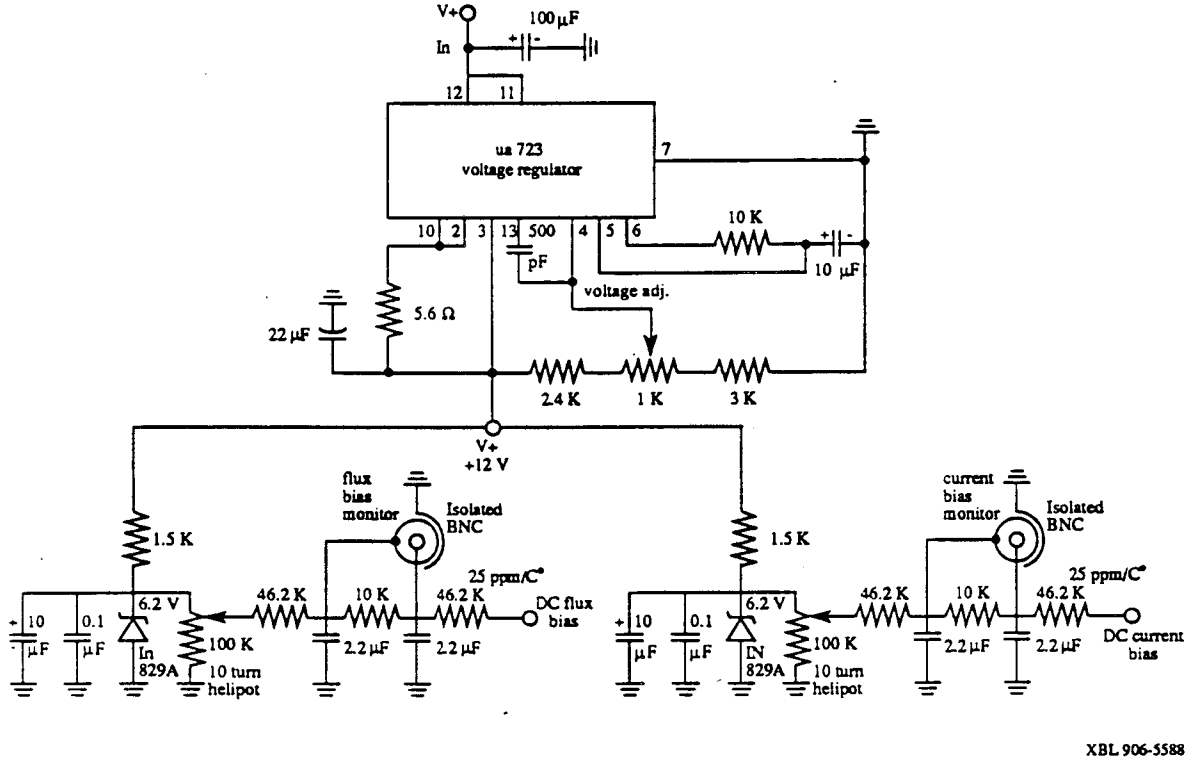

Fig. 2.6 Schematic of circuit for the SQUID current bias and flux bias, based on a drawing by L. Garner.

2.7 Some remaining problems

One of the difficulties in using SQUIDs is making a reliable contact to the Nb contact pad on the chip. We have used tinned Cu wires pressed against the Nb pad. Temperature cycling in liquid helium occasionally causes these contacts to become resistive or open. This is due to thermal stress or oxidation of the Nb pad. The most common mode of destruction of the all-Nb SQUIDs has been breaking the silicon substrate while attempting to remake the pressure contact. A possible solution to this problem is to fabricate SQUIDs with Pb contact pads. Reliable contacts can then be made by pressing Pb wires into the contact pads, as has been done successfully at IBM (Webb, 1989).

Another common mode of failure is accidentally applying too much current through the SQUID. For example, turning an Ohmmeter on or off while it is connected across the SQUID will often destroy the junctions. Care in handling will prevent this problem. Protective devices such as crossed diodes across the SQUID may also help.

References

1. Ketchen, M.B., and J. M. Jaycox, 1982, "Ultra-low-noise Tunnel Junction dc SQUID with a Tightly Coupled Planar Input Coil," Appl. Phys. Lett. 40, 736.

2. Wellstood, F. C., 1988, Ph.D. Thesis, University of California, Berkeley.

3. Savo, B., F. C. Wellstood, and J. Clarke, 1987, "Low Frequency Excess Noise in Nb-Al_2O_3-Nb Josephson Tunnel Junctions," Appl. Phys. Lett. 50, 1757.

4. Fan, N. Q., M. B. Heaney, J. Clarke, D. Newitt, L. L. Wald, E. L. Hahn, A. Bielecki, and A. Pines, 1988, "Nuclear Magnetic Resonance with dc SQUID Preamplifiers," IEEE Trans. Magn. 25, 1193.

5. Hansen, J. B., T. Holst, F. Wellstood, and J. Clarke, 1991, "Low frequency noise in resonant Josephson soliton oscillators," to be published in IEEE Trans. Magn. MAG-27.

6. Fan, N. Q., and J. Clarke, 1990, to be published.

7. Webb, R., 1989, personal communication.

Chapter 3: The dc SQUID as an rf amplifier

3.1 Introduction

In this chapter I review the theory underlying the use of the dc SQUID as an rf amplifier. One model of the dc SQUID as an amplifier was developed by Martinis and Clarke (1985), and Hilbert and Clarke (1985). To understand this chapter, it is helpful to have a familiarity with these two papers. I will outline their main results, and note additional modifications. I will then discuss the optimization of the dc SQUID as an amplifier for rf signals.

3.2 The model circuit

The basic model for the amplifier is a series RLC circuit inductively coupled to a dc SQUID, as shown in Fig. 3.1. In this schematic I have represented the total inductance of the SQUID loop L as two inductances L/2 in each arm of the SQUID. The circulating current in the SQUID loop is $J(t) = I_2(t) - I_1(t)$, where $I_1(t)$ is the total current in one arm of the SQUID, and $I_2(t)$ is the total current in the other arm.

The SQUID is inductively coupled to the tuned RLC circuit (the receiver circuit) via the mutual inductance M. The external flux bias Φ is applied by the inductor above and to the left of the SQUID in Fig. 3.1. The dc current bias I is applied to the top lead of the SQUID. The impedance Z_A represents the impedance of the matching circuit and postamplifier following the SQUID. The voltage V_i is the signal we wish to amplify. The resistance R_i is stray or added resistance in the receiver circuit.

3.3 The equations of motion

The impedance $Z_T(\omega)$ of the receiver circuit is

$$Z_T(\omega) = R_i + 1/j\omega C_i + j\omega L_T\,, \tag{3.1}$$

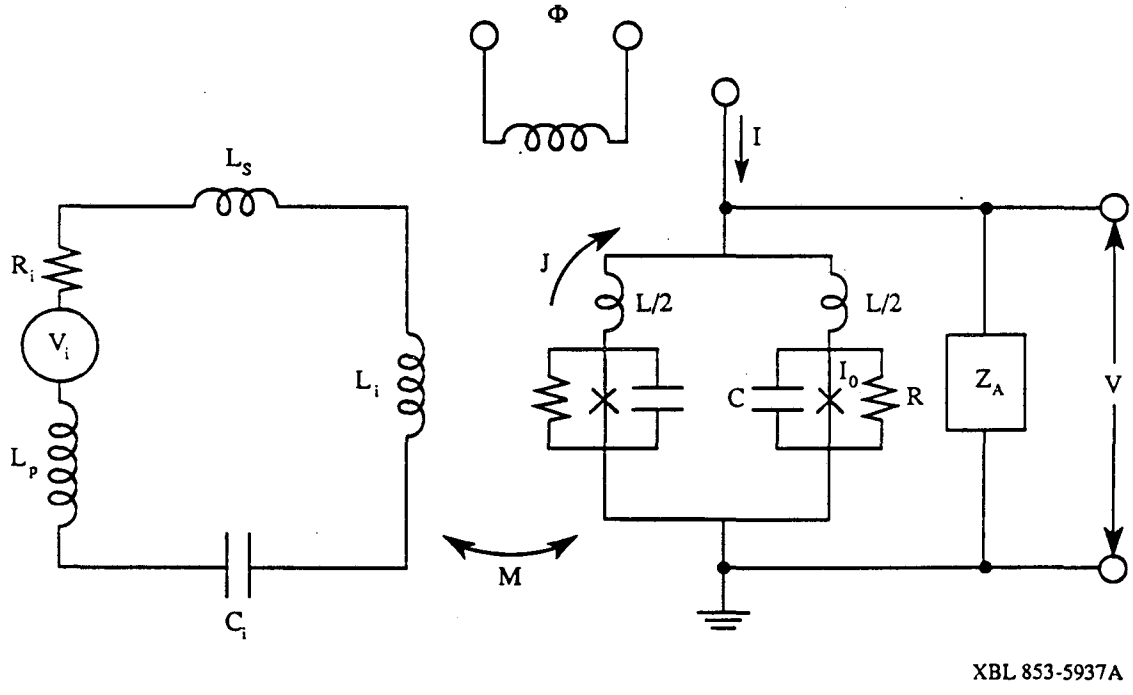

Fig. 3.1 Model circuit for a dc SQUID voltage amplifier.

where the total inductance $L_T = L_i + L_p + L_s$, L_i is the SQUID input coil inductance, L_p is the pickup coil inductance, and L_s is stray inductance. In the time domain, the equations of motion for the SQUID coupled to the RLC circuit and the postamplifier are

$$V(t) = \frac{\Phi_0}{4\pi}[\dot{\delta}_1(t) + \dot{\delta}_2(t)] + \frac{L}{4}[\dot{I}_1(t) + \dot{I}_2(t)] , \tag{3.2}$$

$$\frac{C\Phi_0}{2\pi}\ddot{\delta}_1(t) + \frac{\Phi_0}{2\pi R}\dot{\delta}_1(t) = I_1(t) - I_0\sin\delta_1(t) + I_{N1}(t) , \tag{3.3}$$

$$\frac{C\Phi_0}{2\pi}\ddot{\delta}_2(t) + \frac{\Phi_0}{2\pi R}\dot{\delta}_2(t) = I_2(t) - I_0\sin\delta_2(t) + I_{N2}(t) , \tag{3.4}$$

$$I_1(t) + I_2(t) = I - \widetilde{Z_A^{-1}(\omega)} * V(t) , \tag{3.5}$$

and

$$\frac{\Phi_0}{2\pi}[\delta_1(t) - \delta_2(t)] = \Phi + LJ(t) + MI_i(t) , \tag{3.6}$$

where V(t) is the output voltage across the SQUID, $\Phi_0 = h/2e$ is the flux quantum, $\delta_i(t)$ is the phase difference across junction i, $\dot{f}$ signifies the time derivative $\partial f/\partial t$, L is the inductance of the SQUID loop, C is the capacitance of each junction, R is the resistance of each shunt, I_0 is the critical current of each junction, I_N is the equivalent current noise in each junction due to Nyquist noise in the shunt resistor R, Z_A is the impedance of the circuitry following the SQUID, I_i is the current in the receiver circuit, $\widetilde{f}$ denotes the Fourier transform of f, and $*$ denotes a convolution.

Except for the last term in Eq. (3.2), these equations are identical to those of Martinis and Clarke [the J(t) terms in Eqs. (3) and (4) in Martinis and Clarke were printed incorrectly]. The last term in Eq. (3.2) arises from inclusion of the effects of the postamplifier on the SQUID. Without this additional term Eqs. (3.2) and (3.5) would be

inconsistent, but I will show that this term is negligible for the signal frequencies considered in this dissertation. Using Eq. (3.5), the derivatives in the last term in Eq. (3.2) become

$$[\dot{I}_1(t) + \dot{I}_2(t)] = \frac{d}{dt}[\widetilde{Z_A^{-1}(\omega)} * V(t)] . \tag{3.7}$$

I will now use the low-frequency and high-frequency filter functions introduced by Martinis and Clarke to separate effects near the signal frequency from effects near the Josephson frequency in this term: $V(t) = \{V(t)\}_{LF} + \{V(t)\}_{HF}$. At frequencies near the Josephson frequency, $Z_A(\omega) \rightarrow \infty$ and the HF component of Eq. (3.2) becomes

$$\{V(t)\}_{HF} = \frac{\Phi_0}{4\pi}\{\dot{\delta}_1(t) + \dot{\delta}_2(t)\}_{HF} . \tag{3.8}$$

Near the signal frequency, $Z_A(\omega) = Z_0$ (a constant) and

$$\frac{d}{dt}[\widetilde{Z_A^{-1}(\omega)} * V(t)] = Z_0\dot{V}(t) . \tag{3.9}$$

At the signal frequency, $\dot{V}(t) = -j\omega V(t)$ so that

$$\{V(t)\}_{LF} = \frac{\Phi_0}{4\pi}\{\dot{\delta}_1(t) + \dot{\delta}_2(t)\}_{LF} + \frac{j\omega L}{Z_0}\{V(t)\}_{LF} . \tag{3.10}$$

Since the signal frequencies of interest in this paper are all near 30 MHz, $j\omega L = 0.075\ j\Omega$. When the postamp is matched to the SQUID output impedance at the signal frequency, $Z_0 \approx 8\ \Omega$. Therefore the last term in Eq. (3.2) can be neglected at 30 MHz. This term will be important only at signal frequencies above several hundred MHz.

Martinis and Clarke apply the $\{\ \}_{LF}$ and $\{\ \}_{HF}$ filter functions to Eqs. (3.5) and (3.6), make some simplifying assumptions, and use a small-signal, linear approximation to obtain the equations

$$\begin{pmatrix} V(\omega) \\ J(\omega) \end{pmatrix} = \begin{pmatrix} \frac{-V_I}{Z_A(\omega)} & \frac{-j\omega M^2 V_\phi}{Z_T(\omega)} \\ \frac{-J_I}{Z_A(\omega)} & \frac{-j\omega M^2 J_\phi}{Z_T(\omega)} \end{pmatrix} \begin{pmatrix} V(\omega) \\ J(\omega) \end{pmatrix} + \begin{pmatrix} V_N(\omega) + \frac{M V_\phi V_i(\omega)}{Z_T(\omega)} \\ J_N(\omega) + \frac{M J_\phi V_i(\omega)}{Z_T(\omega)} \end{pmatrix}, \tag{3.11}$$

where $J(\omega)$ is the circulating current in the SQUID loop in the frequency domain, $V(\omega)$ is the voltage across the SQUID in the frequency domain, and the low-frequency transfer functions are $V_I = \partial V/\partial I$, $J_I = \partial J/\partial I$, $V_\phi = \partial V/\partial \phi$, and $J_\phi = \partial J/\partial \phi$.

Note that these equations differ from Eqs. (18) of Martinis and Clarke by the neglect of terms proportional to the effective coupling constant $\alpha_e^2 \equiv M^2/LL_T$. For receiver circuits and SQUID parameters considered in this dissertation, $\alpha_e^2 \approx 0.005$, so this is a good approximation.

Martinis and Clarke solved these equations in the limit $Z_A(\omega) \rightarrow \infty$, assuming the loading of the SQUID by the following circuitry is negligible. This approximates the $-V_I/Z_A(\omega)$ and $-J_I/Z_A(\omega)$ terms to be zero. However, for the high-frequency applications to NMR and NQR (Hilbert et al., 1985; Sleator et al., 1985; Ch. 5; Fan et al., 1988) the SQUID is impedance matched to the postamplifier, and these terms should be retained. The impedance Z_A in Fig. 3.1 represents both the postamplifier and the matching circuit. The impedance matching implies that the low-frequency transfer function $V_I = \partial V/\partial I$ is equal to $Z_A(\omega)$. For the case of a symmetric SQUID the low-frequency transfer function $J_I = \partial J/\partial I$

is equal to zero. Using these values in Eqs. (3.11) and solving for the on-resonance case one finds

$$V(\omega) = \frac{V_N^0}{2} + \frac{MV_\phi}{2R_i}[\, V_i + V_n - j\omega M J_N] \,, \tag{3.12}$$

where $V(\omega)$ is the voltage output of the SQUID, M is the mutual inductance between the SQUID and receiver circuit, V_ϕ is the flux-to-voltage transfer function of the SQUID, V_i is the signal voltage, V_n is the Nyquist noise from R_i , V_N^0 is the voltage noise due to the SQUID, which has spectral density $S_{V_N}^0 = \gamma_v 2k_bTR$, with $\gamma_v \approx 8$, and J_N is the circulating current noise in the SQUID, which has spectral density $S_J = \gamma_j 2k_bT/R$, with $\gamma_j \approx 6$.

Note that Eq. (3.12) differs from Eq. (19) of Martinis and Clarke by a factor of 2 in the two denominators on the right hand side of the equation, in addition to the previously mentioned neglect of terms proportional to α_e^2 and the assumption of resonance. Several important quantities can now be derived from Eq. (3.12). The voltage gain G_v of the SQUID is given by the ratio of $V(\omega)/V_i$ with the noise terms set to zero:

$$G_v = \frac{MV_\phi}{2R_i} \,. \tag{3.13}$$

Matching to the postamplifier loads down the SQUID and reduces the measured voltage gain by a factor of 2. The power gain G_p of the SQUID is given by $G_v^2 R_i / R_d$, where R_d is the dynamic output impedance of the SQUID, nominally equal to the shunt resistance R. The power gain is then

$$G_p = \frac{M^2 V_\phi^2}{4R_i R} \,. \tag{3.14}$$

The spectral density of voltage noise at the output of the SQUID when the temperature of R_i is zero can be derived from the definition $S_V^N = \langle V(\omega)V^*(\omega)\rangle/B$, where $V^*(\omega)$ is the complex conjugate of $V(\omega)$ and B is the bandwidth, to obtain

$$S_V^N = \frac{1}{4} S_{V_N}^0 + \frac{\omega^2 M^4 V_\phi^2}{4R_i^2} S_J . \tag{3.15}$$

The noise temperature of the SQUID is defined by

$$T_N = \frac{S_V^N}{4k_b R_i G_v^2} . \tag{3.16}$$

Using Eqs. (3.14) and (3.15) one can see that the SQUID noise temperature is unchanged by the impedance matching. In terms of the spectral densities, the SQUID noise temperature is

$$T_N = \frac{S_{V_N}^0 R_i}{4k_b M^2 V_\phi^2} + \frac{\omega^2 M^2 S_J}{4k_b R_i} . \tag{3.17}$$

Using the values of $S_{V_N}^0$ and S_J defined following Eq. (3.12), the SQUID noise temperature becomes

$$T_N = \frac{T}{2}\left(\frac{\gamma_v R R_i}{M^2 V_\phi^2} + \frac{\gamma_j \omega^2 M^2}{R R_i}\right). \tag{3.18}$$

The first term is due to voltage noise from the SQUID itself. The second term arises from circulating current noise in the SQUID, which couples to the receiver circuit via the mutual inductance M and induces a noise current in the receiver circuit. This noise current

in the receiver circuit is reflected back via M to the SQUID loop as a flux noise Φ_N, inducing a noise voltage across the SQUID equal to $\Phi_N V_\phi$. We will use these equations for SQUID noise temperature in the discussion of optimization.

3.4 Optimization theory

The optimization of dc SQUIDs as rf amplifiers was first done by Clarke, Tesche, and Giffard (1979). This optimization for an RLC receiver circuit consisted of minimizing the SQUID noise temperature by varying the resistance of the receiver circuit. Solving $\partial T_N/\partial R_i = 0$ gave an optimum receiver circuit resistance

$$R_i^{opt} = \left(\frac{\gamma_i}{\gamma_v}\right)^{1/2} \frac{\omega M^2 V_\phi}{R}, \tag{3.19}$$

where feedback terms are neglected. With some further approximations and the approximation $Q \approx \omega L_T/R_i$ this becomes $Q\alpha_e^2 \approx 1$.

This optimization strategy minimizes the noise temperature of the SQUID but does not necessarily maximize the signal-to-noise ratio of the SQUID rf amplifier, as Wellstood (1988) first pointed out. An example with a conventional amplifier can illustrate this point. Assume one has a voltage source with a source resistance of 1 Ω and an amplifier with a noise temperature which is minimized when 50 Ω is placed across its input. Adding 49 Ω in series with the voltage source would make the amplifier noise temperature look very good, but would make the signal-to-noise ratio much worse. This is a classic error in amplifier design.

This error was apparently made by another group working on SQUID NMR (Freeman et al., 1986). This group added a 0.65 Ω resistor to the receiver circuit, lowering the Q to 42 to satisfy $Q\alpha_e^2 \approx 1$. Another form of this error is to adjust the flux bias point of

the SQUID to lower the Q of the receiver circuit in an attempt to satisfy $Q\alpha_e^2 \approx 1$, as was occasionally done in the experiment described in Ch. 6 of this dissertation.

In any small signal measurement, the most important quantity is the signal-to-noise ratio (S/N). For the circuit shown in Fig. 3.1 and for the case of resonance, the signal power in unity bandwidth is $P_S = (V_i^{rms})^2/R_i$ and the noise power in unity bandwidth is $P_N = 4k_b(T + T_N)$, where T is the bath temperature of the receiver circuit and T_N is the SQUID noise temperature. For simplicity, this neglects any contribution to the noise temperature from the postamplifier following the SQUID. The effect of the postamplifier noise temperature will be treated later. Using Eq. (3.17) for the SQUID noise temperature and assuming a bandwidth B such that the S/N is constant within B, the power S/N is

$$S/N = \frac{M^2V_\phi^2(V_i^{rms})^2B^{-1}}{\omega^2M^4V_\phi^2S_J + (4k_bTM^2V_\phi^2)R_i + S_{V_N}^0R_i^2} . \tag{3.20}$$

To optimize the S/N, it is clear that we want to make R_i as small as possible, subject to signal bandwidth limitations. Given the minimum R_i obtainable, the S/N can be further improved by adjusting the mutual inductance M to balance the noise due to voltage fluctuations and circulating current fluctuations in the SQUID. Setting $\partial(S/N)/\partial M = 0$, and approximating $Q \approx \omega L_T/R_i$ and $V_\phi \approx R/L$ gives the optimization condition

$$M_{opt} = \left(\frac{\gamma_v}{\gamma_j}\right)^{1/4}\left(\frac{LL_T}{Q}\right)^{1/2} . \tag{3.21}$$

With the approximation $\gamma_v \approx \gamma_j$, this is identical in form to the previously derived condition $Q\alpha_e^2 = 1$ (where $\alpha_e^2 \equiv M^2/LL_T$) but now has a different interpretation and result. The earlier optimization condition achieved a balance of SQUID voltage noise and SQUID circulating current noise by minimizing the SQUID noise temperature T_N with respect to R_i,

via $\partial T_N/\partial R_i = 0$. This optimization condition balances the voltage noise and circulating current noise by varying the inductive coupling between the SQUID and the receiver circuit. These two optimization methods give the same minimum T_N, but they do not yield the same signal-to-noise ratio or the same R_i. They give the same minimum T_N because of the similar roles of M and R_i in reducing the amount of SQUID noise that the receiver circuit reflects back to the SQUID. One method changes the amount of coupling between the SQUID and receiver circuit, the other changes the amount of damping in the receiver circuit. The latter method minimizes the noise temperature, but does not necessarily maximize the S/N, since increasing the damping in the receiver circuit will also decrease the strength of the signal induced in the receiver circuit. Therefore, adding a resistor to the receiver circuit may make the SQUID noise temperature lower, but it will also make the total S/N of the spectrometer worse.

Using S_V^N from Eq. (3.15) and the optimum M from Eq. (3.21) in Eq. (3.16), we find the optimum SQUID noise temperature

$$T_N^{opt} = (\gamma_v \gamma_j)^{1/2} \frac{\omega T}{V_\phi} . \tag{3.22}$$

For nominal values of γ_v, γ_j, V_ϕ and for $\omega = 30$ MHz and $T = 4.2$ K the optimum SQUID noise temperature is about 0.3 K.

Note that the S/N [Eq. (3.20)] can be made arbitrarily large by letting $R_i \rightarrow 0$ and $M \rightarrow 0$ (subject to signal bandwidth limitations), but T_N^{opt} [Eq. (3.22)] does not change as $R_i \rightarrow 0$ and $M \rightarrow 0$. This makes it clear that T_N^{opt} may be useful for characterizing the SQUID performance, it does not provide a useful measure of the total system performance.

This optimization theory and the earlier optimization theory (Hilbert and Clarke, 1985) both assume the noise contribution of the postamplifier is zero. However, in both the SQUID NQR experiment (Hilbert et al., 1985) and the SQUID NMR experiment (Ch. 5;

Fan et al., 1988) the postamplifier contributed more noise than the SQUID to the total system noise temperature. A correct optimization theory for these two experiments must include the noise contribution of the postamplifier. I will derive the corrected optimization condition, and discuss its relevance.

The total system noise temperature is

$$T_N^{\Sigma} = T + T_N + T_N^{pa}/G_p, \tag{3.23}$$

where T is the temperature of the tuned circuit, T_N is the noise temperature of the SQUID, T_N^{pa} is the noise temperature of the postamp, and G_p is the power gain of the SQUID. Using this equation in the definition of noise power, Eq. (3.14) for the SQUID power gain, Eq. (3.17) for the SQUID noise temperature, assuming a bandwidth B such that the S/N is constant within B, and calculating the S/N gives

$$S/N = \frac{M^2V_\phi^2(V_i^{rms})^2B^{-1}}{\omega^2M^4V_\phi^2S_J + (4k_bTM^2V_\phi^2)R_i + S_{V_N}^0R_i^2 + 16k_bT_N^{pa}RR_i^2}. \tag{3.24}$$

To optimize the S/N, it is again clear that we want to make R_i as small as possible, subject to signal bandwidth limitations. Given the minimum R_i obtainable, the S/N can be further improved by adjusting the mutual inductance M. Setting $\partial(S/N)/\partial M = 0$ gives the optimization condition

$$M'_{opt} = \left(\frac{\gamma_v}{\gamma_j}\right)^{1/4}\left(\frac{LL_T}{Q}\right)^{1/2}\left(1 + \frac{T_N^{pa}}{T}\right)^{1/4}. \tag{3.25}$$

If the postamplifier has a noise temperature of 100 K and the bath temperature is 4.2 K, then optimizing the total system noise temperature requires a mutual inductance M that is more than twice the value determined by the optimization condition $Q\alpha_e^2 = 1$.

The optimum SQUID noise temperature when the postamplifier is taken into account is found by substituting this M'_{opt} into Eq. (3.18) for SQUID noise temperature and approximating $V_\phi \approx R/L$, and yields

$$T'_N{}^{opt} = (\gamma_v\gamma_j)^{1/2}\frac{\omega T}{V_\phi}\frac{\left(1+\frac{T_N{}^{pa}}{2T}\right)}{\left(1+\frac{T_N{}^{pa}}{T}\right)^{1/2}}. \qquad (3.22)$$

For nominal values of γ_v, γ_j, V_ϕ and for $\omega = 30$ MHz, $T = 4.2$ K, and a postamplifier with a 100 K noise temperature, the optimum SQUID noise temperature is about 0.7 K, which is over twice the value found when the postamplifier noise contribution is neglected.

The optimum total system noise temperature when the postamplifier is taken into account can be calculated by substituting Eq. (3.25) for M'_{opt} into Eq. (3.23). This yields a total system noise temperature which is about 30 % lower than when the postamplifier noise contribution is neglected.

3.5 Conclusions

The optimization theory of the dc SQUID as an rf amplifier must be modified for the experiments described in this dissertation, for three reasons. First, when the SQUID is impedance matched to a postamplifier, the postamplifier will load down the SQUID, reducing the measured power gain by a factor of 4. Second, the previous optimization theory optimized the noise temperature of the SQUID but did not optimize the signal-to-noise ratio, which is the most important quantity. Third, the postamplifier contributes noise, and must be taken into account in the optimization.

References

1. Martinis, J., and J. Clarke, 1985, "Signal and noise theory for a dc SQUID amplifier," J. Low Temp. Phys. 61, 227.

2. Hilbert, C., and J. Clarke, 1985, "DC SQUIDs as radiofrequency amplifiers," J. Low Temp. Phys. 61, 263.

3. Clarke, J., C. D Tesche, and R. P. Giffard, 1979, "Optimization of dc SQUID voltmeter and magnetometer circuits," J. Low Temp. Phys. 37, 405.

4. Wellstood, F. C., 1988, Ph.D. Thesis, University of California, Berkeley.

5. Freeman, M. R., R. S. Germain, R. C. Richardson, M. L. Roukes, W. J. Gallagher, and M. B. Ketchen, 1986, "Low-temperature nuclear magnetic resonance with a dc SQUID amplifier," Appl. Phys. Lett. 48, 300.

6. Hilbert, C., J. Clarke, T. Sleator, and E. L. Hahn, 1985, "Nuclear quadrupole resonance detected at 30 MHz with a dc superconducting quantum interference device," Appl. Phys. Lett. 47, 637.

7. Fan, N. Q., M. B. Heaney, J. Clarke, D. Newitt, L. L. Wald, E. L. Hahn, A.Bielecki, and A. Pines, 1988, "Nuclear Magnetic Resonance with dc SQUID Preamplifiers," IEEE Trans. Magn. 25, 1193.

Chapter 4: Topics in NMR theory

4.1 Introduction

In this chapter I will review the basic principles of pulse NMR and discuss two topics in NMR theory of particular importance to the experiments described in later chapters: the signal-to-noise ratio and the tipping angle optimization. For a more general introduction to the theory of NMR, the reader is referred to standard texts (Slichter, 1980; Abragam, 1961).

4.2 Signal-to-noise theory

In a pulse NMR experiment, the nuclei are given a net magnetization per unit volume M_0 along the z-axis by an externally applied static magnetic field B_0. Then an rf magnetic field B_1 is applied along the x-axis for a time t_θ. If the frequency of B_1 is close to the resonance frequency of the nuclear magnetic moments in the static field B_0, the rf pulse will cause the spins to precess about the x-axis. The angle of precession θ_t is called the tipping angle and is given by $\theta_t = \gamma B_1 t_\theta$, where γ is the gyromagnetic ratio of the nuclei. At the end of the pulse, the magnetization M_0 precesses about the static field B_0 at the Larmor precession frequency $\omega_0 = \gamma B_0$. This precessing magnetization is detected by the voltage induced in a pickup coil surrounding the spins with axis along the x-axis. It is clear that the maximum amplitude signal for a single pulse occurs when the tipping angle is 90°. In the tuned circuit of Fig. 5.1, the signal power for such a pulse is given by V_i^2/R_i, where V_i is the voltage induced in the pickup coil L_p by the precessing spins. For simplicity, this neglects decay of the signal amplitude. The voltage V_i is given by $V_i = -(1/c)\partial\phi/\partial t$, where ϕ is the flux the spins produce in L_p. The flux ϕ is given by $\phi = BAn_t$, where $B = 4\pi M$, $M = M_0 \sin\theta_t \cos\omega_0 t$, A is the cross-sectional area of the sample, and n_t is the number of turns in the pickup coil L_p. The magnetization for spin 1/2 follows a Curie law (Abragam, 1961):

$$M_0 = \frac{N\gamma^2\hbar^2 B_0}{4k_b T}, \tag{4.1}$$

where N is the number of spins per unit volume, and T is the bath temperature.

We wish to measure the signal from the spins. This signal is competing against noise from the amplifier. The equivalent rms noise voltage of the amplifier across the pickup coil is given by $V_n = (4k_b T_N^{\Sigma} R_i B)^{1/2}$, where T_N^{Σ} is the total system noise temperature and B is the bandwidth. The signal-to-noise ratio (S/N ratio) is defined as the ratio of peak signal voltage to rms noise voltage (Ernst, 1966). Using the above equations and solving for the number of spins which gives a S/N of 1, we find

$$N_{mds} = \frac{4\, k_b^{3/2}\, T}{\pi^{1/2}\hbar^2\gamma^{5/2} B_0^{3/2}} \left[\frac{T_N^{\Sigma} V_c B}{Q}\right]^{1/2}, \tag{4.2}$$

where N_{mds} is the minimum detectable number of spins, V_c is the volume of the pickup coil, and $Q \approx \omega_0 L_p/R_i$ is the quality factor of the receiver circuit. This equation will be used in several of the following chapters.

4.3 Pulse optimization

We had initially believed that we needed to pulse at a tipping angle of $\theta_t = 90°$ to obtain maximum signal for the case of many pulses averaged together. This is false, and this section will give an explanation and discuss the implications for SQUID NMR.

Before application of pulses, the spins will have a static equilibrium magnetization M_0 in the static field B_0. Once a pulse is applied and the spins are tipped by an angle θ_t from the z-axis, they precess about B_0 and gradually dephase from each other. This dephasing time is characterized by the spin-spin relaxation time T_2^*. The spins also start

relaxing back along the z-axis, in response to the static field B_0. This longitudinal relaxation time is characterized by the spin-lattice relaxation time T_1. If a second pulse is applied at a time long compared to T_2^* but short compared to T_1, the magnetization will not have had time to relax fully to its maximum value M_0. Instead, it will have some value $M_z < M_0$. This magnetization M_z will be tipped into the x-y plane by the second pulse and precess, giving a smaller detected signal than the first pulse. As the time between the two pulses is decreased, the averaged signal (defined as the sum of the two signals following the two pulses, divided by 2) will decrease. If we were to wait several T_1's between pulses, we would obtain a larger averaged signal. However, the time required to obtain that averaged signal would be longer. The quantity we wish to maximize is the averaged signal (defined as the sum of the n signals following n pulses, divided by n) for a given experimental time T_{ex}, irrespective of the number of pulses n applied. It becomes clear that to obtain maximum averaged signal for a given experimental time, there is a tradeoff between applying many pulses at small tipping angles and applying fewer pulses at large tipping angles. This problem was first addressed by Ernst (1966), for the case of $T_2^* \approx T_1$. The analysis was later extended to the case of $T_2^* << T_1$ by Waugh (1970). For the NMR samples observed in this dissertation, $T_2^* << T_1$. I will outline Waugh's analysis, plot the result, and discuss its importance to the SQUID NMR experiment.

Consider the steady state condition of a set of spins being tipped by identical rf pulses spaced by time τ, where τ is $> T_2^*$. From the Bloch equations,

$$M_z(\tau) = M_0 [1-e^{-\tau/T_1}] + M_{z0}\cos\theta_t\, e^{-\tau/T_1}, \qquad (4.3)$$

where $M_z(\tau)$ is the magnetization along the z-axis right before the $t = \tau$ pulse, M_0 is the equilibrium magnetization along the z-axis in the absence of pulses, and M_{z0} is the

magnetization along the z-axis right before the t = 0 pulse. In steady state, $M_z(\tau) = M_{z0}$. Solving Eq. (4.3) for the steady state value of M_{z0} gives

$$M_{z0} = \frac{M_0 [1-e^{-\tau/T_1}]}{[1 - \cos\theta_t e^{-\tau/T_1}]} . \tag{4.4}$$

The signal voltage is given by $V_S = c_0 M_{z0} \sin\theta$, where c_0 is a constant and θ_t is the tipping angle. The spectrometer system noise can be expressed as an effective Nyquist noise $V_N = (4k_b T_N^{\Sigma} R_i B)^{1/2}$. For a given experimental time T_{ex}, the net signal (defined as the sum of the n signals following n pulses) is $V_{S,T} = V_S(T_{ex}/\tau)$ and the net noise is $V_{N,T} = V_N(T_{ex}/\tau)^{1/2}$, since the signal adds coherently and the noise adds incoherently. The power S/N is then

$$\frac{S}{N} = \left[\frac{V_S}{V_N}\right]^{1/2} \frac{T_{ex}}{\tau} = c_1 M_{z0}^2 \sin^2\theta_t \frac{T_{ex}}{\tau} . \tag{4.5}$$

Using the expression for M_{z0} from Eq. (4.4), we find

$$\frac{S}{N} = c_1 M_0^2 \frac{T_{ex}}{T_1} \frac{[1-e^{-\tau/T_1}]^2 \sin^2\theta_t}{[1-e^{-\tau/T_1}\cos\theta_t]^2 (\tau/T_1)} . \tag{4.6}$$

For a given experimental time T_{ex}, we obtain optimum S/N by maximizing the function

$$G(\theta_t, \tau/T_1) = \frac{[1-e^{-\tau/T_1}]^2 \sin^2\theta_t}{[1-e^{-\tau/T_1}\cos\theta_t]^2 (\tau/T_1)} . \tag{4.7}$$

A computer-generated plot of this function is shown in Fig. 4.1 along with a contour map.

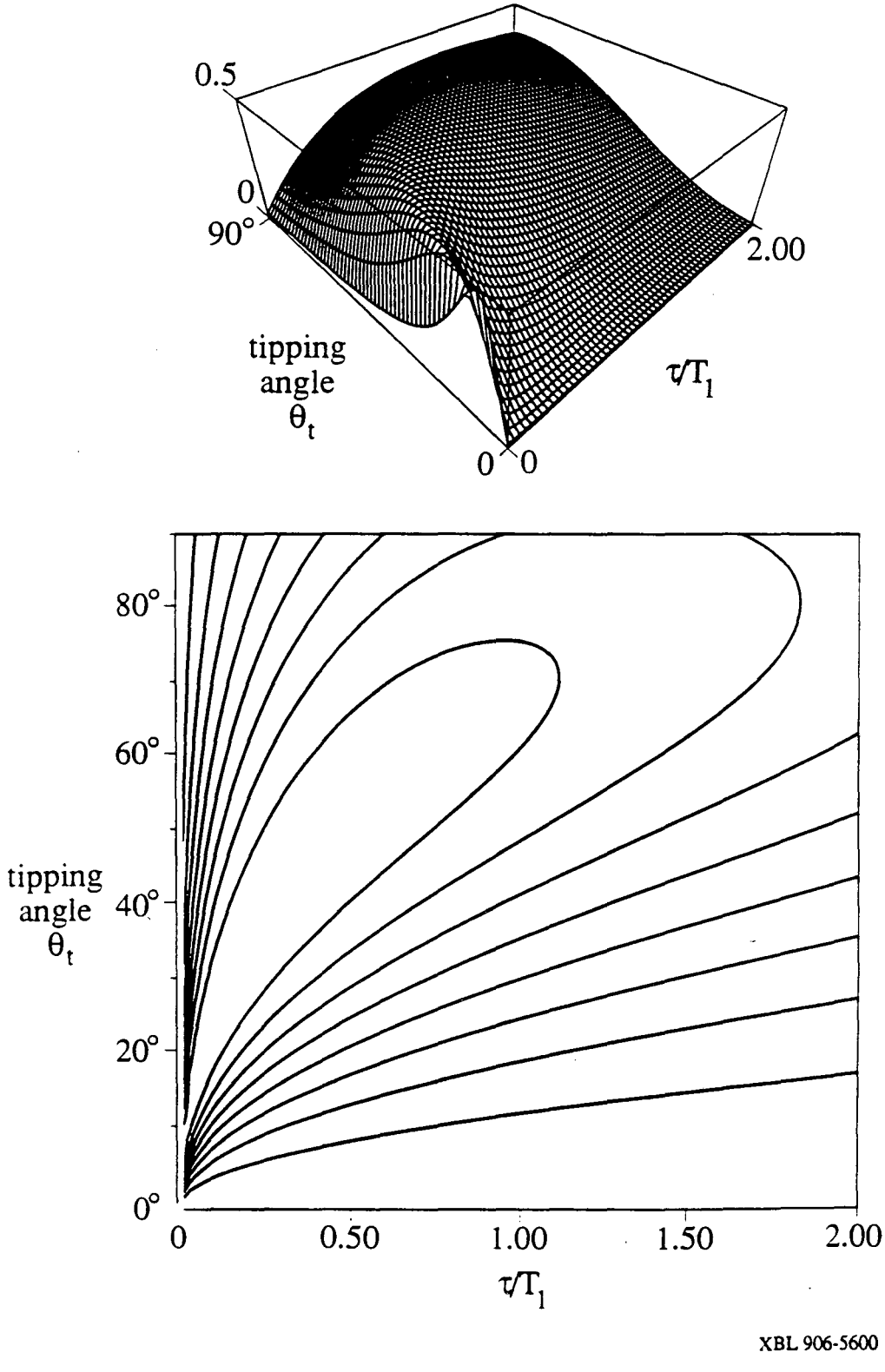

Fig. 4.1 Computer-generated plot of the function $G(\theta_t,\tau/T_1)$:
(a) 3D plot, and
(b) contour map.

We see that maximum S/N is obtained for $\theta_t \rightarrow 0$ and $\tau/T_1 \rightarrow 0$, subject to the lower limit set by T_2^* (pulsing at a rate such that $\tau \approx T_2^*$ would truncate the signal and distort the lineshape). The steepness of $G(\theta_t,\tau/T_1)$ near $\theta_t = 0$ and $\tau/T_1 = 0$ is also of concern: small errors in tipping angle in this region, moving off the "ridge" in $G(\theta_t,\tau/T_1)$, can give large changes in S/N. Not much S/N is lost by moving further away from this region while staying along the top of the ridge in $G(\theta_t,\tau/T_1)$, to a place where $G(\theta_t,\tau/T_1)$ falls off less steeply on either side of the ridge.

This result is important for the SQUID NMR and inverse Stark effect experiments (see Chs. 5 and 6). We were unable to use 90° pulses because of the sensitivity of the SQUID and Q-spoiler junctions to large pulses. This analysis tells us that we do not need 90° pulses to obtain maximum S/N if we are signal averaging. In fact, we can get better S/N by applying pulses with tipping angles less than 90° more often.

However, this analysis neglects the recovery time of the spectrometer following pulses. If we needed to observe a broad line, the recovery time of the spectrometer following a pulse could be much longer than T_2^*, and we would need to use spin echo techniques (Hahn, 1950) which generally require 90° and 180° pulses. As an example, the resonance lines of surface nuclei in platinum catalysts are very broad and can only be detected by using spin echoes (Makowka, 1985). Also, many modern NMR techniques require 90° pulses and echoes, and the inability to achieve these in SQUID NMR would be a serious handicap.

References

1. Slichter, C. P., Principles of Magnetic Resonance (Springer-Verlag, New York, 1980).

2. Abragam, A., Principles of Nuclear Magnetism (Clarendon Press, Oxford, 1961).

3. Ernst, R. R., 1966, "Sensitivity enhancement in magnetic resonance," Adv. Mag. Res. 2, 1.

4. Waugh, J., 1970, "Sensitivity in Fourier transform NMR spectroscopy of slowly relaxing systems," J. Mol. Spectry. 35, 298.

5. Hahn, E. L., 1950, "Spin echoes," Phys. Rev. 80, 580.

6. Makowka, C. D., C. P. Slichter, and J. H. Sinfelt, 1985, "NMR of platinum catalysts: Double NMR of chemisorbed carbon monoxide and a model for the platinum NMR lineshape," Phys. Rev. B31, 5663.

Chapter 5: Pulsed NMR with a dc SQUID amplifier

5.1 Introduction

Nuclear Magnetic Resonance (NMR) has proven to be a very useful tool for the study of a wide variety of phenomena, and the field of NMR continues to grow rapidly. However, NMR signals are relatively small, because of the small magnetic moment of most nuclei ($\mu \approx 5 \times 10^{-24}$ cgs). This low signal level severely limits the possible use of NMR in surface science studies (Rhodes et al., 1982). This chapter describes an attempt to improve the sensitivity by using a dc SQUID to detect NMR signals. The sensitivity can be characterized by N_{mds}, the minimum number of nuclear Bohr magnetons detectable with one pulse (refer to Ch. 4).

5.2 Experimental apparatus

A block diagram of the measurement system is shown in Fig. 5.1. A continuous wave (cw) signal from a PTS 250 rf generator is fed into a gate composed of two HP 10534A rf mixers and triggered by a homemade pulse generator. The resulting rf pulse is amplified by a Granger 500 W distributed amplifier and coupled to the cold transmitter circuit via tunable impedance matching capacitors and a coaxial cable, in order to produce a magnetic field pulse B_1 at the sample. The sample is mounted inside a receiver coil that is inside and orthogonal to the transmitter coil. A grounded Faraday shield (dashed line) between the transmitter and receiver coils minimizes capacitive coupling, thus improving the isolation between the transmitter and receiver circuits. The transmitter and receiver coils are located at the center of a large static magnetic field B_0. When the rf pulse B_1 ends, the precessing magnetization of the sample induces a signal voltage across the receiver coil L_p. The receiver coil is connected in series with an air capacitor C_i (adjustable from the top of the cryostat), the input coil L_i of a dc SQUID, and two series arrays of 21 Josephson tunnel junctions, which act as Q-spoilers, as described in Sec. 5.3. The resistance R_i is due to stray

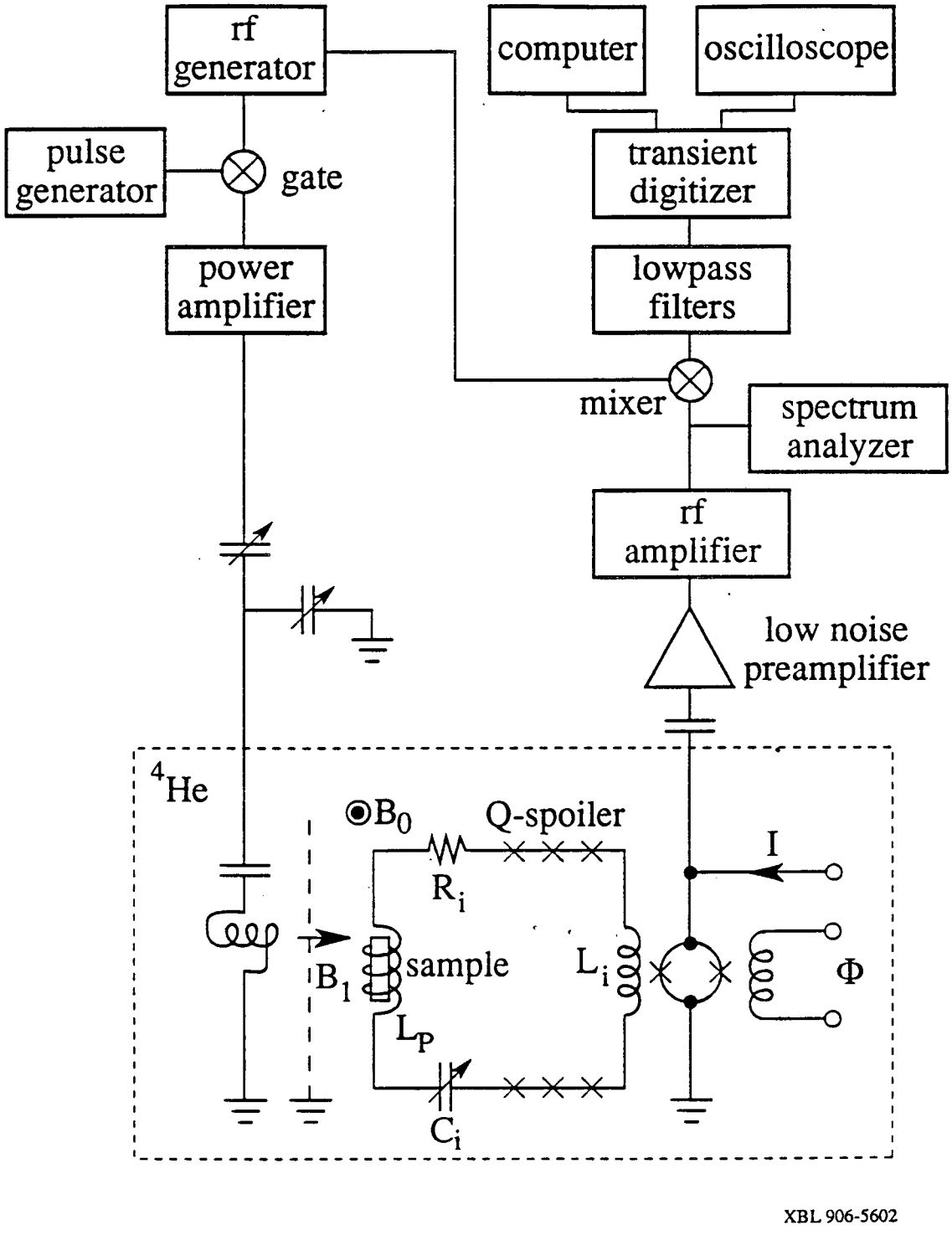

Fig. 5.1 Block diagram of experimental apparatus. Components within the dashed box are inside a liquid helium dewar. The dewar, transmitter matching capacitors, and low noise preamplifier with battery power source are inside a Cu screened room.

losses in the receiver circuit. The SQUID is located outside the field B_0 and enclosed in a superconducting niobium tube, which acts as a magnetic shield. The SQUID is current biased with the dc current I.

The SQUID output signal is fed to a coaxial cable which leads out of the helium dewar and is impedance matched to 50 Ω with a fixed room temperature silver-mica capacitor, C_m in Fig. 5.1. The signal is then further amplified by a low noise Miteq AU-2A-0120 room temperature rf amplifier which has a noise temperature of 83 K. In order to achieve the best system noise performance, it is important to impedance match the SQUID output to the 50 Ω input impedance of the Miteq amplifier. The impedance which the Miteq sees is determined by the SQUID output impedance, the length and characteristic impedance of the coaxial cable between the SQUID and the capacitor C_m, and the capacitance of C_m. The output impedance of the SQUID can be estimated by measuring the dynamic resistance of the SQUID I-V characteristic at the operating point (refer to Ch. 1). The value of capacitance required to match the measured SQUID output impedance to the postamplifier can be readily determined by using a Smith chart. The impedance match was also checked by measuring the impedance presented to the postamplifier with an HP vector impedance meter.

The amplified signal is mixed down and detected in quadrature with a reference supplied by the rf generator. The mixed-down signal is filtered and digitized with a Gould Biomation transient digitizer before storage in a CompuPro computer. The digitized signal can also be displayed on an oscilloscope.

A schematic of the probe is shown in Fig. 5.2. The static magnetic field B_0 is generated by a Cryomagnetics 6 Tesla superconducting solenoid magnet with a specially designed bucking coil to give a high rate of field decay in the region directly above the top of the magnet. This allows the SQUID and Q-spoiler to be placed in a 9 cm long Nb tube close to the magnet, yet in a field below the critical field of the Nb tube. The magnet has a homogeneity of 1 part in 10^5 in a 1 cm diameter spherical volume.

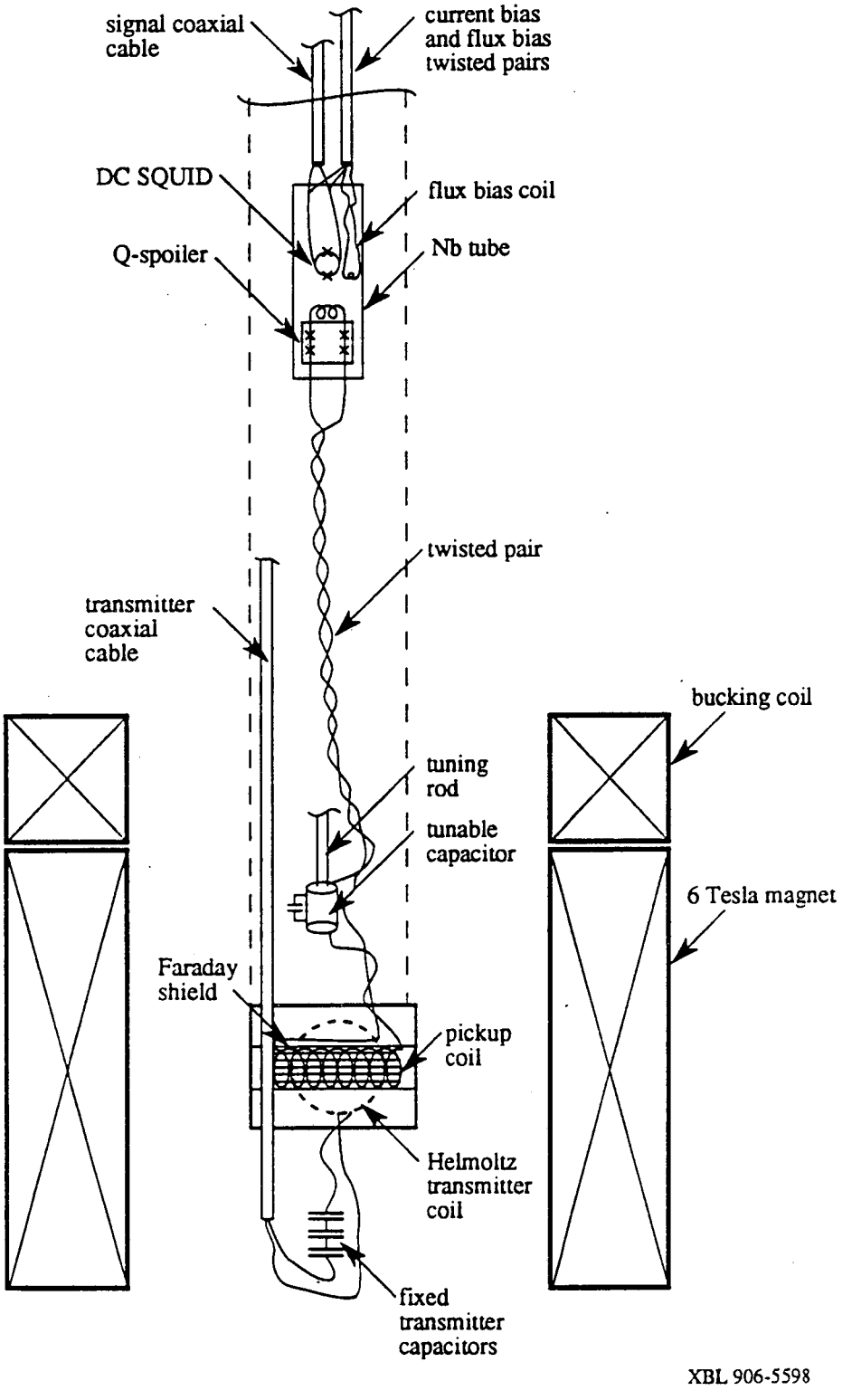

Fig. 5.2 Schematic of probe (not to scale). The portion of the probe shown here is enclosed in a brass can which fits snugly inside the magnet bore.

The magnet dewar and probe, SQUID bias electronics, and Miteq amplifier are enclosed in a Cu-plate "screen" room to shield the SQUID and receiver circuit from external noise. The rest of the spectrometer electronics are located outside the screen room, and connected to the probe via BNC feedthroughs in one wall of the screen room. The entire probe head is enclosed in a brass can, which fits snugly inside the magnet bore. Enclosing the SQUID and receiver circuit in a metal can is essential for shielding from noise. Without the can, the SQUID cannot be stably operated while the screen room door is open. It is necessary to leave the screen room door open when ramping the static magnetic field, since the screen room has no feedthroughs for the high current magnet leads. It is also very convenient to leave the screen room door open while adjusting the flux and current bias of the SQUID, since this is done with a spectrum analyzer located outside the screen room. I also found that if the bottom end of the can was left open, the measured noise temperature was about 1 K higher than if the bottom end were sealed, even with the screen room door closed in both cases.

The brass can also simulates the enviornment of the magnet bore. This is essential for room temperature testing of decoupling and probe arcing, and for testing the probe in a glass or fiberglass dewar.

The pickup coil consists of 8 turns of Cu wire wound on a 1.2 cm diameter, with a 1.1 cm length. The receiver circuit has a Q of about 230, and a total inductance of about 0.7 μH. Thus, the condition $M^{opt} \approx (LL_T/Q)^{1/2}(1 + T_N{}^{pa}/T)^{1/4}$ is approximately satisfied, as required for optimum signal-to-noise ratio (refer to Ch. 3). The transmitter coil is a Helmholtz pair of three turns each of Cu wire, wound on a 3.5 cm diameter. The Faraday shield consists of parallel Cu wires patterned on flexible plastic which can be wrapped around the receiver coil form and grounded to the transmitter coax. The isolation between transmitter and receiver circuits is about 60 dB. The tunable capacitor is a Johanson non-magnetic air capacitor, adjustable from the top of the probe by a fiberglass rod. A fixed capacitor is placed in parallel with the tunable capacitor.

There are several reasons for having a tunable capacitor in the receiver circuit. When we work on the spectrometer, it is often useful to have a real signal for testing. The superconducting magnet dewar requires a liquid nitrogen precool and about 40 liters of liquid helium to cool down and fill, and the helium level in the dewar drops below the level of the SQUID in about 2 1/2 days. Using this magnet every time we need an NMR signal for testing purposes would be costly and time consuming. It is far easier to use an NQR signal from $NaClO_3$, which requires no static magnetic field and can be done in a 15 liter cryostat that is normally kept filled with liquid helium. When the receiver circuit is cooled from room temperature to 4.2 K, its resonance frequency inevitably shifts slightly. Since the NQR signal frequency is fixed, it is necessary to adjust the receiver circuit resonance frequency. The tunable capacitor allows this to be done without trial and error adjustments and cycling of the receiver circuit. When we use the magnet and observe NMR signals, we also want the receiver circuit to be tuned to the resonance frequency of the spins. In principle, this can be accomplished without a tunable receiver circuit by adjusting the static magnetic field so that the spin resonance matches the fixed receiver circuit resonance. In practice, whenever the superconducting magnet is ramped to a new field and then put in persistent mode, the static field shifts slightly as the persistent mode switch goes superconducting. This then requires many iterations to get the spin frequency to match the receiver circuit frequency. A tunable receiver circuit is also useful for looking at two or more nearby resonance lines without changing the static magnetic field. The tunable capacitor allows the receiver circuit frequency to be varied by several MHz. This allows the relative frequencies to be determined accurately, since the above mentioned magnetic field irreproducibility when changing B_0 is avoided. This also makes hunting for a small satellite peak much easier.

We begin a typical experiment by lowering the probe with a spin sample into the liquid helium filled magnet bore while the static field B_0 is zero. I found that lowering the probe into the magnet bore while the static field B_0 was about 3 T resulted in a vibration

dependant modulation of the flux bias point of the SQUID with an amplitude greater than one flux quantum; this would render the SQUID useless as a linear amplifier. This effect may be caused by the fringe field lines from the magnet becoming trapped in the Nb tube when the tube is lowered into the helium bath and becomes superconducting. The field lines in the tube would then be coupled to the vibrational motion of the magnet.

We then monitor the SQUID I-V characteristic on an oscilloscope, and apply current to bias the SQUID slightly above its critical current. The flux bias can also be checked and approximately set to the desired flux bias point $(n \pm 1/4)\Phi_0$, where n is an integer and Φ_0 is the flux quantum. The SQUID output is then fed to the matching capacitor C_m and low noise Miteq amplifier, then out of the screen room to another low noise amplifier and into a spectrum analyzer. The spectrum analyzer displays the Nyquist noise of the spectrometer, with a noise bump at the resonance frequency of the receiver circuit (Sleator et al., 1987). The SQUID current and flux bias points can be optimized to obtain maximum gain by maximizing the noise bump as the current and flux bias are adjusted. The resonance frequency of the receiver circuit can also be adjusted by varying the tunable capacitor C_t and observing the position of the noise bump. The effect of rf pulses on the stability of the SQUID and Q-spoiler can be studied by applying pulses to the transmitter circuit and observing the effect on the noise bump. The spectrum analyzer is normally disconnected while taking NMR data.

The output from the rf amplifier is fed to the mixer, where the rf signal is mixed down to frequencies near zero and detected in quadrature. The two quadrature signals are filtered, digitized, and displayed on an oscilloscope. We ramp up the static magnetic field while applying pulses and observing the signal on the oscilloscope. A resonance signal from protons in the coil form is usually seen first, since protons have a large γ and high abundance in several materials used in probe construction. We sometimes put a small amount of teflon tape, which contains fluorine, in the receiver coil with the spin sample. This is used as a frequency marker, to determine the static magnetic field B_0. The protons in

the probe are distributed over the magnetic field and have varying values of T_1, and are thus less reliable as an accurate gauge of the field at the center of the receiver coil. We then ramp the magnet up to the field at which we expect to see a signal from the spin sample, and put the magnet in persistent mode. The signal from the spin sample can be found by adjusting the resonance frequency of the receiver circuit and signal averaging. Data analysis and Fourier transforms are done with the computer.

5.3 Pulse blocking techniques

The use of high power rf pulses to tip the spins causes several problems for the subsequent detection of the signal. For example, the receiver circuit will ring down after application of a pulse to the transmitter circuit, obscuring the small signal. Likewise, the pulse may cause the flux bias point of the SQUID to be changed irreproducibly, presumably by redistributing trapped flux lines. The pulse may also trap down the minimum critical current of a Josephson junction in the receiver circuit to zero. Two techniques for preventing these problems will be discussed in this section: the Q-spoiler and the Nb microbridge.

The Q-spoiler consists of a series array of 10 μm × 10 μm Nb/NbOx/PbIn Josephson tunnel junctions (Hilbert et al., 1985). The current-voltage characteristic of a typical Q-spoiler is shown in Fig. 5.3. The 21 junctions of the Q-spoiler have critical currents ranging from about 10 μA to 24 μA, and hysteretic current-voltage characteristics with a net resistance of about 1 kΩ above the sum of the energy gaps. The Q-spoilers are placed in the receiver circuit between the receiver coil and the SQUID. When a large rf pulse is applied to the transmitter coil, a current larger than the maximum critical current of the Q-spoiler is induced in the receiver circuit, causing the junctions to switch to the resistive state, with $Q \approx 0.1$. This prevents large pulses from reaching the SQUID, and also reduces the ringdown time of the receiver circuit. After the pulse transients have died

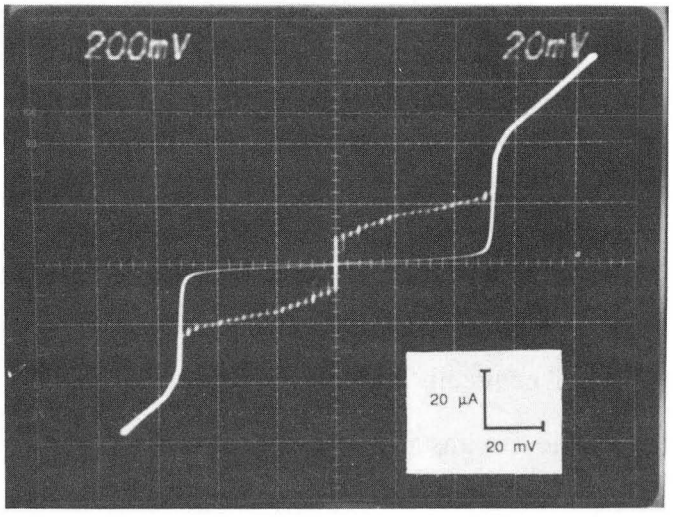

XBB 900-9369

Fig. 5.3 Current-voltage (I-V) characteristic of a Q-spoiler, consisting of a series array of 21 10 μm x 10 μm area cross-strip Josephson junctions.

down the Q-spoiler switches back to the supercurrent state, restoring the high Q receiver circuit.

Without the Q-spoiler in the receiver circuit, very small rf pulses cause the flux bias point of the SQUID to change irreproducibly. This Q-spoiler can also be used in a conventional NMR spectrometer, to reduce the ringdown time of the receiver circuit. It has an advantage over other possible switches in that it is passive, it does not ring down after a pulse, and it has a fast switching time. On the other hand, the Q-spoiler has some limitations. The minimum critical current of the Q-spoiler could be trapped down to zero μA following application of pulses. This kills the Q of the receiver circuit and damps out the signal. This effect was observed in all of the pulsed NQR and NMR experiments carried out by the Clarke and Hahn groups, and will be discussed further in Sec. 5.7.

A second method of blocking pulses, proposed by Prof. Clarke, is to insert a niobium microbridge in the receiver circuit. This would function in a manner similar to the Q-spoiler, but presumably be able to withstand larger pulses without permanent damage or trapping down of the critical current. The microbridge could be used in series with the Q-spoiler to prevent large pulses from trapping down the minimum critical current of the junctions in the Q-spoiler. Since the microbridge would not have as small a critical current as the Q-spoiler, the Q-spoiler would still be needed to reduce the recovery time of the receiver circuit. We were also concerned that in the proposed single-coil SQUID NMR experiment (see Sec. 5.9) the pulses reaching the Q-spoiler and SQUID would be much larger than in the cross-coil configuration, perhaps enough to cause permanent damage to the Q-spoiler junctions. For large pulses, the critical current of the microbridge would be exceeded, and it would act like a resistor with resistance of about 1.5 kΩ and attenuate pulses. Once the pulse had ended, the microbridge would return to the superconducting state and allow the signal to pass without attenuation.

To explore the feasibility of using Nb microbridges in this manner, I fabricated a series of microbridges and studied their response to dc pulses. The Nb microbridges were

fabricated in a manner similar to the fabrication of the Nb base layer for SQUIDs described in Ch. 3. The microbridges were 3 mm long, 4 μm wide, and 100 nm thick, and were patterned from Nb sputter deposited on oxidized silicon substrates. The microbridges had a resistance of about 1.7 kΩ at room temperature, and were superconducting at 4.2 K, with a typical critical current of about 30 mA. I applied current pulses (with current greater than the critical current of the microbridge) 0.5 msec long at 10 msec intervals. I found that the critical current of the Nb microbridge was reduced to values as low as 500 μA by the pulses, and the microbridge developed a resistance in series with its supercurrent. The I-V characteristic of a microbridge before application of pulses looked similar to Fig. 5.4(b). The I-V characteristic after application of pulses is shown in Fig. 5.4(a). I found that removing the microbridge from liquid helium for 30 sec, so that it is no longer superconducting but still below room temperature, and then reimmersing it caused no change in the I-V characteristic shown in Fig. 5.4(a). However, removing the microbridge from liquid helium for 5 minutes before reimmersing caused the microbridge to revert to its state prior to application of pulses as shown in Fig. 5.4(b). The critical current returned to its value before application of pulses, and the resistance in series vanished. This effect was seen in several different microbridges sputter deposited in different pumpdowns. Examination of the microbridges with an optical microscope revealed no visible changes.

This is quite different behavior than what has been reported by others in Nb microbridges. Duret et al. (1975) formed 10 μm × 10 μm microbridges in a 40 nm thick Nb film evaporated onto quartz substrates. Pulses were applied to the microbridge while it was at a temperature slightly above T_c. The microbridge resistance was observed to decrease slightly and then increase. The critical current was then observed to have decreased. This was attributed to a rapid tempering phenomenon. Pascal (1980) fabricated 0.3 μm × 0.5 μm microbridges in a 100 nm thick Nb film evaporated onto quartz substrates. He applied rf pulses to a coil coupled inductively to a loop of Nb interrupted by the microbridge, and observed a brief increase followed by a decrease in the critical current of the microbridge.

(a)

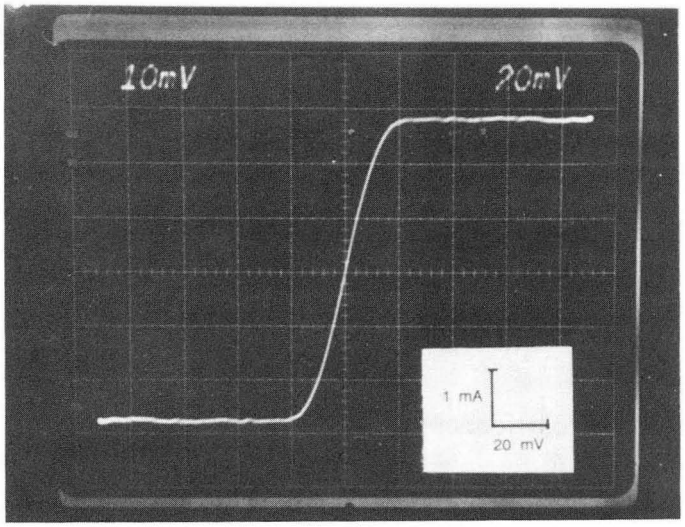

(b)

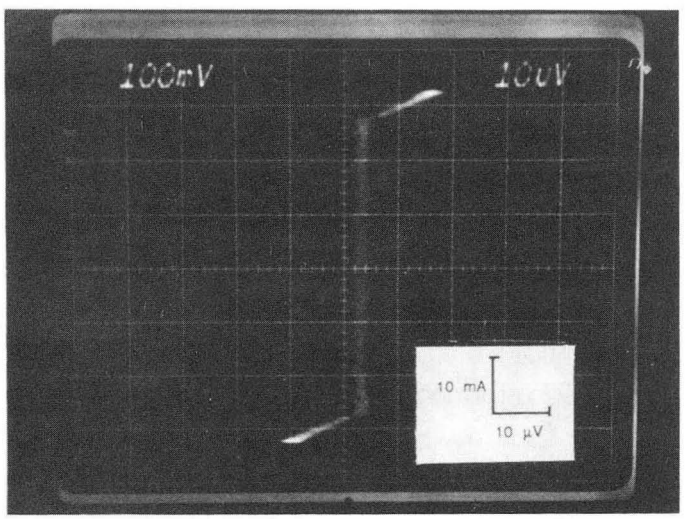

XBB 900-9370

Fig. 5.4 Current-voltage (I-V) characteristic of a Nb microbridge, made with a 4-point technique:
(a) after application of dc pulses, and
(b) after cycling to room temperature for 5 minutes.

The critical current decreased further after room temperature cycling, reaching an equilibrium. Monfort et al. (1984) formed a microbridge by patterning a 20 μm constriction in a 160 nm Nb film evaporated onto a silicon substrate. They placed the microbridge in liquid helium and applied 1 μsec current pulses. The critical current of the microbridge decreased, and room temperature cycling caused an additional reduction of critical current. Analysis of the microbridge revealed an increase in grain size by an order of magnitude and formation of Nb_5Si_3. The decrease in critical current was attributed to the decrease in critical temperature caused by the silicon contamination. These studies all show a permanent decrease in the critical current of Nb microbridges following application of current pulses. I have observed a decrease in critical current and appearance of a resistance that are fully reversed by cycling to room temperature for about 5 minutes. It is possible that intrinsic differences in Nb film characteristics (grain size, microstructure, etc.) may be responsible for these differences. The three other groups mentioned all deposited the Nb by evaporation onto a substrate heated to 400°C. I deposited the Nb by sputtering onto an unheated substrate. It is known that the microstructure of deposited films can vary greatly depending on deposition conditions (Thornton, 1975). The difference in substrate may also play a role.

If the microbridges became resistive after application of pulses, the Q of the circuit would be seriously reduced and the signal-to-noise would be degraded. However, these effects were observed for dc pulses, and the effects might not occur for the rf pulses of the proposed experiment. I tested the effect of rf pulses on the microbridges and found a decrease in the critical current of the microbridge following application of rf pulses that could be reversed by allowing the film to go normal several times. No resistance appeared, as was observed with dc pulses. These results suggested that the Nb microbridge might work for the purpose of blocking rf pulses in a SQUID NMR experiment.

5.4 The Pb sample and skin depth considerations

The spin sensitivity N_{mds} of the spectrometer was calibrated using a thin Pb film. Lead was chosen as a calibration standard for several reasons. Since it is a metal, the longitudinal relaxation time T_1 at liquid helium temperatures is short, due to conduction electron scattering (Slichter, 1980). We have measured T_1 to be about 50 ms at 4.2 K. The short T_1 greatly facilitates signal acquisition, since we can apply large tipping angle pulses and signal average many such pulses in a short period of time. For comparison, the T_1 of $NaClO_3$ at 4.2 K is > 72 h. (The T_1 of $NaClO_3$ can be reduced to about 20 min by introducing defects, but below this value the lineshape becomes distorted). Also, Pb has only one isotope which has a nuclear magnetic moment (Pb^{207}), with a reasonably high gyromagnetic ratio of 9 MHz/T and a natural abundance of 21%. Pb^{207} has spin 1/2, and thus has no electric quadrupole moment. This simplifies the analysis of experimental results, and prevents quadrupolar broadening of the line. Lead is one of the few metals that has these desirable properties and yet can be easily evaporated.

The lead film was evaporated to a thickness of 3 μm on a thin glass substrate, and contained about 6×10^{18} nuclei. The number of nuclei in the sample was checked by measurement of the mass of an identical larger-area film and measurement of the sample film area. Since the film is metallic, the rf field will be attenuated exponentially as it penetrates the film. This has the effect of reducing the effective number of spins detected, and complicates the sensitivity analysis. If the skin depth were infinite, all the nuclei would contribute to the signal, and the net signal would be given by $M_\Sigma = M_0 \sin\theta_\tau$, where M_Σ is the magnetization detected, M_0 is the total magnetization of the sample in the static field B_0, $\theta_\tau = \gamma B_1' \tau$ is the tipping angle, γ is the gyromagnetic ratio, B_1' is the pulse field in the rotating frame, and τ is the pulse length. With the measured tipping angle of 0.67 rad, this would give a signal of $M_\Sigma = 0.62 M_0 \cos\omega t$ in the lab frame. I will show that the effect of the skin depth on the calibration of N_{mds} is negligible.

The skin depth can be inferred from measurements of the conductivity and resistivity ratio of an identical film on an identical substrate. The resistivity ratio was 254 between 295 K, 0 T and 4.2 K, 3.5 T. This gives a skin depth of 2.58 μm under the conditions of the sensitivity calibration. The rf field B_1' penetrates the Pb film from both sides, and is given by

$$B_1'(x) = B_1^0\left[\frac{e^{-x/\delta}\,e^{ix/\delta} + e^{x/\delta}\,e^{-ix/\delta}}{e^{-d/\delta}\,e^{id/\delta} + e^{d/\delta}\,e^{-id/\delta}}\right], \tag{5.1}$$

where B_1^0 is the field outside the Pb film in the rotating frame, x is the distance measured from the center of the film, δ is the skin depth, and d is the thickness of the film.

The local magnetization is $dM(x) = dM_0 \sin\theta_\tau(x)$, where dM_0 is the net magnetization of a slice dx of the Pb film at equilibrium in the static field B_0. Since the skin depth attenuation and phase shift cause the magnetization to vary across the film, the net magnetization is

$$M_\Sigma = \frac{M_0}{2d}\int_{-d}^{d}\sin\left\{(\theta_\tau^0)\left[\frac{e^{-x/\delta}\,e^{ix/\delta} + e^{x/\delta}\,e^{-ix/\delta}}{e^{-d/\delta}\,e^{id/\delta} + e^{d/\delta}\,e^{-id/\delta}}\right]\right\}dx \quad , \tag{5.2}$$

where $\theta_\tau^0 = \gamma B_1^0\tau$ is the tipping angle for the case of infinite skin depth. Note that both amplitude attenuation and phase shifting effects of the rf tipping field are fully accounted for in this calculation. The rf signals from the spins will also suffer attenuation and phase shifting as they pass out of the film. This can be accounted for by squaring the term in [ ] brackets. The net measured magnetization is then

$$M_\Sigma = \frac{M_0}{2d} \int_{-d}^{d} \sin\left\{(\theta_\tau^0)\left[\frac{e^{-x/\delta}\, e^{ix/\delta} + e^{x/\delta}\, e^{-ix/\delta}}{e^{-d/\delta}\, e^{id/\delta} + e^{d/\delta}\, e^{-id/\delta}}\right]^2\right\} dx \,. \tag{5.3}$$

This integration can be done numerically, using the measured tipping angle of 0.67 rad. The signal in the lab frame is found to be $M_\Sigma = M_0\,(0.55\cos\omega t + 0.23\sin\omega t)$. Since the detection is done in quadrature, the net signal will be the magnitude of the vector defined by these two phase components, $0.60M_0$. With no attenuation or phase shift, setting $\delta = \infty$ in Eq. 5.3 reduces it to the expected relation $M_\Sigma = M_0 \sin\theta_\tau^0$ and gives a net magnetization of $0.62M_0$, as obtained earlier. Therefore the net effect of the finite skin depth is expected to be less than 5%.

5.5 Noise temperature calibration

The spectrometer gain and noise temperature can be calibrated by using the periodic nature of the voltage vs. flux (V-Φ) characteristic of the current biased SQUID (refer to Ch.1). If the V-Φ curve is approximated as a sine wave, then the voltage across the SQUID is given by

$$V(\Phi_a) = V_0 \sin\frac{2\pi\Phi_a}{\Phi_0} \,, \tag{5.4}$$

where V_0 is the maximum amplitude of the ac component of the V-Φ curve, Φ_a is the external flux applied to the SQUID, and Φ_0 is the flux quantum. We produce the flux Φ_a by applying a cw signal at frequency Ω to the transmitter coil of the spectrometer. The applied flux is then given by $\Phi_a = \tilde{\Phi}\sin\Omega t$, and the voltage across the SQUID becomes

$$V(t) = V_0 \sin\frac{2\pi\,\tilde{\Phi}\sin\Omega t}{\Phi_0} \,. \tag{5.5}$$

This can be expanded in a Fourier sine series

$$V(t) = \sum_{n=1}^{\infty} V(\omega_n)\sin\omega_n t \quad , \tag{5.6}$$

where

$$V(\omega_m) = \frac{2}{T}\int_{-T/2}^{T/2} V_0 \sin\frac{2\pi\,\tilde{\Phi}\sin\Omega t}{\Phi_0}\sin\omega_m t\,dt \tag{5.7}$$

and $T = 2\pi/\Omega$ is the period of the cw signal. Now we can use the identity

$$\sin(z\sin\theta) = 2\sum_{k=0}^{\infty} J_{2k+1}(z)\sin[(2k+1)\theta] \quad , \tag{5.8}$$

where $J_{2k+1}(z)$ is a Bessel function of the first kind, to obtain

$$V(\Omega) = 2V_0 J_1\left(\frac{2\pi\,\tilde{\Phi}}{\Phi_0}\right) . \tag{5.9}$$

When $\tilde{\Phi}$ is increased to the point at which the SQUID output reaches a maximum, $\tilde{\Phi} = 0.29\Phi_0$ (the first maximum of the Bessel function). The absolute current in the receiver circuit can now be determined, since $\tilde{\Phi} = MI_i$, where I_i is the current in the receiver circuit. For the 4-turn SQUIDs, $M = 0.6\ \Phi_0/\mu A$, so the current in the receiver circuit is 0.5 μA at the first maximum in SQUID output.

The flux $\tilde{\Phi}$ is attenuated by 20 dB to ensure that the SQUID is being operated on the linear approximation of the V-Φ curve. The current in the receiver circuit is then

0.05 μA. The resistance in the receiver circuit can be determined by measurement of the Q, and the total power in the receiver circuit P_i calculated. The power at the output of the spectrometer is measured with a spectrum analyzer, and the total system power gain G_Σ determined.

The total system noise temperature can now be measured. Removing the flux $\tilde{\Phi}$ leaves the resonance spectrum of the receiver circuit (the noise bump) visible on the spectrum analyzer. The power P_0 at the peak of the noise bump is measured, as well as the resolution bandwidth B of the spectrum analyzer. The total system noise temperature is then given by

$$T_N^\Sigma = \frac{P_0}{4k_b B G_\Sigma} \,. \tag{5.10}$$

For the spectrometer described here, the total system noise temperature was measured to be 11 K. Subtracting the 4.2 K bath noise temperature gives an amplifier noise temperature of about 7 K. The power gain of the SQUID was measured to be about 19, in reasonable agreement with Eq. 3.14. The Miteq noise temperature is about 83 K. If we use Eq. 3.23, the Miteq postamplifier is expected to contribute about 4.5 K to the amplifier noise temperature. About 1 K of the remaining amplifier noise temperature was later found to be attributable to external noise reaching the receiver circuit via a hole in the shielding, as mentioned in Sec. 5.2. The SQUID is expected to contribute less than 1 K to the amplifier noise temperature (refer to Eq. 3.22). The remaining 1.5 K of amplifier noise temperature is due to unknown sources, possibly additional external noise.

5.6 Spin sensitivity calibration

The spin sensitivity N_{mds} of this NMR spectrometer was measured using the free induction signal at 31.8 MHz from a lead film in a 3.5 Tesla static field. The

superconductivity of the lead film is completely quenched by the 3.5 Tesla static field. A nuclear resonance signal is shown in Fig. 5.5. The free induction decay followed a 38 μs rf pulse which tipped the spins 38°. For larger pulses, the flux bias point of the SQUID occasionally changed irreproducibly, presumably due to rearrangement of trapped flux lines in or near the SQUID. The signal is detected in quadrature and mixed down from 31.8 MHz. The signal shown is the average of 1000 pulses, and was measured in a 25 kHz bandwidth. The time between pulses was 0.2 sec. Referring to Fig. 4.1, we see that for a 38° tipping angle the optimum t_p/T_1 is about 0.25, where t_p is the time between pulses. For the T_1 of this sample, this gives an optimum time between pulses of 0.01 sec. Using Eq. 4.6, the total S/N for the given experimental time of 200 sec could have in principle been improved by a factor of 5, by decreasing the time between pulses to 0.0125 sec. We did not do this because we were not aware of the tipping angle optimization theory presented in Ch. 4 at the time of this experiment. This does not change any of the quoted values of spin sensitivity N_{mds}, since these are all referred to the S/N following a single pulse, not the total S/N for a given experimental time of a large number of pulses averaged together. An exponential fit to an off-resonance signal (not shown) gave a T_2^* of 93 μs. The recovery time is about 90 μs for one phase of the quadrature signal, and less than this for the other phase. Taking 90 μs as the recovery time and extrapolating to a 90° tipping angle gives a sensitivity of 3×10^{17} Pb^{207} spins. The magnetic moment of a Pb^{207} spin is equivalent to 0.58 nuclear Bohr magnetons, so the experimental sensitivity of our spectrometer is $N_{mds} \approx 2 \times 10^{17}$ nuclear Bohr magnetons in a 25 kHz bandwidth.

The theoretical sensitivity , derived in Ch. 4, is given by

$$N_{mds} = \frac{4\, k_b^{3/2}\, T}{\pi^{1/2}\, \hbar^2\, \gamma^{5/2}\, B_0^{3/2}} \left[\frac{T_N^{\Sigma}\, V_c\, B}{Q} \right]^{1/2} . \qquad (5.11)$$

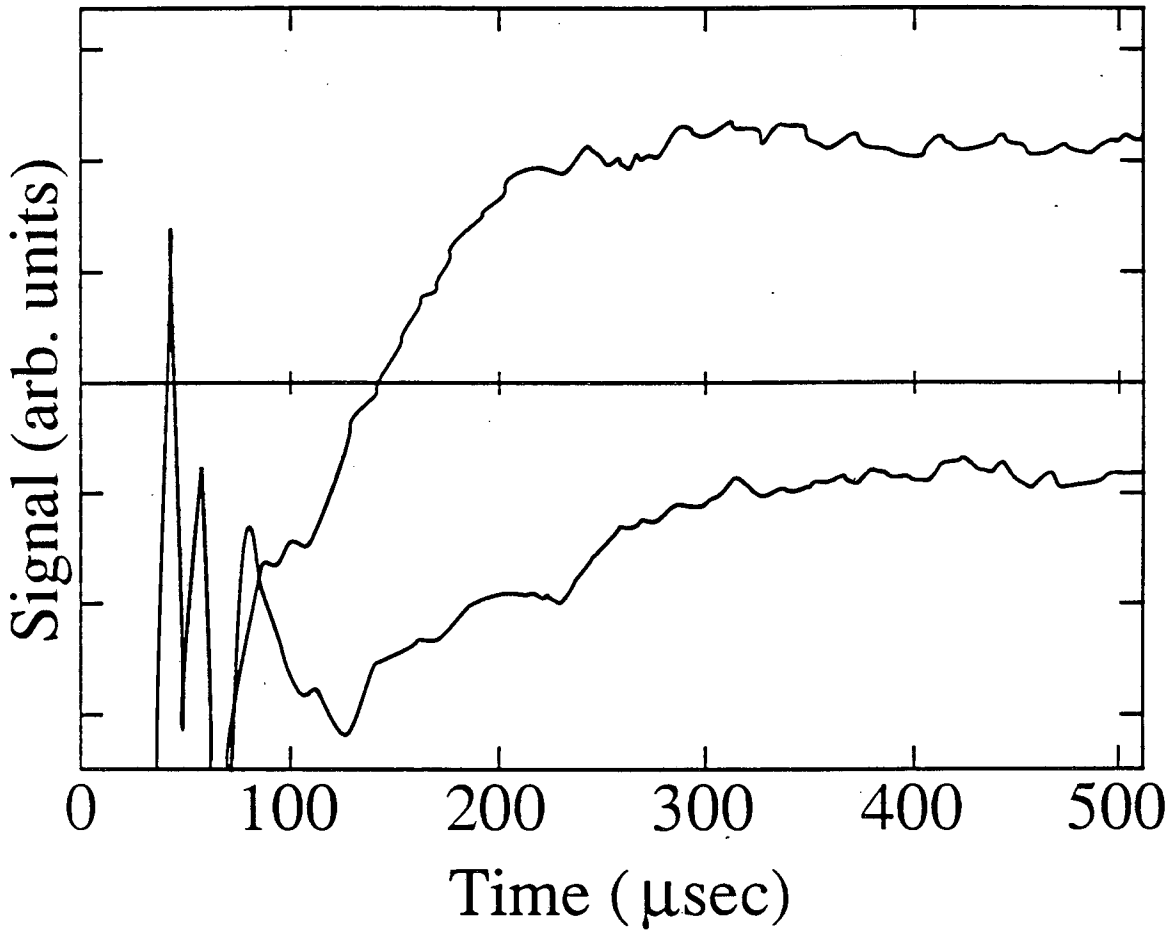

Fig. 5.5 Free induction decay, mixed down to near zero frequency, from a thin Pb film. The signal is detected in quadrature, and both phases are shown. The upper trace is the 0° phase, and the lower trace is the 90° phase.

For the signal measured above, the parameters are T = 4.2 K, γ = 5.66 10^2 Hz/Gauss (the Knight-shifted value, since we are observing lead in metal form), B_0 = 35.3 kGauss, T_N^{Σ} = 11 K, V_c = 1.24 cm^2, B = 25 kHz, and Q = 235. Assuming an exponential decay and a 90 μs recovery time, the theoretical spin sensitivity is $N_{mds} \approx 8.6 \times 10^{16}$ nuclear Bohr magnetons in a 25 kHz bandwidth. The discrepancy between theoretical and experimental spin sensitivities is about a factor of 3. The source of this discrepancy is not known.

5.7 Comparison to the SQUID NQR experiment

The SQUID NMR experiment was motivated in part by the results of an earlier SQUID NQR experiment (Hilbert et al., 1985). This earlier experiment used a dc SQUID to detect the NQR signal at 30 MHz from the ^{35}Cl nuclei of $NaClO_3$ in zero static magnetic field at 4.2 K. The total system noise temperature was measured to be 6 K, the Q of the receiver circuit 2,500, and the spin sensitivity $N_{mds} \approx 2 \times 10^{16}$ nuclear Bohr magnetons in a 10 kHz bandwidth. The decoupling between transmitter and receiver circuits was ≥ 90 dB.

The spin sensitivity N_{mds} was based on the observation of a S/N of 1 at time 75 μs after a 600 μdegree tipping angle pulse which was 4 μs long . The 600 μdegree tipping angle was estimated from a geometric calculation of the tipping field B_1 of the transmitter coil and a measurement of the pulse power applied at the top of the dewar. This S/N was extrapolated from 600 μdegrees to a 90° tipping angle pulse to obtain the quoted spin sensitivity of 2×10^{16} nuclear Bohr magnetons. This calibration was done without a Q-spoiler in the receiver circuit. Basing the sensitivity calibration on an extrapolation from 600 μdegrees to 90° and a geometric calculation of the tipping field B_1 raises doubts about the accuracy of the quoted spin sensitivity N_{mds}. A more reliable estimate of the spin sensitivity can be made from the response after applying a 90° tipping angle pulse, since a

90° pulse angle can be determined fairly confidently by application of a second pulse immediately afterward to look for a null signal (Fukushima and Roeder, 1981). An estimate of the spin sensitivity of the SQUID NQR spectrometer based on a 90° tipping angle pulse gives an $N_{mds} \approx 4 \times 10^{16}$ nuclear Bohr magnetons. Using Eq. 5.11 and the parameters of the SQUID NQR experiment gives a theoretical spin sensitivity of about 1×10^{16} nuclear Bohr magnetons. The discrepancy between theoretical and experimental spin sensitivities for the SQUID NQR experiment is then about a factor of 4. The source of this discrepancy is not known. Using 4×10^{16} for N_{mds}, the measured spin sensitivities of the SQUID NQR spectrometer and the SQUID NMR spectrometer differ by about a factor of 6. In theory, the difference in Q (neglecting any accompanying changes in T_N^{Σ}) accounts for a factor of about 3. The difference in T_2^* combined with the difference in recovery time accounts for a factor of about 2. The difference in noise temperature accounts for a factor of about 1.4.

The spin-spin relaxation time T_2^* is important because if it is comparable to the recovery time of the spectrometer then significant S/N will be lost. For the SQUID NQR experiment, T_2^* was 240 μsec and the recovery time (with a Q-spoiler present) was about 50 μsec. Thus the recovery time would not in principle seriously degrade the S/N. For the SQUID NMR experiments, we were observing resonance signals from metals, and the spin-spin relaxation time was about 93 μsec. The recovery time was about 90 μsec, and the pulse length was 38 μsec. Thus the recovery time seriously degraded the S/N. We were also unable to attain the same recovery time, presumably due to the differences in decoupling between the transmitter and receiver coils for the two spectrometers (60 dB for the SQUID NMR experiment compared to 90 dB for the SQUID NQR experiment) and the differences in critical currents of the Q-spoilers used (minimum $I_c \approx 12$ μA for the SQUID NMR experiment compared to minimum $I_c \approx 4$ μA for the SQUID NQR experiment). We needed to use Q-spoilers with larger critical currents in the SQUID NMR experiment because the minimum critical current of Q-spoilers with critical currents less

than about 10 μA would occasionally be permanently trapped down to zero or near zero μA following application of pulses, dramatically reducing the Q and damping out the signal.

A major problem with the use of SQUIDs and Josephson junction Q-spoilers to detect NQR and NMR is their recovery from rf pulses. It is observed that the rf pulses typically used in NMR and NQR experiments can permanently change the flux bias point of a SQUID (Freeman et al., 1986; Fan et al., 1988). This renders the SQUID useless as an amplifier. These pulses can also trap down the critical current of a Josephson junction Q-spoiler, as observed in the SQUID NQR experiment, the nuclear-quadrupole induction of atomic polarization experiment (see Ch. 6), and the SQUID NMR experiment . The SQUID NQR experiment (Hilbert et al., 1985) used a gradiometer configuration to attain a decoupling of 90 dB between the transmitter and receiver coils. With this decoupling, the SQUID and Q-spoiler did not suffer changes in flux bias point or critical current ("flux knocking") following application of rf pulses. Hilbert et al. found that if this decoupling was reduced to 78 dB, the critical current of the Q-spoiler junctions would permanently trap down to zero or near zero μA following application of pulses.

The SQUID NQR experiment was performed in zero static magnetic field, and the coil geometry was limited only by the 7.6 cm diameter throat of the fiberglass helium dewar. The NQR signal was linearly polarized and colinear with the rf pulse field B_1. The receiver and transmitter coils could be colinear with each other and with the 7.6 cm diameter helium dewar throat . This allowed a gradiometer configuration to be used to isolate the receiver circuit, SQUID, and Q-spoiler from the transmitter circuit. On the other hand, the SQUID NMR experiment was performed in a 3.5 Tesla axial field magnet with a 5.6 cm diameter bore. The static magnetic field direction required the receiver and transmitter coils to be perpendicular to the bore of the magnet. This did not allow room for a gradiometer configuration. Instead, the receiver and transmitter were built in a cross-coil configuration. The isolation between transmitter and receiver was about 30 dB worse than in the SQUID

NQR experiment. The 60 dB decoupling achieved in the SQUID NMR probe is comparable to the decoupling obtained by other groups for cross-coil configurations (Hoult, 1978; Freeman et al., 1986; Chingas, 1988). Based on the earlier results of the SQUID NQR experiment, it is not surprising that flux knocking was a serious problem in the SQUID NMR experiment.

The fact that the SQUID NQR experiment could be performed in zero static magnetic field had many other advantages. It permitted use of Nb wire and solder-coated wire in the receiver circuit. It allowed the SQUID to be located close to the receiver pickup coil and capacitor, and for the entire receiver circuit to be compact. The entire probe head could be enclosed in a superconducting container, providing shielding and allowing superconducting grounds. The 3.5 Tesla field of the SQUID NMR experiment necessitated locating the SQUID remote from the receiver coil. This caused a clear decrease in Q. For a compact receiver circuit located near the SQUID, a Q of 2,000 was easily obtained. For the circuit required to locate the SQUID remotely, the maximum Q obtainable was about 230 for Cu wire, and about 600 for NbTi wire.

5.8 Attempts to improve Q

In an attempt to improve the spin sensitivity of the SQUID NMR spectrometer, I expended considerable effort in attempts to increase the quality factor Q. In normal conductors at radio frequencies, most of the current flows within a skin depth of the surface of the wire. The skin depth is about 12 μm for Cu at 30 MHz and 295 K. It seemed that using wire with more surface area should increase the Q. I obtained Litz wire, which consists of many fine strands of insulated Cu wire woven together, with a surface area much larger than an equivalent diameter of single strand Cu wire. The number of strands in the Litz wire was 175, and the diameter of a single strand was about 63 μm. RLC circuits built from this wire had a Q of about 100 at 30 MHz and room temperature, compared to a Q of 200 for a similar RLC built using 20 AWG Cu wire. This was a surprising result. In

an attempt to understand this, I measured the resistance of Litz wire and 20 AWG single strand Cu wire as a function of frequency. The results are shown in Fig. 5.6. Two types of Litz wire were measured: the earlier mentioned wire and a second length from a different manufacturer consisting of 210 strands of 48 AWG Cu wire. The Litz wire shows a smaller increase in resistance compared to the 20 AWG Cu wire as the frequency is increased from 1 kHz to 1 MHz. Above about 3 MHz, both types of Litz wire show a sharp increase in resistance. This sharp increase in resistance may be due to the "proximity effect" between the individual strands of the Litz wire: the magnetic fields generated by two nearby wires carrying the same rf current approximately cancel each other along some parts of the wires, reducing the effective cross-section of the wires and increasing the resistance (Hoult, 1978). Thus building the receiver circuit from Litz wire would not improve the Q.

The need to isolate the SQUID from the 3.5 T static magnetic field of the magnet required a receiver circuit with about 25 cm of twisted pair between the pickup coil and the SQUID. I found that the relative location of the pickup coil and the capacitor in the receiver circuit had a noticeable effect on the Q. The closer the pickup coil and capacitor were, the higher the Q. I believe this is caused by the voltage drop to ground at a given point in the receiver circuit. If the inductor and capacitor are right next to each other, then the voltage changes across their impedances are localized to the immediate vicinity of the inductance and capacitance. If the inductor and capacitor are at opposite ends of the 25 cm twisted pair, then the voltage drop will occur along the length of the twisted pair, and between the twisted pair and any nearby grounds. This provides more opportunity for losses from coupling to the enviornment. This is related to the theory behind birdcage resonators, which have small capacitors interrupting the receiver coil.

The high magnetic fields required for SQUID NMR precluded use of Nb wire and superconducting tinned receiver circuits, as had been used in the SQUID NQR

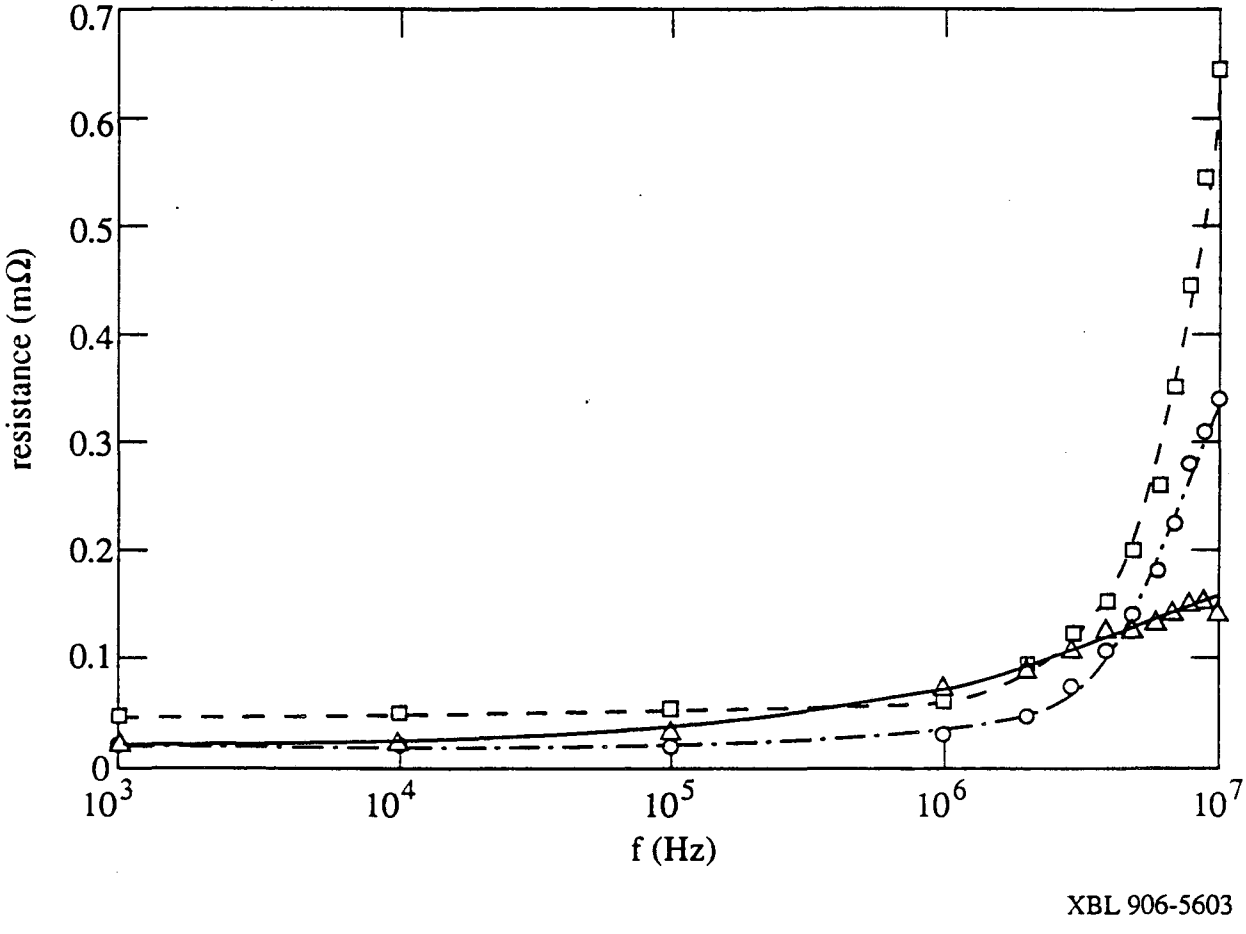

Fig. 5.6 Resistance as a function of frequency for Litz wire (circles are 175 strands of 42 AWG Cu wire, boxes are 210 strands of 48 AWG Cu wire) and for a single strand of 20 AWG Cu wire (triangles).

experiments. We used Cu wire for most of the SQUID NMR experiments. However, I made significant improvements in the Q by using NbTi wire to construct the receiver circuit. Wire with a 5 mil NbTi core and 1.5 mil Cu sheath was dipped in dilute nitric acid for several minutes to remove all but 5 mm of Cu at each end of the wire. The coil was then formed and connections made to the capacitor and SQUID connector by soldering to the remaining Cu sheath. I obtained Q values of over 600 with this method. Similar Cu receiver coils had Q values of about 200. An estimate of the static magnetic field distortion in a 6 Tesla field due to the NbTi wire using the Bean model gives a ΔB of about 0.04 Gauss at a distance of 0.1 cm from the wire. This is an order of magnitude less than the rated inhomogeneity of the Cryomagnetics magnet. We tested the wire with a 6 kHz wide Sn^{119} resonance line and saw no measurable distortion.

It should be noted that improving the Q of the receiver circuit will in principle improve the spin sensitivity of the receiver circuit, but it will also in principle exacerbate the flux knocking problem. A larger Q receiver circuit implies that the same strength transmitter pulse will induce a larger current in the SQUID input coil and Q-spoiler junctions.

5.9 Single-coil SQUID NMR

The experimental apparatus described in Sec. 5.2 uses a cross-coil probe: the transmitter and receiver are two separate circuits, with the transmitter coil orthogonal to the receiver coil and both coils orthogonal to the static magnetic field. This arrangement permits a high degree of electrical isolation between the transmitter and receiver circuits. This is useful for obtaining a low receiver noise temperature, since otherwise room temperature noise from the transmitter could couple to the receiver circuit. This isolation also reduces the previously mentioned deleterious effects of the transmitter pulse on the receiver circuit recovery time, the Q-spoiler critical currents, and the SQUID flux bias point. However, most modern NMR probes use a single coil as both a transmitter and receiver. The single-coil probe has two main advantages over the cross-coil probe. First of all, the single-coil

probe gives a much larger tipping angle for a given transmitter power. This is because a cross-coil probe transmitter coil has a larger volume (smaller filling factor) and is generally a Helmholtz pair, both of which make it less efficient than a solenoidal single-coil. Secondly, the single-coil probe is simpler to construct and use. For example, we had plans to build a SQUID NMR spectrometer with a variable temperature sample space. This requires building a transmitter and receiver coil around the outside of a cylindrical double-walled insulated insert which contains the sample. Unfortunately, this configuration makes the filling factor worse, and necessitates the use of saddle coils. We concluded that designing cross-coil saddle coils in the limited space available, achieving good decoupling between the transmitter and receiver, and maintaining a reasonable filling factor was impractical. In view of these practical difficulties, Prof. Hahn proposed building a single-coil SQUID NMR system.

The experimental configuration is shown in Fig. 5.7. The crossed diodes at room temperature allow the rf pulses through with little attenuation, and prevent noise from the power amplifier from reaching the single-coil circuit after the pulse ends. When a rf pulse from the power amplifier is applied, the crossed diodes at room temperature and at 4.2 K allow the pulse to pass to the single-coil circuit. The crossed diodes at 4.2 K also reduce the possibility of room temperature noise from the transmitter from reaching the single-coil circuit. The large currents of the rf pulse drive the Nb microbridge normal and cause the Q-spoiler junctions to switch to the resistive state, which blocks the large pulses from reaching the SQUID. The Nb microbridge, when driven normal by the pulse, would limit the current reaching the Q-spoiler below the threshold for critical current trapping or permanent damage. After the pulse ends, the Nb microbridge switches to the superconducting state, and the Q-spoiler damps down the ringdown of the single-coil circuit. The diodes at 4.2 K act as an open circuit for the small signals, which can then be coupled to the SQUID.

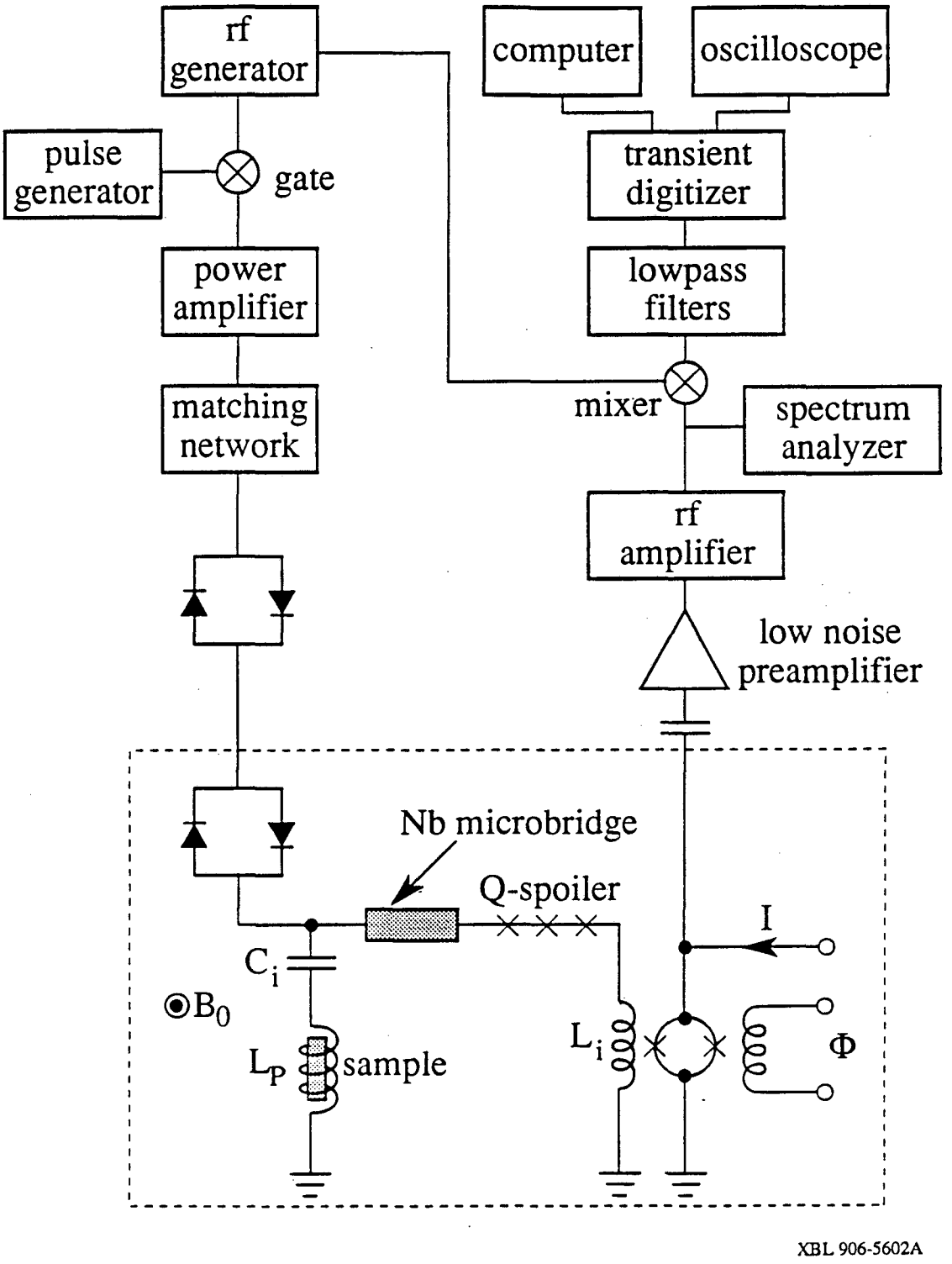

Fig. 5.7 Configuration of the single-coil SQUID NMR experiment. The RLC single-coil circuit is constructed with NbTi wire.

We tested the single coil SQUID NMR system with a circuit built with NbTi wire. We obtained Q values of about 500 without the transmitter leads connected to the circuit. Connecting the transmitter leads lowered the Q to about 100. We were able to observe the resonance signal at 36 MHz from a Sn^{119} sample in a 2 Tesla static field. We also observed a serious flux-knocking problem: a 4 Watt pulse would cause the SQUID flux bias point to change irreproducibly. The microbridge and Q-spoiler apparently did not provide sufficient blocking of the transmitter pulse in this single-coil configuration. The problems with the low quality factor Q and the low power flux knocking led us to abandon this approach. The low power flux knocking problem might be overcome by the use of a fast feedback system.

5.10 Conclusions

In conclusion, we have developed a NMR spectrometer using a dc SQUID amplifier. We have used this spectrometer to detect the free induction decay from Pb nuclei at 30 MHz in a 3.5 Tesla static magnetic field. The measured spin sensitivity is $N_{mds} \approx 2 \times 10^{17}$ Pb^{207} spins. We have also developed NbTi receiver circuits to improve the Q.

The main problems with the SQUID NMR spectrometer are the recovery of the SQUID and Q-spoiler following application of rf pulses, and the low Q of the receiver circuit. The recovery problem might be overcome by improving the isolation between the transmitter and receiver circuits. One could try building a gradiometer configuration for the transmitter and receiver circuits which would work in the limited dimensions of the magnet bore. Standard techniques in decoupling conventional NMR probes could be applied to the SQUID NMR probe, such as the use of moveable metal paddles near the transmitter coil to redistribute the transmitter flux lines. The recovery problem might also be overcome by using a feedback circuit, to return the SQUID to the optimum flux bias point after the end of the pulse. The quality factor Q might be improved by building a receiver coil with microchip capacitors interrupting it, which would place the inductor and capacitor as close together as possible.

References

1. Rhodes, H. E., P. K. Wang, H. T. Stokes, C. P. Slichter, and J. H. Sinfelt, 1982, "NMR of platinum catalysts. I. Line shapes," Phys. Rev. B26, 3559.

2. Sleator, T., E. L. Hahn, C. Hilbert, and J. Clarke, 1987, "Nuclear-spin noise and spontaneous emission," Phys. Rev. B36, 1969.

3. Hilbert, C., J. Clarke, T. Sleator, and E. L. Hahn, 1985, "Nuclear quadrupole resonance detected at 30 MHz with a dc superconducting quantum interference device," Appl. Phys. Lett. 47, 637.

4. Slichter, C. P., Principles of Magnetic Resonance (Springer-Verlag, New York, 1980), 144.

5. Fukushima, E., and S. B. W. Roeder, Experimental Pulse NMR (Addison-Wesley, Reading, Massachussetts, 1981) 434.

6. Freeman, M. R., R. S. Germain, R. C. Richardson, M. L. Roukes, W. J. Gallager, and M. B. Ketchen, "Low-temperature nuclear magnetic resonance with a dc SQUID amplifier," Appl. Phys. Lett. 48, 300.

7. Fan, N. Q., M. B. Heaney, J. Clarke, D. Newitt, L. L. Wald, E. L. Hahn, A. Bielecki, and A. Pines, 1988, "Nuclear Magnetic Resonance with dc SQUID Preamplifiers," IEEE Trans. Magn. 25, 1193.

8. Chingas, G., 1988, personal communication.

9. Hoult, D. I., 1978, "The NMR receiver: a description and analysis of design," in Progress in NMR Spectroscopy 12 (Pergamon Press, Great Britain) 61.

10. Duret, D., P. Bernard, and D. Zenatti, 1975, "A uhf superconducting magnetometer utilizing a new thin film sensor," Rev. Sci. Instrum. 46, 474.

11. Pascal, D., 1980, "Simple fabrication and characterization of thin-film niobium SQUIDs working at 4.2 K," in SQUID ' 80 (de Gruyter, New York) 417.

12. Monfort, Y., D. Bloyet, J. C. Villegier, and D. Duret, 1985, "Nb metallurgical transformations occuring in the microbridge area of an rf SQUID during its critical current adjustment," IEEE Trans. Magn. MAG-21, 866.

13. Thornton, J. A., 1975, "Influence of substrate temperature and deposition rate on structure of thick Cu coatings," J. Vac. Sci. Tech. 12, 830.

Chapter 6: Detection of an inverse Stark effect in magnetic resonance with a dc SQUID amplifier

6.1 Introduction

In this chapter I will describe the detection of an inverse Stark effect in the NQR (Nuclear Quadrupole Resonance) of $NaClO_3$ with a dc SQUID amplifier. Most of the material in this chapter has appeared in two papers by Sleator et al. (1986, 1988) and in Sleator's thesis (1986).

Before describing the inverse Stark effect, I will first discuss the better known Stark effect. The Stark effect in magnetic resonance occurs when an electric field is applied to a crystal containing a nucleus possessing an electric quadrupole moment located at a non-centrosymmetric crystal site. The electric field induces changes in the electron orbitals and relative displacements of the ions in the crystal which alter the electric field gradient seen by the nucleus (Dixon, 1965). Note that, by symmetry, the electric field gradient at a centrosymmetric crystal site must be zero. Since the electric field gradient couples to the electric quadrupole moment of the nucleus, this causes changes in the NQR and NMR resonance lines of the nucleus.

The Stark effect was first discussed by Pound (1950), who applied a 20 kV/cm static electric field across a potassium iodide crystal while looking for changes in the NMR line of the iodine nuclei, which has an electric quadrupole moment. The iodine nuclei are located at centrosymmetric sites in the crystal, so normally there would be no electric field gradient and thus no NQR energy levels. Pound hoped to induce an electric field gradient and thus a quadrupole broadening or splitting of the NMR line by applying a large static electric field to displace the ions from their equilibrium positions. He saw no effect, and a later calculation suggested the effect was too small to be observed with the given sample and apparatus. Gutowsky and Williams (1957) applied a 20 kV/cm static electric field to a $NaClO_3$ crystal and observed no change in the NQR resonance frequency of the Cl^{35}

nucleus. Later observation of the shift in resonance frequency upon application of pressure indicated that the expected Stark shift was smaller than the 2 kHz resolution of their apparatus. The first successful detection of the Stark effect in magnetic resonance was made by Kushida and Saiki (1961). They applied a $0 \rightarrow 9$ kV/cm static electric field to a $NaBrO_3$ crystal while observing the Br^{81} NQR line. The center frequency of the line changed linearly with applied electric field by up to 500 Hz at 9 kV/cm. Shortly after this, Armstrong et al. (1961) applied a static electric field of $0 \rightarrow 3$ kV/cm to powdered $KClO_3$ and $NaClO_3$, and observed increases in both the resonance frequencies and the linewidths of the Cl^{35} NQR lines. Collins and Bloembergen (1964) then observed the Stark effect in single crystals of $NaClO_3$ placed between the plates of a capacitor. A static magnetic field was applied to the sample, to lift the energy level degeneracies. The NQR resonance lines were observed to shift as the static electric field across the capacitor was varied.

Bloembergen (1961) first proposed that rf electric fields could induce transitions between nuclear spin levels, by an ac Stark effect. If the externally applied electric field is varying at a frequency corresponding to the NQR resonance frequency, the electric field gradient seen by the nucleus will oscillate at resonance, coupling to the electric quadrupole moment of the nucleus and inducing spin transitions. This effect was first observed in nuclear spins by Brun et al. (1962). They placed a GaAs crystal in a static magnetic field B_0 and observed a decrease in the magnetic free induction decay signal amplitude following a magnetic rf pulse when an rf electric field was applied across the crystal.

Gill and Bloembergen (1963) then proposed an inverse Stark effect (which they named the "quadrupole-electric effect"), in which a dc electric polarization is induced across a crystal as a result of nuclear spin transitions induced by an rf magnetic field. They calculated the effect for GaAs at 10 MHz and 77 K, obtaining an estimated induced dc potential of 0.4 mV/cm across the crystal. They also estimated the effect in the quadrupole resonance of crystals containing Br or I isotopes at about 400 MHz and 4 K, obtaining an

estimated dc potential of order 100 mV/cm across the crystal. To the best of our knowledge, this quadrupole-electric effect has never been observed.

This chapter describes yet another effect, the theoretical prediction and experimental detection of an ac electric polarization induced across a $NaClO_3$ crystal as a result of nuclear spin transitions induced by an rf magnetic field. The Cl^{35} nucleus possesses a magnetic dipole moment and an electric quadrupole moment, and undergoes a nuclear spin transition and precesses following the application of an rf magnetic pulse. The Cl^{35} nucleus is located at a non-centrosymmetric site in the $NaClO_3$ crystal, so the electron orbitals around the Cl^{35} nucleus are not symmetric. The electric field of the precessing electric quadrupole moment of the nucleus induces electric polarization of the nearby electron orbitals. The electric polarization induced by all of the Cl^{35} nuclei in the crystal sums to give a net electric polarization across the crystal. This net electric polarization has frequency components at and near dc, and at and near the rf precession frequency. (This effect also implies that without an external static electric field or rf magnetic pulse there exists a spontaneous electric polarization in crystals containing a quadrupole at a non-centrosymmetric site, due to the Boltzmann distribution of states.) We measured the net electric polarization of the crystal at frequencies near the rf precession frequency. This is the inverse of the effect predicted by Bloembergen in 1961, and is the extension to ac frequencies of the effect predicted by Gill and Bloembergen in 1963. We found that the size of the effect was much larger than anticipated, but observable by detecting the off-diagonal induced dipole signal at the Larmour frequency. This could be described as the "ac quadrupole-electric effect". This effect can yield information about the electronic polarization of bonds and atoms in a crystal, without introducing the complications of bond angle distortions and ionic displacements caused by the large static electric fields needed to see the direct Stark effect.

An estimate of the expected signal-to-noise ratio can be made using a simple classical model. The electric field of an electric quadrupole moment (the Cl nucleus) is

$E = eQS/r^4$, where e is the proton charge, Q is the quadrupole moment, S is the Sternheimer nuclear quadrupole enhancement factor, and r is the distance from the quadrupole. This electric field will polarize a nearby atom (one of the oxygen atoms), giving it a polarization $p = \alpha E$, where α is the atomic polarizability. The net electric polarization of the crystal is $P = (\hbar\omega_0/2k_bT)np$, where ω_0 is the NQR resonance frequency, T is the bath temperature, and n is the number of polarized oxygen atoms per unit volume. The factor $(\hbar\omega_0/2k_bT)$ accounts for the Boltzmann distribution of states. The voltage induced across the crystal is given by $V = 4\pi Pd/\varepsilon$, where d is the thickness of the crystal and ε is the dielectric constant of $NaClO_3$. Combining the above terms gives a voltage across the crystal of

$$V = \frac{2\pi\hbar\omega_0 n\alpha eQSd}{\varepsilon k_b T r^4} . \qquad (6.1)$$

The NQR frequency for the Cl nucleus in $NaClO_3$ is about 2×10^8 s^{-1}, n is about 4×10^{22} oxygen atoms/cm^3, α is of order 10^{-24} cm^3, $Q = -8 \times 10^{-26}$ cm^2 for the Cl^{35} nucleus, the Sternheimer factor S is of order 30, the crystal thickness d = 0.4 cm, the dielectric constant ε is about 5, the bath temperature is 4.2 K, and the Cl-O distance is r = 1.5 Å. Using these values in Eq. (6.1) and converting to MKS units gives an estimated induced voltage of order 50 μV across the crystal. The electric polarization is detected with a capacitor of capacitance $C_p = 7$ cm. The signal voltage induced across this capacitor is given by $V_s = PA/C_p$, where the area A of the crystal face is about 0.7 cm^2. The signal voltage induced across the capacitor is then $V_s = 5$ μV. The Nyquist noise voltage is $V_n = \sqrt{4k_bTR_iB}$, where the resistance R_i of the receiver circuit is about 0.47 Ω and the circuit bandwidth B is about 20 kHz. This gives a Nyquist noise voltage of about 1 nV. The voltage signal-to-noise ratio is then about 5,000, if amplifier noise is neglected. If a conventional, room temperature rf amplifier with a noise temperature of 100 K is used, the

voltage signal-to-noise ratio will be about 500. This suggests that a SQUID was not needed to observe the ac quadrupole-electric effect.

6.2 Theory of the ac quadrupole-electric effect

I will now give a more rigorous derivation of the expected magnetic signal, produced by the well-known mechanism of nuclear magnetic dipole precession, and then derive the electric polarization signal, produced by the ac quadrupole-electric effect. The nuclear state of the Cl nucleus (which has spin 3/2) in a small static field H_0 after application of an rf pulse is given by (Bloom et al., 1955):

$$|\psi\rangle = C_{3/2}(t)|3/2\rangle + C_{1/2}(t)|1/2\rangle + C_{-1/2}(t)|-1/2\rangle + C_{-3/2}(t)|-3/2\rangle, \tag{6.2}$$

where:

$$\left.\begin{aligned} C_{3/2}(t) &= C_{3/2}(0)\exp[i\omega_0 t/2 + i\Omega'' t], \\ C_{-3/2}(t) &= C_{-3/2}(0)\exp[i\omega_0 t/2 - i\Omega'' t], \\ C_{1/2}(t) &= e^{-i\omega_0 t/2}\{[b^2 e^{i\Omega' t} + a^2 e^{-i\Omega' t}]C_{1/2}(0) + [2abi\, e^{-i\phi_0}\sin(\Omega' t)]C_{-1/2}(0)\}, \\ C_{-1/2}(t) &= e^{-i\omega_0 t/2}\{[b^2 e^{-i\Omega' t} + a^2 e^{i\Omega' t}]C_{-1/2}(0) + [2abi\, e^{i\phi_0}\sin(\Omega' t)]C_{1/2}(0)\}, \end{aligned}\right\} \tag{6.3}$$

and where $C_{3/2}(0) = 2^{-1/2}\cos(\sqrt{3}/2\ \omega_1 t_w \sin\theta_1)$, $C_{1/2}(0) = i2^{-1/2}\cos(\sqrt{3}/2\ \omega_1 t_w \sin\theta_1)$, $C_{-3/2}(0) = e^{i\xi}C_{3/2}(0)$, $C_{-1/2}(0) = e^{i\xi}C_{3/2}(0)$, $\omega_1 = \gamma H_1$, t_w = pulse length, $\sqrt{3}\omega_1 t_w \sin\theta_1$ is the tipping angle, ξ is a random phase factor used to keep track of incoherence between different states, $\omega_o = e^2qQ/2$ is the NQR frequency, e = proton charge, eq = electric field gradient at the nucleus, Q = quadrupole moment of the nucleus, $\Omega'' = (3/2)\Omega_0\cos\theta_0$,

$\Omega_0 = \gamma H_0$, $a = \cos\theta_0/|\cos\theta_0|\,[(f-1)/2f]^{1/2}$, $b = [(f-1)/2f]^{1/2}$, $f = (1 + 4\tan^2\theta_0)^{1/2}$, $\Omega' = (1/2)\Omega_0 f\cos\theta_0$, θ_0 = angle between H_0 and $\hat{z}$ (see Fig. 6.2), ϕ_0 = angle between H_0 and $\hat{x}$, and θ_1 = angle between H_1 and $\hat{z}$.

The magnetic signal from a single nucleus is given by $\langle\psi|\mu|\phi\rangle$, where μ is the magnetic moment operator $\gamma\hbar I$. The magnetic signal from a single nucleus is $\mu = \sqrt{3}/2\gamma\hbar W[(a^2\cos\Omega_a t + b^2\cos\Omega_b t)\hat{x} + (a^2\sin\Omega_a t + b^2\sin\Omega_b t)\hat{y}]$, where $W = \sin(\sqrt{3}\omega_1 t_w \sin\theta_1)\sin\omega_0 t$, $\Omega_a = \Omega'' + \Omega'$, $\Omega_b = \Omega'' - \Omega'$, and t_w is the pulse length. The net magnetic signal for the entire crystal is

$$\mathbf{M} = \frac{\hbar\omega_0}{2k_bT} N\gamma\hbar\sin(\sqrt{3}\,\omega_1 t_w \sin\theta_1)\sin\omega_0 t\,(a^2\cos\Omega_a t + b^2\cos\Omega_b t)\hat{x}', \qquad (6.4)$$

where N = total number of Cl nuclei in the crystal, and the vector $\hat{x}'$ is along the crystal (111) axis.

The electric signal can be found by first calculating the quadrupole moments of the nucleus following a pulse, then calculating the electric field produced by the precessing quadrupole moment, then assuming an electric polarization $\mathbf{P} = \alpha\mathbf{E}$, where α is the polarizability of the nearby electron orbitals. The net electric dipole moment induced across the crystal is then given by the sum of $\mathbf{P}$ over all nuclei in the crystal. Carrying this out for the (111) crystal face coplanar with the capacitor plate and retaining only terms near the Larmour frequency gives an electric polarization signal

$$\mathbf{P}(t) = \frac{\hbar\omega_0}{2k_bT} Np_0\sin(\sqrt{3}\omega_1 t_w \sin\theta_1)\cos\omega_0 t$$
$$\times [0.14\sin\Omega_a t - 0.92\sin\Omega_b t + \{\pm\}0.78\cos\Omega_a t - \{\pm\}0.78\cos\Omega_b t]\hat{x}', \qquad (6.5)$$

where $p_0 = \alpha Q/r_0^4$, r_0 = the Cl-O distance, and the sign in the brackets { } refers to the particular crystal enantiomer.

Similar calculations for the (100) crystal face coplanar with the capacitor plate gives a net magnetic signal of

$$M = 0.24 \frac{\hbar\omega_0}{2k_bT} N\gamma\hbar\sin(\sqrt{3}\,\omega_1 t_w \sin\theta_1)\sin\omega_0 t\,[2 + \cos(\sqrt{3}\Omega_0 t)]\hat{x}'', \qquad (6.6)$$

and a net electric polarization signal of

$$P(t) = -\{\pm\}\, 0.86 \frac{\hbar\omega_0}{2k_bT} Np_0\sin(\sqrt{3}\omega_1 t_w \sin\theta_1)\cos\omega_0 t\,[1 - \cos(\sqrt{3}\Omega_0 t)]\hat{x}'', \qquad (6.7)$$

where the vector $\hat{x}''$ is along the crystal (100) axis.

6.3 The $NaClO_3$ sample

The structure of a unit cell of $NaClO_3$ is shown in Fig. 6.1. The Cl nuclei are located at non-centrosymmetric sites. While I was constructing a ball and stick model of this crystal, I learned that the crystal has two enantiomorphs, and realized that this would have an effect on the calculated electric polarization signal (we had not known these facts before). The two enantiomorphs differ by a 39° rotation of the oxygen atoms about the Na-Cl axis.

The spin-lattice relaxation time T_1 of $NaClO_3$ at 4.2 K was measured to be > 72 hours (Sleator, 1986). This would make NMR impractical: one would have to wait days between pulses. The T_1 was decreased to 20 min. by irradiation with γ-rays, which introduces paramagnetic defects.

We built a one-position goniometer to hold and position the crystal when we cut it along the (111) faces, using a circular diamond saw. We also cut a second crystal

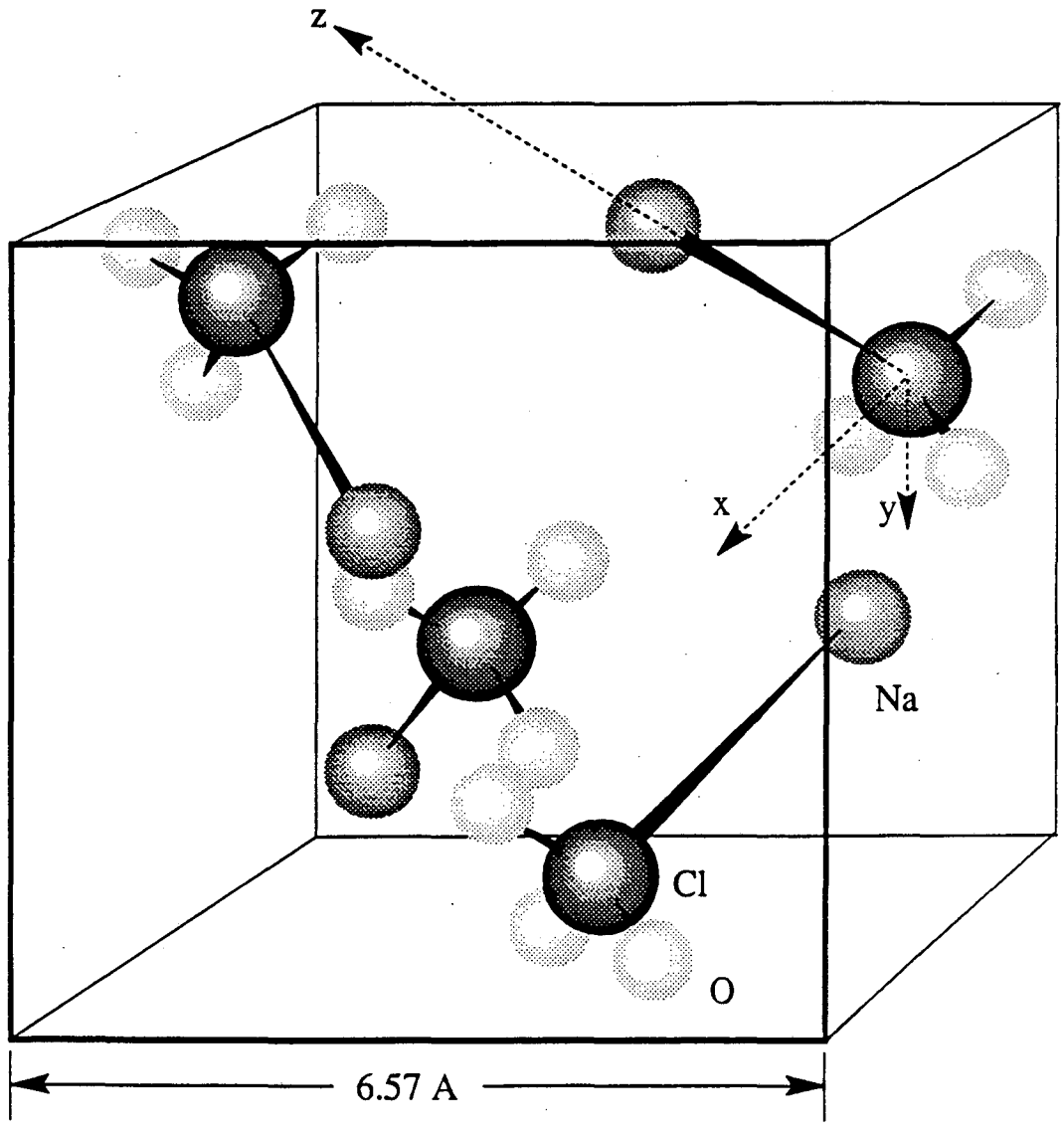

Fig. 6.1 Structure of a unit cell of $NaClO_3$. There are four molecules per unit cell, and the space group is $P2_13$.

along the (100) faces. The two crystals were cut into slabs 0.4 cm thick. We then used a belt sander to round the slabs into 0.95 cm diameter cylinders, to match the diameter of the capacitor C_p.

6.4 The experimental apparatus

A block diagram of the experimental configuration is shown in Fig. 6.2(a). A cw signal from a rf generator is fed into a gate and triggered by a pulse generator. The resulting rf pulse is amplified and coupled to the cold transmitter circuit via a 50 Ω resistor in series with the transmitter circuit and coaxial cable. The sample is mounted between the plates of a capacitor C_p which is inside the transmitter coil. The sample, capacitor, and transmitter coil are located inside a Helmholtz coil (not shown) colinear with the transmitter coil, which is used to generate small static magnetic fields. When the rf pulse B_1 ends, the electric polarization **P** of the sample induces a signal voltage across the receiver capacitor C_p.

The sample also has a precessing magnetization **M**, which will couple to the receiver circuit via stray inductance, and may obscure the electric polarization signal. We cancel out this magnetic signal by using a variable inductor L_c shown in detail in Fig. 6.2(b). One end of this variable inductor is connected to a rotatable rod which can be turned from the top of the dewar. The number of turns and handedness of this inductor can then be varied to cancel out any stray magnetic signal the receiver circuit picks up from the sample. The electric polarization signal is zero and the magnetic signal is maximum when the externally applied static magnetic field is zero. By setting the externally applied static magnetic field to zero and then adjusting the variable inductor to minimize the signal observed following a pulse, we could cancel out the magnetic signal. I was able to get this variable inductor to work properly by trying various modifications in a clear plexiglass block with a cylindrical hole (which simulated the experimental location of the inductor) while visually observing the sources of failure.

The receiver capacitor is connected in series with L_c and in parallel with an air capacitor C_i (also adjustable from the top of the cryostat). The resistance R_i is due to

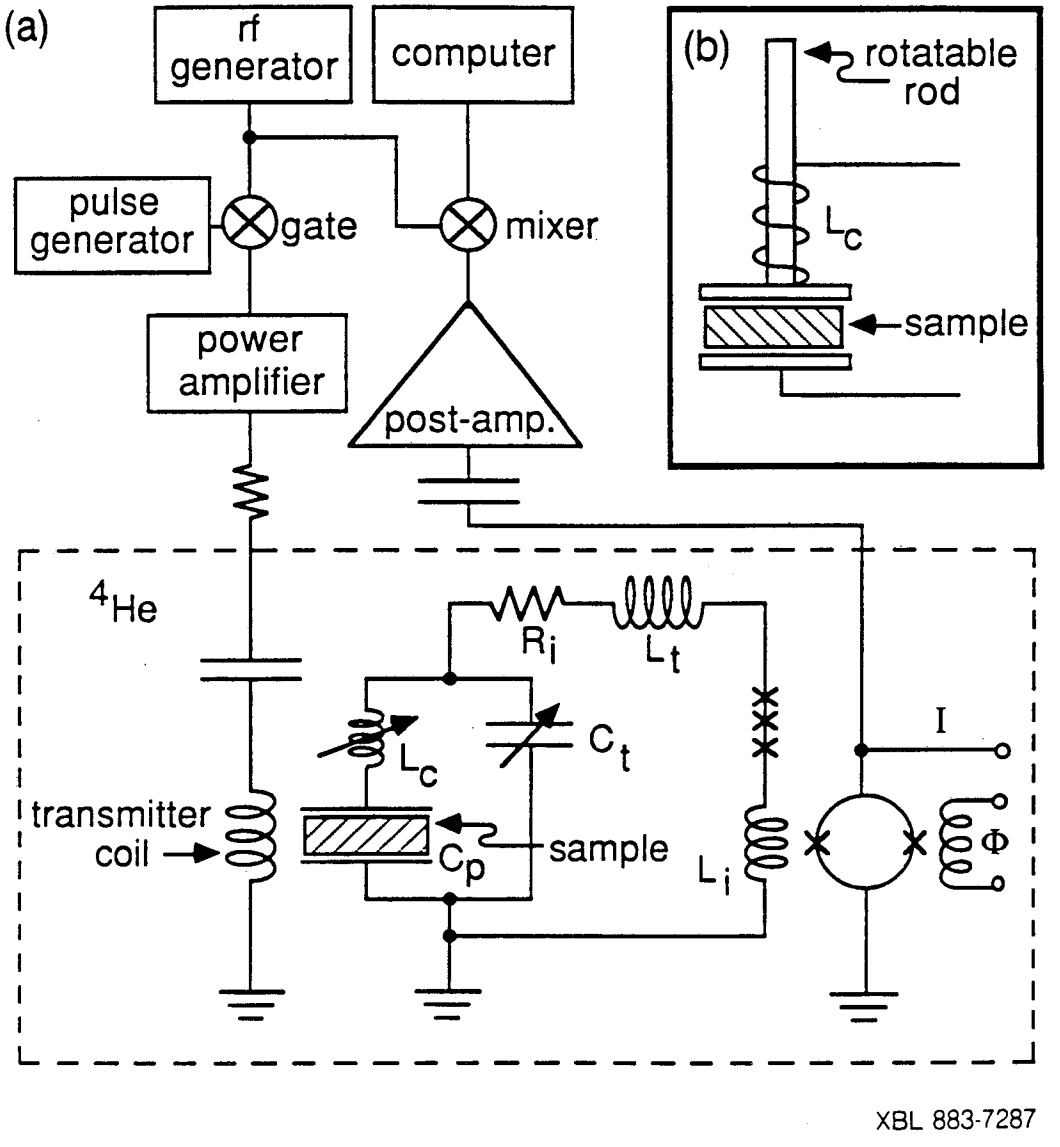

Fig. 6.2 (a) Block diagram of experimental apparatus. Components within the dashed box are inside a liquid helium dewar. (b) Detail of the inductor L_c, used to cancel out stray magnetic signal from the sample.

stray losses in the receiver circuit. These components are part of a tuned RLC circuit in series with the input coil L_i of a dc SQUID and a series array of 20 Josephson tunnel junctions, which act as a Q-spoiler (Hilbert et al., 1985). We found that the minimum critical current of the Q-spoiler occasionally trapped down to zero μA following application of pulses, even at pulse powers corresponding to a tipping angle of 0.07 °. When this occurred it was necessary to remove the probe from the helium bath and allow the Q-spoilers to go normal, then reimmerse the probe. This was usually effective at untrapping the Q-spoiler.

The SQUID output signal is fed to a coaxial cable which leads out of the helium dewar and is impedance matched to 50 Ω with a fixed room temperature capacitor, and then further amplified by a low noise room temperature rf amplifier. The amplified signal is mixed down and detected in quadrature with a reference supplied by the rf generator. The mixed-down signal is filtered and digitized before storage in a computer.

The receiver circuit has a Q of about 1200 [the value of 1500 quoted in Sleator et al. (1986, 1988) includes feedback effects which change the true Q of the circuit], and a total inductance of about 2.8 μH. This corresponds to a receiver circuit resistance of 0.47 Ω. The optimization theory of Hilbert and Clarke (1985) states that the optimum resistance for this receiver circuit is given by $R_i^{opt} = \alpha^2 \omega L_i = 0.7\ \Omega$. The revised optimization theory (see Wellstood, 1988 and Sec. 3.4) had not yet been developed, and it was believed that increasing the effective circuit resistance (by using feedback effects) to match the predicted R_i^{opt} more closely would improve the signal-to-noise ratio. This was actually done in some cases.

6.5 Experimental results

Fig. 6.3 shows experimental data for the crystal (111) face coplanar with the capacitor plate. We first observed the magnetic signal due to stray pickup of the precessing magnetic moments of the Cl^{35} nuclei, while the externally applied static magnetic field was

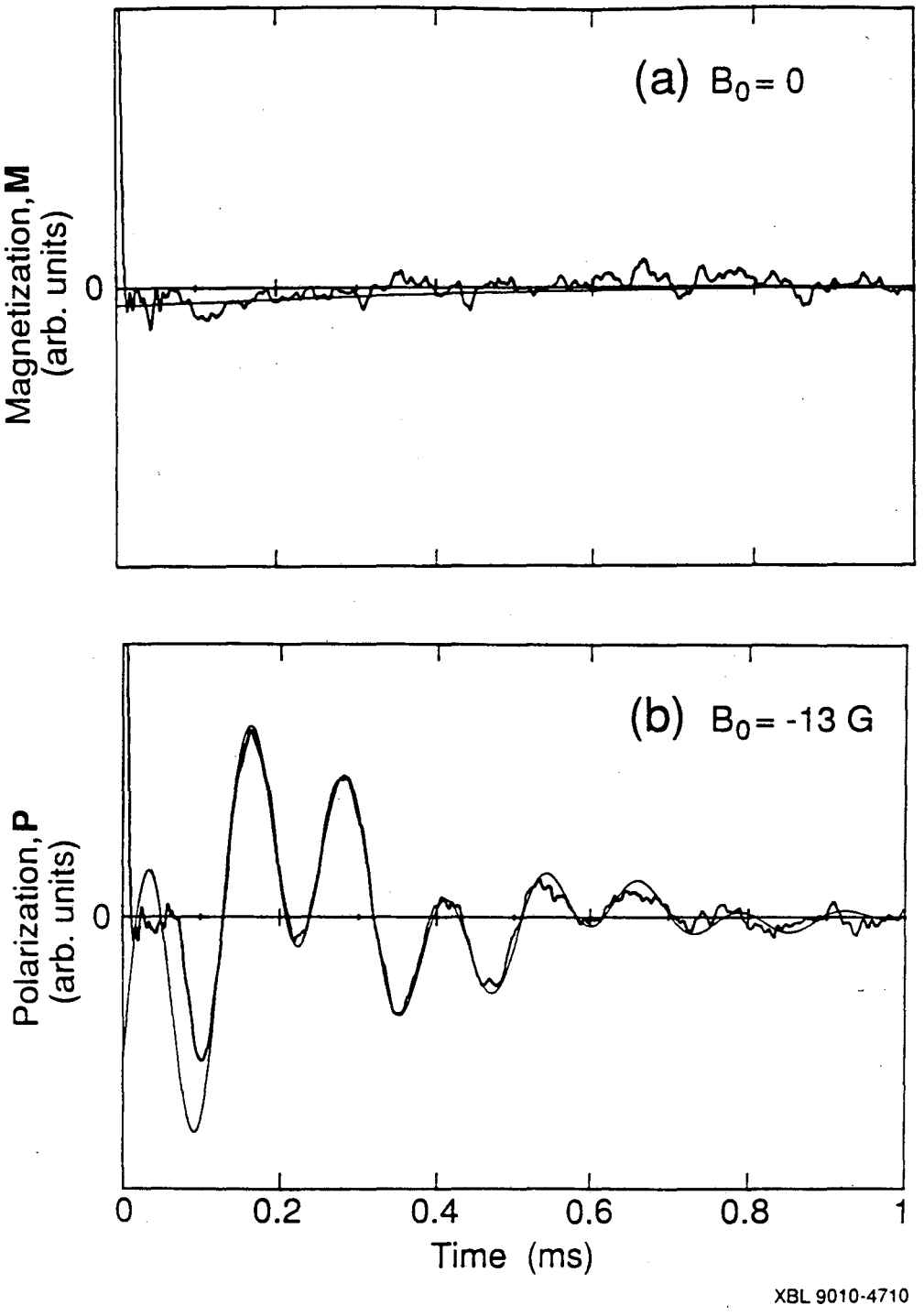

Fig. 6.3 (a) Free induction decay, mixed down from 30 MHz to near dc, when $B_0 = 0$, for the (111) crystal orientation.
(b) All conditions identical to (a), except for the application of a static 13 G magnetic field.

zero. We adjusted the inductor L_c to minimize this magnetic signal, as shown in Fig. 6.3(a). The magnetic signal will then be maximum for the given coupling, since $\Omega_a \propto H_0$ and $\Omega_b \propto H_0$ (refer to Eq. 6.4), and the electric polarization signal will be zero (refer to Eq. 6.4). We then apply a 13 G static magnetic field to the crystal, which lifts the degeneracy between the quadrupole energy levels. We see a clear signal due to electric polarization of the crystal, as shown in Fig. 6.3(b). The signals shown in Figs. 6.3 are each the sum of 100 identical pulses; each pulse tipped the spins by 0.056°. Although we could demonstrate the existence of this "ac quadrupole-electric effect", the experimental signal did not match our theoretical predictions. The fitted function shown in Fig. 6.3(b) is an arbitrary combination of the various terms of the predicted signal, Eq. (6.4) (Sleator et al., 1988). We concluded that the "ball and stick" model we had used to calculate the expected signal was inadequate. Later theoretical work (Harris et al., 1988) supported this conclusion.

We also performed the experiment with a $NaClO_3$ crystal cut along the (100) faces. We again minimized the magnetic signal by adjusting the variable inductor while observed the signal in zero externally applied magnetic field, as shown in Fig. 6.4(a). The magnetic signal will be at a maximum [see Eq. (6.6)] and the electric polarization signal will be zero [see Eq.(6.7)] for this case. We then applied a small static magnetic field and saw the electric polarization signal shown in Fig. 6.4(b). For this case, the form of the experimental signal was in reasonable agreement with the calculated theoretical signal.

6.6 Conclusions

In conclusion, we have used the dc SQUID as an rf amplifier to detect an inverse Stark effect in nuclear quadrupole resonance. Nuclei with magnetic dipole and electric quadrupole moments located at non-centrosymmetric sites in a crystal are induced to precess by an rf magnetic pulse. The precessing nuclei generate a magnetic signal which is cancelled out by a variable inductor located near the crystal. The precessing nuclei also generate an rf electric field which polarizes the nearby electron orbitals. Due to the

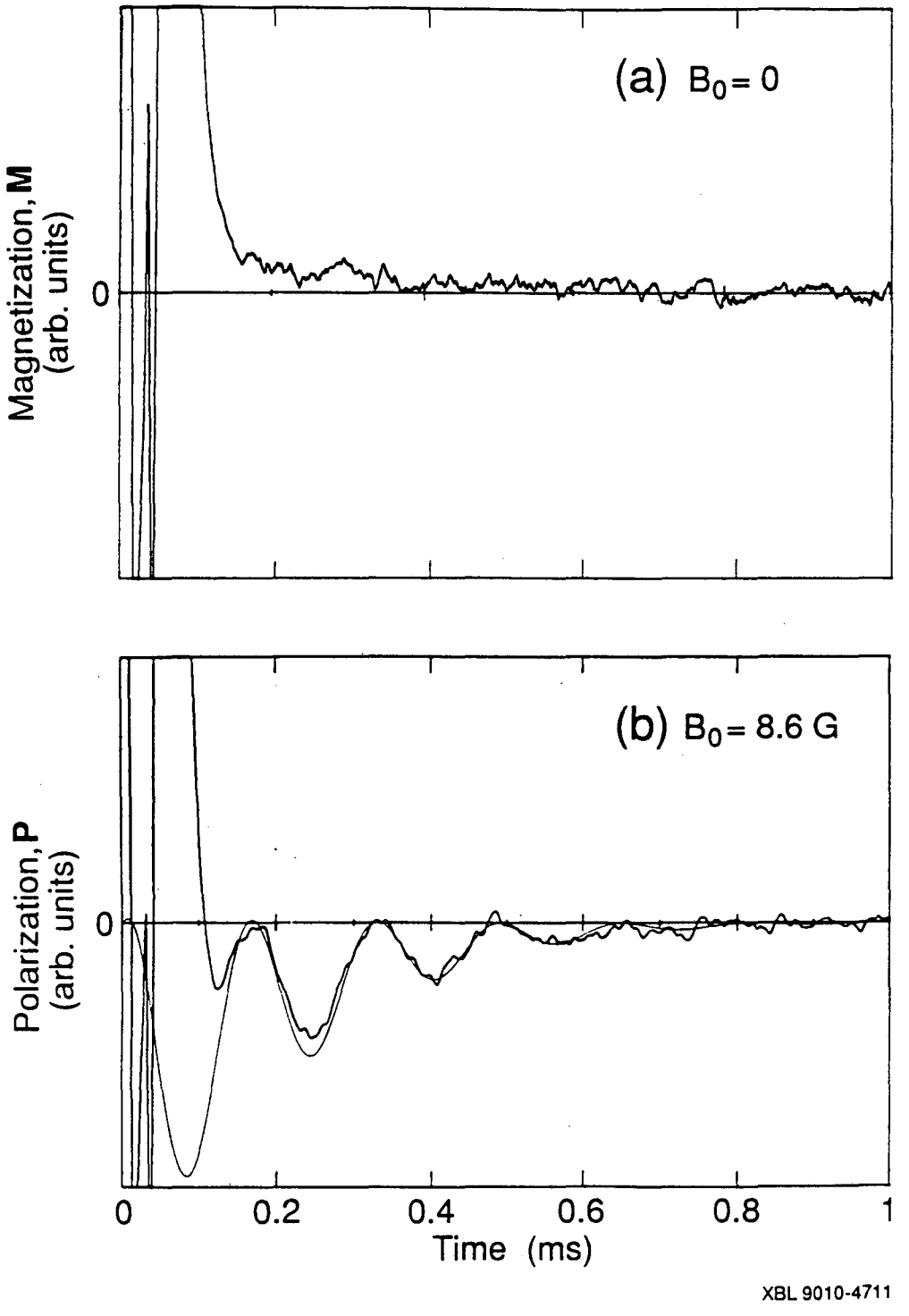

Fig. 6.4 (a) Free induction decay, mixed down from 30 MHz to near dc, when $B_0 = 0$, for the (100) crystal orientation.
(b) All conditions identical to (a), except for the application of a static 8.6 G magnetic field.

non-centrosymmetric location of the nuclei, this polarization causes a net electric polarization of the crystal, which is detected. This effect can yield information about the local electronic environment in a crystal, without producing bond angle distortions. The signal is reasonably large, and did not require the use of a SQUID to detect it.

References

1. Sleator, T., E. L. Hahn, C. Hilbert, and J. Clarke, 1986, "Nuclear electric quadrupole induction of atomic polarization," Phys. Rev. Lett. 57, 2756.

2. Sleator, T., E. L. Hahn, C. Hilbert, and J. Clarke, 1988, "Nuclear-quadrupole induction of atomic polarization," Phys. Rev. B38, 8609.

3. Sleator, T., 1986, Ph.D. Thesis, University of California, Berkeley.

4. Dixon, R. W., 1964, "Perturbations of nuclear quadrupole interactions induced by dc electric fields", Proc. XIIIth Colloque Ampere, in Nuclear Magnetic Resonance and Relaxation in Solids (North-Holland Publishing Co., Amsterdam), 213.

5. Pound, R. V., 1950, "Nuclear electric quadrupole interactions in crystals," Phys. Rev. 79, 685.

6. Gutowsky, H. S., and G. A. Williams, 1957, "Sodium nuclear quadrupole interactions in $NaClO_3$ and $NaBrO_3$," Phys. Rev. 105, 464.

7. Kushida, T., and K. Saiki, 1961, "Shift of nuclear quadrupole resonance frequency by electric field," Phys. Rev. Lett. 7, 9.

8. Armstrong, J., N. Bloembergen, and D. Gill, 1961, "Linear effect of applied electric field on nuclear quadrupole resonance," Phys. Rev. Lett. 7, 11.

9. Collins, F. A., and N. Bloembergen, "Stark effects on the nuclear quadrupole coupling of ^{35}Cl in sodium chlorate," J. Chem. Phys. 40, 3479.

10. Bloembergen, N., 1961, "Linear Stark effect in magnetic resonance spectra," Science 133, 1363.

11. Brun, E., R. Hann, W. Pierce, and W. H. Tanttila,1962, "Spin transitions induced by external rf electric field in GaAs," Phys. Rev. Lett. 8, 365.

12. Gill, D., and N. Bloembergen, 1963, "Linear Stark splitting of nuclear spin levels in GaAs," Phys. Rev. 129, 2398.

13. Hilbert, C., J. Clarke, T. Sleator, and E. L. Hahn, 1985, "Nuclear quadrupole resonance detected at 30 MHz with a dc superconducting quantum interference device," Appl. Phys. Lett. 47, 637.

14. Hilbert, C., and J. Clarke, 1985, "DC SQUIDs as radiofrequency amplifiers," J. Low Temp. Phys. 61, 263.

15. Wellstood, F.C., 1988, Ph.D. Thesis, University of California, Berkeley.

16. Bloom, M., E. L. Hahn, and B. Herzog, 1955, "Free magnetic induction in nuclear quadrupole resonance," Phys. Rev. 97, 1699.

17. Harris, R. A., C. J. Grayce, and E. L. Hahn, 1988, "The nuclear-quadrupole-induced dipole moment of HD," Chem. Phys. Lett. 147, 443.

Chapter 7: Comparison to conventional magnetic resonance techniques

7.1 Introduction

This chapter discusses the various means of improving the sensitivity of an NMR experiment. The sensitivity of the SQUID spectrometer can be expressed in the same terms as the sensitivity of a conventional NMR spectrometer [Eq.(4.2)], so direct comparisons of noise temperatures, quality factors Q, and operating frequencies ω can be made. The use of a dc SQUID as an rf amplifier will be compared to conventional amplifiers and other techniques of improving the sensitivity. A brief summary of the application of dc SQUIDs to high frequency magnetic resonance is given.

7.2 Experimental techniques to improve sensitivity

The ultimate sensitivity of an NMR experiment depends on several factors. This section will examine some of these factors in detail. The problem of sensitivity in NMR can be divided into two general classes: the signal strength and the noise strength. I will first discuss the signal strength.

The signal strength derivation was outlined in Sec. 4.2. Combining the various terms gives a signal voltage

$$V_i = \frac{\pi}{c} A n_t \sin\theta_t \sin\omega_0 t \left[\frac{N\gamma^3\hbar^2 B_0^2}{k_b T}\right], \tag{7.1}$$

where V_i is the voltage induced across an inductor L_p which contains the spin sample, A is the cross-sectional area of the sample, n_t is the number of turns in the inductor L_p, θ_t is the tipping angle, ω_0 is the Larmour frequency, N is the total number of spins in the sample, γ is the gyromagnetic ratio, B_0 is the static magnetic field, and T is the bath temperature.

The temperature dependance of Eq. (7.1) implies that the signal voltage increases inversely as the bath temperature, due to the Boltzmann factor. This is only an approximation, valid in the limit $\gamma\hbar B_0 << 2k_bT$. The correct equation is (Abragam, 1961)

$$V_i = \frac{2\pi}{c} A n_t \sin\theta_t \sin\omega_0 t\, \hbar\gamma^2 B_0 N \tanh\left\{\frac{\gamma\hbar B_0}{2k_bT}\right\}. \qquad (7.2)$$

As an example, consider the NMR of Pt^{195} in a 6 Tesla field. The temperature at which $\gamma\hbar B_0 = 2k_bT$ is about 1 mK. Below this temperature, the signal voltage increases only slowly with further decreases in bath temperature. With all other parameters held constant, decreasing the temperature of the Pt spin sample from room temperature to 1 mK will increase the signal voltage by $> 10^5$. The problem with this idea is that the spin-lattice relaxation time T_1 generally increases as the bath temperature is decreased.

In metals, the relation between spin-lattice relaxation time and temperature is given by the Korringa relation T_1T = constant (Slichter, 1980). This is because the predominant relaxation mechanism is the coupling of nuclei to the magnetic moment of electrons in the tail of the Fermi distribution. As the temperature is decreased, the tail of the Fermi distribution becomes less broad, with the number of electrons in the tail scaling with T. The Korringa constant for Pt is about 30 msec-K, so at 1 mK the T_1 would be 30 sec.

The arguments given above for increasing the signal voltage by cooling the sample are only valid for the case of a single pulse, when T_1 is of no consequence. For many pulses averaged together, T_1 becomes very important and we must use the pulse optimization theory presented in Ch. 4. Combining Eqs. (4.1) and (4.6) gives a power signal-to-noise of

$$\frac{S}{N} \propto \frac{1}{T^2 T_1} G(\theta_t, \tau/T_1). \qquad (7.3)$$

If we assume that the function $G(\theta_t,\tau/T_1)$ can be approximately optimized at the different experimental temperatures, then $G(\theta_t,\tau/T_1)$ will be a constant independent of T and T_1. If we then assume the Korringa relation (T_1T = constant) holds, the voltage signal-to-noise becomes

$$\frac{V_S}{V_N} \propto \frac{1}{\sqrt{T}}, \tag{7.4}$$

so for an experiment requiring signal averaging on metal samples, cooling the sample from room temperature to 1 mK will give an increase in averaged voltage signal-to-noise ratio of about 500. The increase in T_1 at low temperatures has greatly reduced the initially expected $> 10^5$ gain in signal-to-noise.

In insulators, the spin-lattice relaxation mechanisms are more complicated (Abragam, 1961), but T_1 generally increases exponentially as the temperature is decreased. This makes spin echo techniques and signal averaging problematic at low temperatures. The spin-lattice relaxation time can be reduced by introduction of paramagnetic defects, as was done for the $NaClO_3$ crystal described in Ch. 6. The T_1 at 4.2 K was reduced from > 72 hours to 20 min (reduction of T_1 below 20 min by this technique caused noticeable distortion of the line). A T_1 of 20 min is still unreasonably large for spin echo techniques and signal averaging. A relatively new relaxation technique (Friedman et al., 1981) has solved the long T_1 problem for surface species. The spin sample is immersed in a liquid ^{3}He bath, and spin coupling between the ^{3}He nuclear spins and the surface nuclei of the sample induces relaxation. Using this technique, T_1's of about 20 sec for ^{1}H and ^{19}F can be achieved at 8 mK (Gonen et al., 1989). For comparison, the T_1 of ^{19}F without a ^{3}He bath is already > 1 hour at 1.3 K (Friedman et al., 1981).

Cooling a spin sample to millikelvin temperatures while maintaining a short T_1 via ^{3}He spin coupling has been successfully used to increase the sensitivity of NMR: the

experimentally measured minimum detectable number of spins following a single pulse is 10^{15} protons, or equivalently 2.8×10^{15} nuclear Bohr magnetons (Kuhns, 1989). This is achieved with a conventional room-temperature amplifier with a noise temperature of 50 K, a receiver coil at 1.2 K, and a receiver Q of about 50. For comparison, a monolayer of Pt atoms with area 1 cm^2 contains 3×10^{14} nuclear Bohr magnetons. This technique has been used to study catalysis on SnO_2 powder (Gonen et al., 1989b).

The magnetic field dependance of Eq. (7.1) implies that the signal voltage increases as the square of the static magnetic field B_0. Superconducting magnets for NMR capable of static fields of up to 13 Tesla are commercially available (Chemagnetics), and the expected increase in S/N is experimentally realized (B. Q. Sun, 1990).

The γ^3 dependence of the signal voltage in Eq. (7.1) is due partly because the voltage induced in a receiver coil by precessing spins is proportional the precession frequency, and partly because the Curie magnetization depends on γ. This implies an increase in sensitivity of over 100 for protons in comparison to Pt.

The geometric terms A and n_t in Eq. (7.1) can also be optimized (Hoult, 1978), but in general have much less effect in increasing the S/N than the terms discussed above.

I will now discuss the noise, and methods of minimizing the noise so as to maximize the S/N. The noise voltage in a NMR spectrometer is given by

$$V_n = (4k_b T_N^{\Sigma} R_i B)^{1/2}, \tag{7.5}$$

where T_N^{Σ} is the total system noise temperature, R_i is the resistance of the receiver circuit, and B is the bandwidth. Building a NMR spectrometer with a low noise temperature and receiver circuit resistance would clearly improve the signal-to-noise. This was the fundamental reason for building a SQUID NMR spectrometer. A NQR spectrometer using a dc SQUID as an amplifier was built and measured to have a total system noise

temperature of 6 K and a Q of 2,500 (R_i = 0.2 Ω) at 30 MHz (Hilbert et al., 1985). It was claimed that this SQUID spectrometer was an improvement of 1-2 orders of magnitude in voltage sensitivity over conventional spectrometers with room-temperature amplifiers. This was attributed to the low noise temperature of the SQUID and the ability to use a high Q receiver circuit. I will examine these claims in more detail.

The total system noise temperature of 6 K appeared to be an impressive improvement over conventional amplifiers. One basis for claiming an improvement of 1-2 orders of magnitude in voltage sensitivity was a comparison of the noise temperature of the SQUID amplifier with the noise temperature of a commercial room-temperature amplifier. The overall system noise temperature of the SQUID spectrometer, including the Nyquist noise from the receiver coil at 4.2K, was measured to be 6 K. A comparison was made to a Miteq (model AU-2A-0150) room-temperature rf amplifier with a noise temperature of about 100 K. Properly matched to a receiver coil at 4.2 K, the conventional Miteq-based spectrometer would have a total system noise temperature of about 104 K. The SQUID-based spectrometer would be an improvement by a factor of about 17 in total system noise temperature compared to the Miteq amplifier. However, the voltage sensitivity is proportional to the square root of the total system noise temperature [refer to Eq. (7.5)], so the SQUID-based spectrometer would be an improvement by a factor of about 4 in voltage sensitivity, all other parameters held constant.

It was believed that this Miteq amplifier had about the lowest noise temperature available. The Miteq is a broadband (1-500 MHz) amplifier. Room-temperature broadband (5-500 MHz) amplifiers with noise temperatures of 50 K are now commercially available (Doty Scientific). The SQUID-based spectrometer would in principle be an improvement by a factor of 3 in voltage sensitivity over a Doty-based spectrometer, all other parameters held constant.

However, if one is attempting to get the lowest noise temperature possible, then one would not want to use a broadband amplifier such as the Miteq or Doty. Broadband

amplifiers are used for other reasons. If one is going to do NMR and NQR experiments at a variety of frequencies and there is no pressing need for the ultimate sensitivity possible, then it makes sense to buy one broadband amplifier. A second reason for using a broadband amplifier is if one will be doing multiple irradiation (Fukushima and Roeder, 1981). In multiple irradiation NMR, two or more distinct frequencies are applied to the same receiver circuit. One reason this is done to "decouple" spins. If a spin sample contains protons and carbon-13 nuclei which see each others field, the resonance lines will be broadened and complicated. If one irradiates the protons, this will average out the proton fields seen by the carbon-13, and simplify the carbon-13 line. If the carbon-13 line is at 30 MHz, the protons will have to be irradiated at 120 MHz, since the proton gyromagnetic ratio is about four times the carbon-13 gyromagnetic ratio. Other uses of multiple irradiation are in multiple quantum coherence, cross-polarization, and two-dimensional NMR. Multiple irradiation is a widespread and useful technique in NMR.

If one wants to achieve the best sensitivity possible at a particular frequency, then the best choice is a narrowband rf amplifier. Narrowband (5 MHz bandwidth) room-temperature rf amplifiers are commercially available with noise temperatures of about 30 K at 30 MHz (Advanced Receiver Research). These amplifiers are successfully used for pulse NMR (Besah, 1990). The SQUID-based spectrometer would in principle be an improvement by a factor of about 2 in voltage sensitivity over a spectrometer using one of these narrowband amplifiers, if all other parameters were the same.

However, this is still not the lowest noise temperature achievable with a conventional rf amplifier. If one is going to compare the voltage sensitivity of a SQUID NMR spectrometer, which is operating at 4.2 K, with a conventional NMR spectrometer, then it is only fair to compare the cooled SQUID amplifier to a cooled conventional amplifier. Gallium arsenide field effect transistors (GaAs FET's) have been cooled to 77 K for use as amplifiers for pulsed NMR spectrometers. One group (Hoult and Richards, 1975) built a liquid-nitrogen-cooled GaAs FET for NMR which achieved an amplifier

noise temperature of 20 K with a gain of 22 dB at 129 MHz. A second group (Conradi and Edwards, 1977) built a liquid-nitrogen-cooled GaAs FET for NMR which achieved an amplifier noise temperature of 9 K at 20 MHz. The total system noise temperature of the NMR spectrometer is 15 K, with the receiver circuit at 4.2 K and losses in the coaxial cable between the receiver circuit and the amplifier contributing 2 K. A third group (Styles et al., 1989) built a liquid-nitrogen-cooled GaAs FET-based NMR spectrometer which achieved an amplifier noise temperature of 15 K and a gain of 20 dB (Styles, 1990) at 90 MHz.

Conventional amplifiers have also been cooled to 4.2 K for use as amplifiers for pulsed NMR spectrometers. One group (Miyoshi and Cotts, 1968) placed a silicon metal oxide semiconductor field effect transitor (MOSFET) in a liquid helium bath and measured an amplifier noise temperature of 88 K at 20 MHz. A second group (Long et al., 1979) developed a liquid-helium-cooled GaAs FET amplifier for a SQUID magnetometer which achieved an amplifier noise temperature of 13 K and a gain of 19 dB at 80 MHz. A third group (Styles et al., 1984) achieved a total system noise temperature of 11 K at 46 MHz, with a gain of 20 dB and a Q of 1,000. The noise temperature measurement was made using the "hot and cold load" method (Doty et al., 1988), and is believed to be fairly accurate (Styles, 1990b). In terms of noise temperature, the SQUID-based NQR spectrometer is in principle an improvement by a factor of 1.4 in voltage sensitivity over this conventional spectrometer, all other parameters being the same. Since the conventional spectrometer is operating at a higher frequency than the SQUID NQR spectrometer, it actually has a slightly better absolute spin sensitivity in principle [refer to Eq.(4.2)] This neglects recovery effects, which do not significantly change this conclusion, and will be discussed later. This group (Styles et al., 1984) has since abandoned the liquid-helium-cooled GaAs FET NMR spectrometer with a total system noise temperature of 11 K, in part because the voltage sensitivity is not impressive compared to conventional spectrometers with room-temperature amplifiers operating at higher static field strengths (Styles et al., 1989).

A second reason the SQUID NQR spectrometer was claimed to be an improvement in voltage resolution of 1-2 orders of magnitude over conventional spectrometers was the high Q of the receiver circuit. The SQUID input impedance is negligible, and a series RLC tuned circuit can be used for a receiver circuit, as shown in Fig. 1.2. It was believed that since conventional amplifiers have high input impedances, one could not use a high Q receiver circuit because of impedance matching considerations. Actually, conventional NMR spectrometers avoid this problem by using a parallel tuned RLC circuit, allowing high Q receiver circuits and good impedance matching to conventional high-input-impedance amplifiers (Hoult, 1978). Pennington and I have built an NMR probe using a parallel RLC receiver circuit made of copper wire which is impedance matched to a room-temperature, 50 Ω input impedance conventional amplifier. When the receiver circuit is cooled to 4.2 K, the Q is about 1,000 at 56 MHz. It may be possible to get even higher Q's by building the receiver circuit out of type II superconducting wire, as was done in the SQUID NMR experiment (see Sec. 5.8).

A third reason the SQUID NQR spectrometer was claimed to be an improvement in voltage resolution of 1-2 orders of magnitude over conventional spectrometers was the recovery time of the spectrometer. The recovery time is inversely proportional to Q, and a long recovery time can obscure a decaying resonance signal. Using a Josephson junction Q-spoiler reduced the recovery time of the Q = 2,500 receiver circuit from 250 μs to 50 μs (Hilbert et al., 1985). Conventional NMR spectrometers get around this problem by using pulse sequences (Pennington, 1989). The ringdown of the tuned receiver circuit in an NMR spectrometer will have a phase determined by the phase of the pulse. If the phase of the pulse is changed by 180°, the phase of the ringdown will also change by 180°. By applying pulse sequences with alternating phases, one can get the NMR signals to add coherently while the circuit ringdowns cancel. Using this technique, Pennington and I achieved an effective recovery time of 60 μs in the conventional NMR spectrometer with a Q of about 1,000 described earlier. In principle, the Q of 2,500 of the SQUID-based NQR

spectrometer would give it an improvement in voltage sensitivity of about a factor of 1.6 over this conventional spectrometer, all other parameters being the same.

7.3 Summary

If the sample, bandwidth, recovery time, and receiver coil geometries are the same, then the expression for the relative minimum detectable number of spins (equivalent to voltage sensitivity) of a SQUID-based NMR spectrometer and an FET-based NMR spectrometer is

$$\frac{N_{mds}(SQUID)}{N_{mds}(FET)} = \frac{T_{bath}^{squid}}{T_{bath}^{fet}} \frac{B_0^{3/2}(fet)}{B_0^{3/2}(squid)} \left[\frac{T_N^{\Sigma}(squid)\, Q^{fet}}{T_N^{\Sigma}(fet)\, Q^{squid}} \right]^{1/2}, \tag{7.6}$$

where T_{bath} is the bath temperature of the spin sample in the spectrometer, B_0 is the static field strength, the total spectrometer noise temperature $T_N^{\Sigma} = T_{coil} + T_N^{amp}$. T_{coil} is the temperature of the tuned receiver circuit, T_N^{amp} is the amplifier noise temperature, and Q is the quality factor of the receiver circuit for each system.

Most of the increase in sensitivity of the SQUID NMR spectrometer with a spin sample at 4.2 K compared to a conventional room-temperature spectrometer with a spin sample at 290 K is due to the Boltzmann factor enhancement of spin polarization (the factor T_{bath}) and the decreased Nyquist noise of the receiver circuit (the factor T_{coil}). The best sensitivity obtained with a SQUID NQR spectrometer with the SQUID amplifier and the sample at 4.2 K was 4×10^{16} nuclear Bohr magnetons (refer to Sec. 6.7), and the best sensitivity obtained with a SQUID NMR spectrometer with the SQUID amplifier and the sample cooled to 4.2 K was 2.5×10^{17} nuclear Bohr magnetons (refer to Sec. 6.6). The best sensitivity obtained with a conventional NMR spectrometer with the FET amplifier at room temperature and the sample at 10 mK was 2.8×10^{15} nuclear Bohr magnetons (Gonen, 1989b). Other comparisons are complicated by the different ways of measuring

sensitivity and different experimental conditions: most NMR sensitivities are given in terms of the S/N of a standard liquid spin sample which has multiple lines. Comparisons can still be made between the noise temperatures and Q values. The best total system noise temperature obtained with a SQUID NQR spectrometer was 6 K with a Q of 2,500, and the best total system noise temperature obtained with a SQUID NMR spectrometer was 11 K with a Q of 600. The best total system noise temperature obtained with a FET NMR spectrometer was 11 K with a Q of 1,000. A SQUID-based NMR spectrometer has a voltage sensitivity which is about the same as a FET-based NMR spectrometer, at these temperatures and operating frequencies.

The trend in modern NMR is to go to higher static magnetic fields and frequencies, to improve the sensitivity. NMR systems capable of operating at frequencies over 500 MHz are commercially available and used in NMR laboratories. The SQUID performance is expected to decrease at frequencies higher than 30 MHz: the noise temperature increases and the Q obtainable in the tuned receiver circuit decreases, lowering the gain of the SQUID and decreasing the signal current in the receiver circuit.

The advantages of techniques such as going to higher frequencies and choosing a favorable spin sample (narrow signal bandwidth and high γ) in NMR is vividly illustrated by the results of recent spin noise experiments. The second experiment using a dc SQUID to detect a high frequency magnetic resonance signal was the observation of nuclear spin noise (Sleator et al., 1985). It was stated that "the very low noise temperature of the dc SQUID as a radiofrequency amplifier has made possible the first observation of spontaneous emission from nuclear spins" (Sleator et al., 1987). In fact, it was not necessary to use a dc SQUID to observe spontaneous emission from nuclear spins: two separate groups have since observed spontaneous emission from nuclear spins using conventional room-temperature amplifiers with room-temperature receiver circuits and room-temperature spin samples (Gueron and Leroy, 1989; McCoy and Ernst, 1989). The lower sensitivity of the conventional room-temperature spectrometer was compensated by

operating at about 300 MHz and using a liquid sample, which has a narrower linewidth than a solid. Both the absorption dip and the spin noise bump were detected, with signal averaging times as short as 3 seconds for the spin noise bump. For comparison, the signal averaging time required to see the spin noise bump in the SQUID experiment was about 7 hours.

References

1. Abragam, A., 1961, Principles of Nuclear Magnetism (Clarendon Press, Oxford).

2. Slichter, C. P., 1980, Principles of Magnetic Resonance (Springer-Verlag, New York).

3. Friedman, L. J., P. Millet, and R. C. Richardson, 1981, "Surface relaxation of ^{3}He on small flourocarbon spheres," Phys. Rev. Lett. 47, 1078.

4. Gonen, O., P. L. Kuhns, C. Zuo, and J. S. Waugh, 1989, "Mechanism of ^{3}He-mediated nuclear spin-lattice relaxation at surfaces," J. Magn. Reson. 81, 491.

5. Kuhns, 1989, personal communication.

6. Gonen et al., 1989b, "Observation of surface intermediates by NMR below 1 K: CO chemisorbed on a SnO_2 oxidizing catalyst," J. Phys. Chem. 93, 504.

7. Chemagnetics, 208 Commerce Street, Fort Collins, Colorado, 80524.

8. B. Q. Sun, 1990, U. C. Berkeley, personal communication.

9. Hoult, 1978, "The NMR receiver: a description and analysis of design," in Progress in Nuclear Magnetic Resonance Spectroscopy, 12, Eds. J. W. Emsley, J. Feeney, and L. H. Sutcliffe (Pergamon Press, New York), p. 41.

10. Hilbert, C., J. Clarke, T. Sleator, and E. L. Hahn, 1985, "Nuclear quadrupole resonance detected at 30 MHz with a dc superconducting quantum interference device," Appl. Phys. Lett. 47, 637.

11. Miteq, Inc., 125 Ricefield Lane, Hauppage, New York, 11788.

12. Doty Scientific, Inc., 600 Clemson Road, Columbia, South Carolina, 29223.

13. Advanced Receiver Research, P. O. Box 1242, Burlington, Connecticut, 06013.

14. Fukushima, E., and S. B. W. Roeder, 1981, Experimental pulse NMR: a nuts and bolts approach (Addison-Wesley, Reading, Mass.).

15. Besah, 1990, MIT, personal communication.

16. Hoult, D. I., and R. E. Richards, 1975, "V.H.F. F.E.T. preamplifier with 0.3 dB noise figure," Electron. Lett. 11, 596.

17. Conradi, M., and C. M. Edwards, 1977, "Low-noise circuitry for low-temperature NMR and SQUIDs," Rev. Sci. Instrum. 48, 1219.

18. Styles, P., N. F. Soffe, and C. A. Scott, 1989, "An improved cryogenically cooled probe for high-resolution NMR," J. Magn. Reson. 84, 376.

19. Miyoshi, D. S., and R. M. Cotts, 1968, "Helium cooled radio frequency preamplifier for use in NMR," Rev. Sci. Instrum. 39, 1881.

20. Long, A., T. D. Clark, R. J. Prance, and M. G. Richards, 1979, "High-performance UHF SQUID magnetometer," Rev. Sci. Instrum. 50, 1376.

21. Ahola, H., G. J. Enholm, P. Ostman, and B. Rantala, "Cryogenic GaAs-FET amplifiers for SQUIDs," J. Low Temp. Phys. 35, 313.

22. Styles, P., Soffe, N. F., C. A. Scott, D. A. Cragg, F. Row, D. J. White, and P. C. J. White, 1984, "A high-resolution NMR probe in which the coil and preamplifier are cooled with liquid helium," J. Magn. Reson. 60, 397.

23. Styles, 1990, personal communication.

24. Doty, F. D., T. J. Connick, X. Z. Ni, and M. N. Clingan, 1988, "Noise in high-power, high-frequency double-tuned probes," J. Magn. Reson. 77, 536.

25. Styles, 1990b, personal communication.

26. Pennington, C. H. P., 1989, Ph. D. Thesis, University of Illinois at Urbana-Champaign.

27. Sleator, T., E. L. Hahn, C. Hilbert, and J. Clarke, 1985, "Nuclear-spin noise," Phys. Rev. Lett. 55, 1742.

28. Sleator, T., E. L. Hahn, C. Hilbert, and J. Clarke, 1987, "Nuclear-spin noise and spontaneous emission," Phys. Rev. B36, 1969.

29. Gueron, M., and J. L. Leroy, 1989, "NMR of water protons. The detection of their nuclear-spin noise, and a simple determination of absolute probe sensitivity based on radiation damping," J. Magn. Reson. 85, 209.

30. McCoy, M. A., and R. R. Ernst, 1989, "Nuclear spin noise at room temperature," Chem. Phys. Lett. 159, 587.

LAWRENCE BERKELEY LABORATORY
UNIVERSITY OF CALIFORNIA
INFORMATION RESOURCES DEPARTMENT
BERKELEY, CALIFORNIA 94720